University of Tennessee, Knoxville
Trace: Tennessee Research and Creative Exchange

Masters Theses   Graduate School

5-2005

Modeling and Analysis of Active Front-End Induction Motor Drive for Reactive Power Compensation

Pankaj Prabhakar Pandit
University of Tennessee - Knoxville

To the Graduate Council:

I am submitting herewith a thesis written by Pankaj Prabhakar Pandit entitled "Modeling and Analysis of Active Front-End Induction Motor Drive for Reactive Power Compensation." I have examined the final electronic copy of this thesis for form and content and recommend that it be accepted in partial fulfillment of the requirements for the degree of Master of Science, with a major in Electrical Engineering.

Leon M. Tolbert, Major Professor

We have read this thesis and recommend its acceptance:

Jack S. Lawler, John N. Chiasson

Accepted for the Council:
Dixie L. Thompson

Vice Provost and Dean of the Graduate School

(Original signatures are on file with official student records.)

To the Graduate Council:

I am submitting herewith a thesis written by Pankaj Prabhakar Pandit entitled "Modeling and Analysis of Active Front-End Induction Motor Drive for Reactive Power Compensation." I have examined the final electronic copy of this thesis for form and content and recommend that it be accepted in partial fulfillment of the requirements for the degree of Master of Science, with a major in Electrical Engineering.

<div align="right">

Leon M. Tolbert

Major Professor
</div>

We have read this thesis
and recommend its acceptance:

Jack S. Lawler

John N. Chiasson

<div align="right">

Accepted for the Council:

Anne Mayhew

Vice Chancellor and

Dean of Graduate Studies
</div>

(Original signatures are on file with official student records)

Modeling and Analysis of Active Front-End Induction Motor

Drive for Reactive Power Compensation

A Thesis

Presented for the

Master of Science

Degree

The University of Tennessee, Knoxville

Pankaj Prabhakar Pandit

May 2005

Dedication

I wish to dedicate this thesis to my family:

Shri. Prabhakar B. Pandit

Sau. Jayashree P. Pandit

Sharad and Dipak

Papa, Akka, Anna, and Dipu, thank you for your unending love, support, and above all for being my inspiration which made the completion of this thesis possible.

Acknowledgments

I wish to thank all those who helped me complete my M.S. in Electrical Engineering at the University of Tennessee. I would like to thank Dr. Leon M. Tolbert for giving me an opportunity to work on this thesis by funding my research, serving as my major professor, and providing valuable advice from time to time. I would like to thank Dr. Chiasson for serving on my thesis committee, and teaching ECE 617 which helped me towards my research. I would like to thank Dr. Lawler for his valuable suggestions regarding the research, and serving on my thesis committee.

I am also grateful to Dr. Bimal K. Bose for igniting my interest in power electronics, his support, and guidance.

I would also like to thank my lab mates, Surin, Ben, Weston, Niranjan, Michael, Pierre, and Gerry for their heartfelt support, and making my graduate school experience so much more enjoyable.

A special thanks to all my Indian friends at The University of Tennessee.

Abstract

In this thesis, an active front end induction motor drive for reactive power compensation is analyzed. The classical vector control approach for high performance control of an induction motor drive is a well established industry standard today. The same idea of decoupled control is extended to the line-side PWM converter for achieving better dynamic performance.

The system model is obtained using *d-q* rotating frame theory. The i_{qe} component of line currents is used to control the reactive power. The i_{de} component is used to control the dc-link voltage and also to supply active power required by the motor. A high gain feedback controller with input-output linearization is presented to remove coupling between i_{qe} and i_{de} currents. A load power feed-forward loop is added to the dc-link voltage controller for fast dynamic response.

The drive performance is analyzed to define system specifications. The motor acceleration, deceleration, and variable power factor operation (reactive power compensation) of the active drive system are demonstrated. The motor load is varied from no load to full load in steps of 10% each. For each step the device currents, switching power loss, line harmonics, and dc-link ripples are plotted. This data is used to derive conclusions that define system specifications and also state operating limits.

The control of the drive system is implemented in MATLAB-SIMULINK. The complete system hardware is implemented in commercially available simulation tool, PSIM. The two software packages are interlinked using an interface module.

Table of Contents

List of Tables

List of Figures

1   Introduction

1.1   Chapter Overview

The purpose of this chapter is to introduce the research presented in this thesis. Section 1.2 provides a brief overview of the research undertaken. In Section 1.3, the general idea of Active Front End Inverters is presented. The circuit topology for the complete power converter system used for reactive power compensation is explained.

Section 1.4 discusses the basic operating principle using single-phase equivalent circuit of the system. The different modes of operation are elaborated using phasor diagrams. Section 1.5 examines the key features and suitable applications of the Active Front End Inverter system. Section 1.6 defines research goals. The scope of the research is discussed here. Section 1.7 concludes Chapter 1 by presenting the thesis outline.

1.2   Thesis Research

In this thesis, an active front-end induction motor drive for reactive power compensation is analyzed. The vector control approach for high performance control of an induction motor drive is now a well accepted industry standard control. The same idea of decoupled control is extended to the line-side PWM converter for achieving better dynamic performance. The sine-triangle PWM scheme is used to control IGBT switches in both rectifier and inverter bridges.

The system model is obtained using d-q rotating frame theory. The line currents are decomposed into i_{qe} and i_{de} components. The i_{qe} component is used to control the

reactive power. The i_{de} component is used to control the dc-link voltage and also to supply active power required by the motor. A high gain feedback with input-output linearization control is presented to remove coupling between i_{qe} and i_{de} currents. A load power feed-forward loop is added to the dc-link voltage controller for fast dynamic response.

Using the dynamic *d-q* model, the drive performance is analyzed to define system specifications. The motor acceleration, deceleration, and variable power factor operation (reactive power compensation) of the active system are demonstrated. The motor load is varied from no load to full load in steps of 10% each. For each step the device currents, reverse blocking voltage, switching power loss, line harmonics, and dc-link ripples are plotted. This data is used to derive conclusions that define system specifications and also state operating limits.

The control of the drive system is implemented in MATLAB-SIMULINK. The complete system hardware comprising of switches, line inductors, dc-link capacitor bank, and the motor is implemented in commercially available simulation tool, PSIM. The two software packages are interlinked using an interface module.

1.3   Active Front-End Inverters

In this work, the term Active Front End Inverter refers to the power converter system consisting of the line-side converter with active switches such as IGBTs, the dc-link capacitor bank, and the load-side inverter. The line-side converter normally functions as a rectifier. But, during regeneration it can also be operated as an inverter, feeding power back to the line. The line-side converter is popularly referred to as a PWM rectifier

in the literature. This is due to the fact that, with active switches, the rectifier can be switched using a suitable pulse width modulation technique.

The PWM rectifier basically operates as a boost chopper with ac voltage at the input, but dc voltage at the output. The intermediate dc-link voltage should be higher than the peak of the supply voltage [1]. This is required to avoid saturation of the PWM controller due to insufficient dc link voltage, resulting in line side harmonics. The required dc-link voltage needs be maintained constant during rectifier as well as inverter operation of the line side converter. The ripple in dc-link voltage can be reduced using an appropriately sized capacitor bank. The active front-end inverter topology for a motor drive application is shown in Figure 1.1
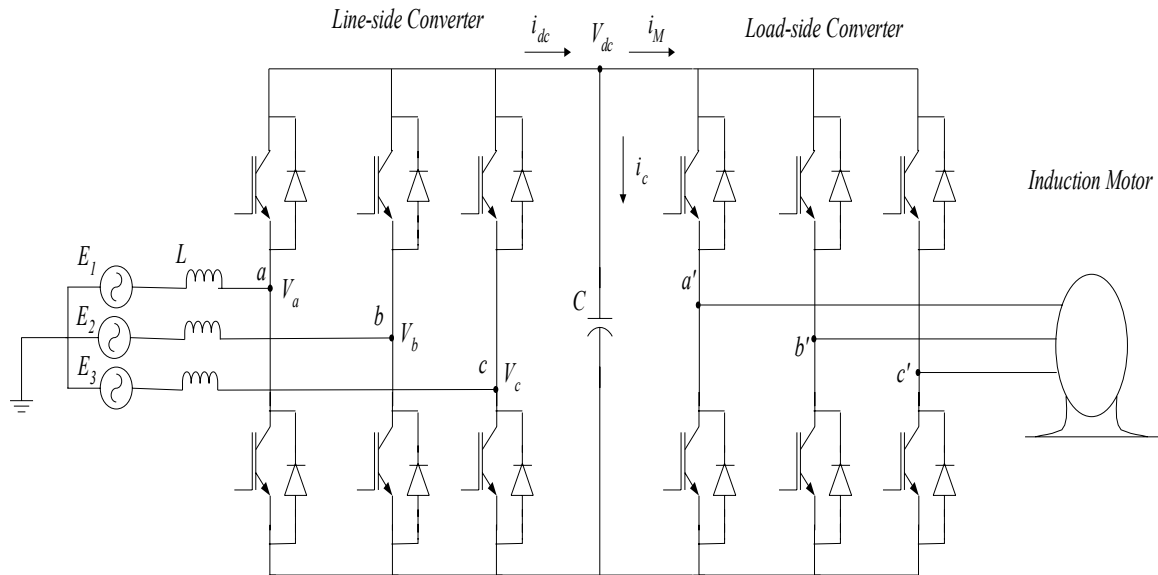
Figure1.1 Active front-end induction motor drive system

3

The topology shown in Figure 1.1 has two three-phase, two-level PWM converters, one on the line side, and another on the load side. The configuration uses 12 controllable switches. The line-side converter is connected to the utility through inductor. The inductor is needed for boost operation of the line-side converter. A transformer on the supply side with appropriate secondary impedance also serves the same purpose.

For a constant dc-link voltage, the IGBTs in the line-side converter are switched to produce three-phase PWM voltages at a, b, and c input terminals. The line-side PWM voltages, generated in this way, control the line currents to the desired value. When dc-link voltage drops below the reference value, the feed-back diodes carry the capacitor charging currents, and bring the dc-link voltage back to reference value.

1.4   Operating Principle

A per-phase equivalent circuit of the three-phase, line-side PWM converter is shown in Figure 1.2. The source voltage E_S, and line inductance L represent the utility system. The three-phase voltages at the three input legs of the line side converter are represented by V. The voltage V can be viewed as a PWM voltage wave constructed from the dc link voltage V_d. The magnitude and phase of the fundamental component of V is controlled by the line-side converter. The voltage V_L, across inductor L, is $I_S \omega L$ where, ω is the angular frequency of supply voltage. Note that, the synchronous machine connected to an infinite bus can also be represented by the same per-phase equivalent circuit shown in Figure 1.2. Similar to an overexcited or under-excited synchronous machine, the PWM converter can also draw line currents at leading, lagging or unity power factor.
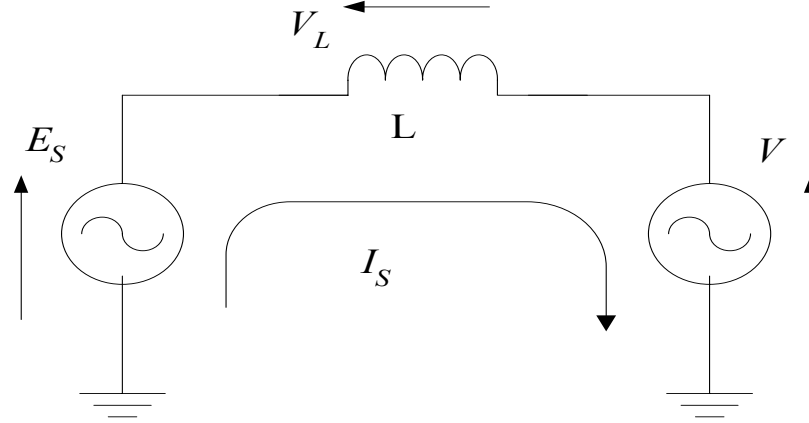
Figure 1.2 Per-phase equivalent circuit

As illustrated in Figure 1.3 (a), for unity power factor operation in rectifier mode of the line-side converter, the PWM voltage V needs to be larger than the supply voltage phasor E_S in magnitude and lags E_S by an angle δ. This makes E_S and line current I_S, to be co-phasal. The angle δ is called the power angle because it controls the power flow between the two sources.

The regenerative mode of the line-side converter is shown in Figure 1.3 (b). The I_S phasor now reverses, causing reversal of $I_S\omega L$ phasor. In order to satisfy the phasor diagram, the V phasor should lead phasor E_S by an angle δ. Thus the power angle δ also reverses. Likewise, the leading power factor operation is illustrated in Figure 1.3 (c).

The active power P, and reactive power Q, are given by following expressions:

$$P = 3 \cdot E_S I_S \cos\varphi \tag{1.1}$$

$$Q = 3 \cdot E_S I_S \sin\varphi \tag{1.2}$$

where E_S and I_S are supply voltage and line current, while φ is power factor angle.
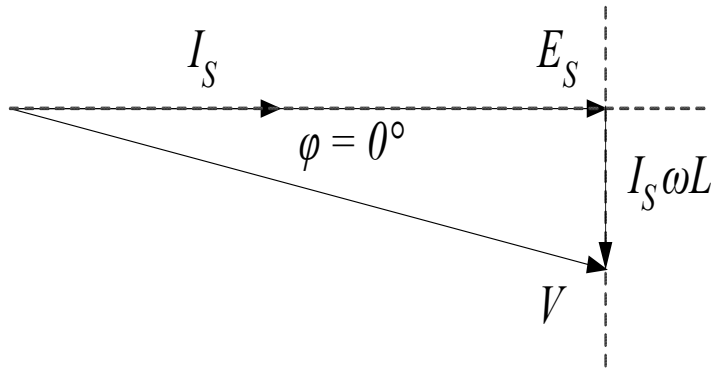
a) Unity power factor during motoring mode
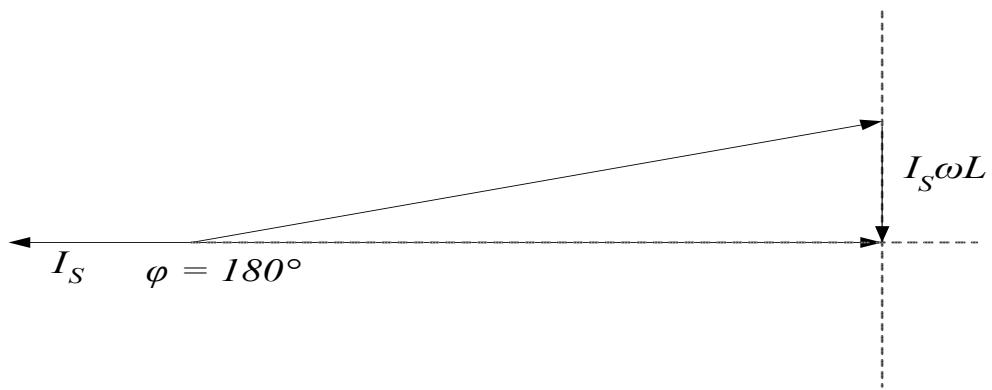
b) Unity power factor during regenerating mode
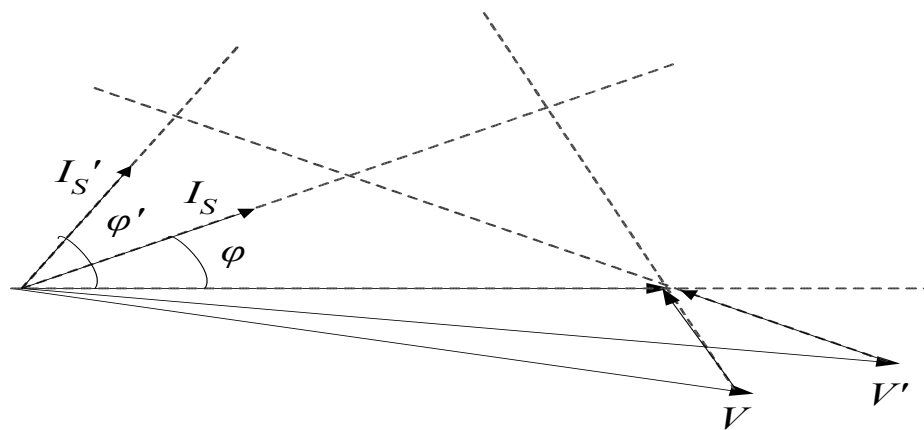
c) Leading power factor operation during motoring mode

Figure 1.3 Operating principle

From Figure 1.3 (b) we can write,

$$I_S \omega L \cos\varphi = V \sin\delta \qquad (1.3)$$

$$I_S \omega L \sin\varphi = V \cos\delta \qquad (1.4)$$

Substituting the values of $I_S \cos\varphi$ and $I_S \sin\varphi$ in Equation 1.1 and 1.2 respectively,

$$P = 3 \cdot E_S \frac{V \sin\delta}{\omega L} \qquad (1.5)$$

$$Q = 3 \cdot E_S \frac{V \cos\delta - E_S}{\omega L} \qquad (1.6)$$

The equations 1.1 through 1.6 indicate that the PWM voltage, V, and power angle, δ, can be controlled to control active and reactive power. It is also possible to maintain reactive power constant while varying active power. This is done by keeping phasors $V \cos\delta$ constant and varying phasor $V \sin\delta$. An effective control strategy for achieving this are discussed in detail in Chapter 4.

1.5   Key Features of Active Front-End Inverters

The power electronics equipments are often viewed as a source of troublesome line-side interactions in the form of non-linear reactive currents and harmonics. However, with the advent of high power semiconductor devices capable of switching adequately fast, many new applications of power electronics equipments are being envisaged. One amongst them is Active front-end inverter, which can provide a solution to some power quality problems. The key features of this topology are discussed here.

- **Regenerative Capabilities –** In normal motoring mode of the drive, power flows from supply-side to the motor. The line-side converter operates as rectifier, whereas the load-side converter operates as an inverter. During regenerative braking mode, their respective roles are reversed. The system can continuously regenerate power if the machine is a generator, such as in wind generation system.

- **Unity Power Factor Operation –** With the line currents in phase with the line voltages, the unwanted reactive currents are eliminated. Since regeneration is also possible at unity power factor, the overall power quality is improved significantly. The converter will be able to supply the same active power but at reduced current ratings. Thus an increased cost of the converter on account of using active power switches can be justified for high power applications.

- **Reactive Power Compensation –** Alternatively, the kVA ratings saved due the unity power factor operation can be used to provide reactive power compensation to the utility system. The double-sided power converter thus acts as static VAR compensator while driving a variable speed motor load. This scheme can be an attractive alternative to the overexcited synchronous motor used as a VAR compensator.

- **As an Interface between Distributed Energy Source and Utility –** The line-side PWM converters are applicable whenever a DC bus is to be connected to the AC grid. Usually this is the case for distributed energy sources such as fuel cells, microturbines, or variable speed wind energy plants employing a dc-link.
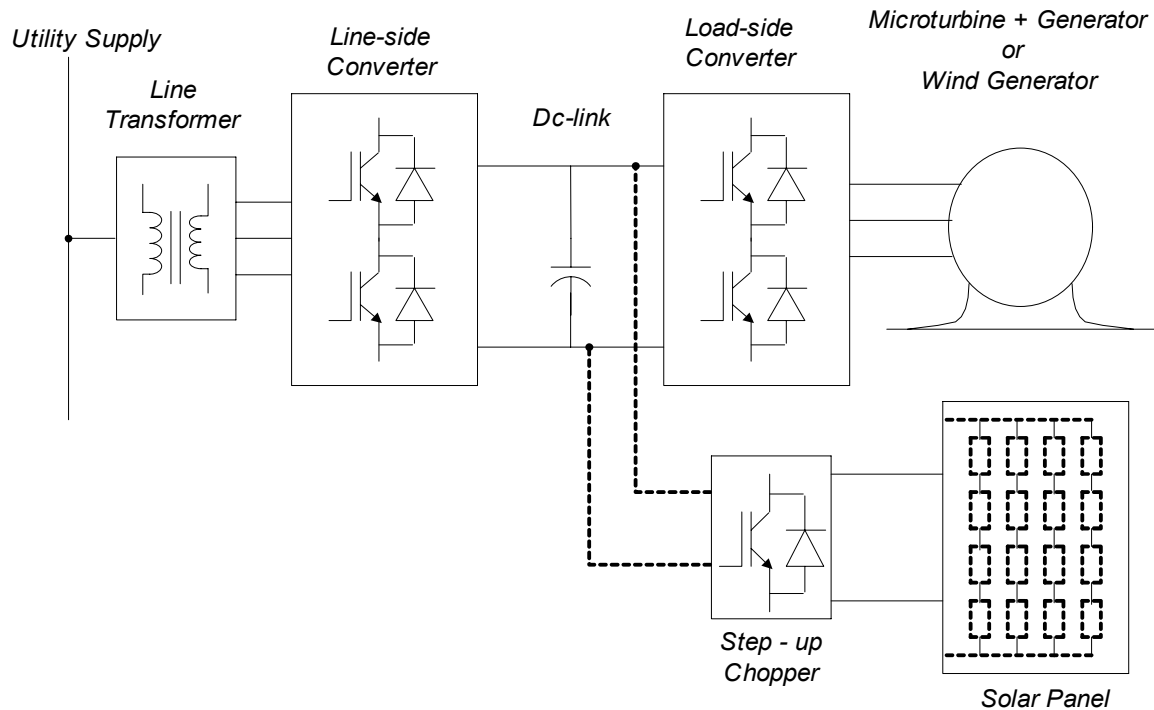
Figure 1.4 Distributed energy source and utility interface

Figure 1.4 shows schematic representation of distributed energy sources connected to the utility grid. The line-side PWM converter facilitates the flow of power from distributed sources to the Utility at fixed frequency, and at desired power factor.

1.6   Research Goals

Evaluating the system performance by accurate simulations is the first important step in the development of any power electronics system prototype. By simulating the expected performance of the system, technical risks in the actual development can be reduced significantly. Thus to identify device selection, system specifications, and design

issues prior to the actual design, is the principal motivation behind undertaking this research.

The broader objective stated above is further articulated into specific goals mentioned below.

1. Demonstrate application of an Active Front End Motor Drive topology, shown in Fig. 1.1, for supplying variable reactive power compensation to the utility, while driving a variable speed motor load.

2. Obtain the system dynamic model and present effective decoupling control strategies for better transient performance.

3. Implement the system model and suitable control scheme in SIMULINK.

4. Evaluate the system performance at variable load by plotting system parameters such as line currents, line harmonics, dc-link voltage ripple, device peak currents and voltages. Use the device loss model to plot conduction, and switching losses for the active switches.

5. Draw conclusions about the system operating efficiency, device selection, and discuss optimum system design issues.

The research presented in this thesis aims to achieve these goals.

1.7   Chapter Summary and Thesis Outline

In this chapter, several topics were discussed. A brief overview of the research to be presented in this thesis is first provided. A circuit topology used for an Active Front End motor drive system is discussed as well. Further the principle of operation for this topology is explained with the help of phasor diagrams. Several key features and some

potential applications of Active Front End Inverters are examined further. At the end, the primary motivation behind this research and the precise goals that this research set out to achieve are also stated.

In Chapter 2, a detailed discussion on power quality, stability, and reactive power compensation will be presented. In addition the Instantaneous Active and Reactive power definitions will be reviewed. Further, different methods for compensation will be compared. In particular, the power compensation using induction motor drive will be discussed.

In Chapter 3, the d-q rotating frame theory as applied to the active front end inverter system will be discussed. The system dynamic model in d-q coordinates will be derived. The active and reactive power definitions in dq-frame will be derived as well. This will set up the control problem, which will be solved in the next chapter.

In Chapter 4, the control strategy is formulated. The input-output linearization for decoupled control of i_{de} and i_{qe} current components will be discussed. The load power feed-forward compensation is also discussed to achieve better transient performance.

The main purpose of Chapter 5 will be to simulate all possible modes of operation of the complete drive system. The simulation set up and implementation issues in SIMULINK as well as PSIM will be discussed. In addition, this chapter will set down the approach for determining the system specifications, loss calculations, and optimum system performance. The detailed simulation results will also be presented.

In Chapter 6, a brief summary of the thesis will be given. Based on the simulation results, important conclusions regarding the research will be made. Lastly, several suggestions on possible future research will be made.

2 Background

2.1 Chapter Overview

In the previous chapter, the general idea of active front-end inverters and the thesis outline was presented. The purpose of this chapter is to provide a detailed background pertaining to other research useful in analyzing the active front-end drive. In Section 2.2 power quality issues including cause and effects of harmonics are discussed.

In Section 2.3 the role of power electronics in improving the ac grid power is reviewed. The interesting interpretations of instantaneous real and reactive power are discussed in Section 2.4. At the end, the comparison between traditional drives with phase-controlled rectifiers and drives with active front-ends is presented. This comparison is the motivation for preferring active front-end drives over traditional drives for some high power applications.

2.2 Power Quality Issues

An uninterrupted, sinusoidal voltage at rated magnitude and frequency represents the power supply of highest quality. The factors that define the quality of electric power are harmonic distortion, voltage regulation, voltage sag, and voltage unbalance in addition to the continuity of power supply.

The universal use of non-linear loads, mainly power electronic converters, has increased the presence of non-linear and reactive currents in the power system. In most applications, the switching of these converters is done synchronously with the line

voltage. The harmonic components produced in this case are integer multiples of the fundamental frequency, also referred to as superharmonics. The presence of lagging, non-linear currents lead to the line voltage distortions, increased transmission losses, additional transmission and distribution capacity, in addition to affecting power system stability.

In many other industrial loads such as arc furnaces, spot wielding machines, rolling mills, and mine hoists, the load currents are rapidly changing and non-sinusoidal in shape. The harmonic spectrum of the rectifier input currents for these loads contain subharmonic components, which are not integer multiples of the fundamental line frequency, in addition to the superharmonics components [2]. These waveforms are considered as non-periodic.

These reactive currents along with periodic and non-periodic harmonic currents need to be eliminated from the power system to improve the overall power quality to an acceptable level. Before discussing the details of various power compensation methods, it is useful to investigate the sources of harmonics and their effects in different types of electrical loads.

2.2.1 Sources of Harmonics

Any component of voltage or current waveform, other than specified frequency sinusoidal component is referred to as harmonics. Non-linear loads change the sinusoidal nature of the ac power current, thereby, resulting in the flow of harmonic currents in an ac power system. A brief review of these loads and harmonics produced by them is presented here [3].

- Static Power Converters - Thyristor and/or diode based power converters are the largest non-linear loads connected to the power system. These are extensively used in industry to convert power from ac-to-dc, dc-to-ac, dc-to-dc, and ac-to-ac. The current commutation phenomenon results in voltage notching and the poor displacement power factor (DPF) draws additional VAR from the source.

- Arc furnaces, mine hoists loads – The harmonics produced by these loads are highly unpredictable because of cycle-by-cycle variation of the mechanical torque. The line current is non-periodic. The harmonic spectrum shows presence of both integer and non-integer order of frequencies [2]. These types of loads often require a shunt compensator to maintain voltage levels, improve power factor, and increase power system stability.

- Switch Mode Power Supplies (SMPS) – Most electronic equipment uses a SMPS to provide the stabilized voltage to the equipment. It feeds the capacitor that supplies voltage to the equipment. Since the load, as seen from the power system, is a capacitor, the current to the power supply is discontinuous, producing line harmonics.

- Pulse Width Modulated (PWM) Drive – The dc link drive has a diode at the input and a large capacitor on the dc link to regulate the dc voltage. For light loads (30-50%), the current only flows when the voltage output of the diode rectifier is above that of the capacitor. Thus at light loads current in the ac circuit is discontinuous.

- Utility Interface with Distributed Energy Sources – With the increasing use of distributed energy sources such as fuel cells, wind generators, micro-turbines, and

14

solar cells, there are various topologies available to connect these sources to the utility. These interfacing power converters may act as current sources attached to the electric utility or as voltage sources tied to the utility through a series impedance. Depending on the topology used, the outputs of these power converters may contain harmonics of various orders and power factors that may cause unacceptable power quality for the utility grid.

2.2.2 Effects of Harmonics

Most power equipment are designed to operate at fixed frequency sinusoidal voltages and currents. The presence of harmonics will naturally have unwarranted effects on these equipments. The degree to which harmonics can be tolerated depends on the type of load consuming these harmonics. In case of heating loads, such as oven or furnaces, the harmonic currents are utilized for heating and thus presence of harmonics do not have any adverse impact.

In rotating machines, such as induction motors and synchronous generators, the harmonics cause increased iron and copper losses, resulting in increased heating and reduced efficiency. Harmonic currents also give rise to higher audible noise compared to the sinusoidal currents. The harmonic currents can also cause or enhance cogging (refusal to start smoothly) or crawling (high slip) phenomenon in an induction motor. The interaction between harmonic currents and fundamental frequency stator current leads to pulsating torque and may cause mechanical oscillations. In the case of transformers, the harmonics cause higher iron and core losses resulting in increased heating.

15

Power cables carrying harmonic currents are prone to heating due to skin and proximity effects. Power cables acting as parallel capacitors may be involved in system resonance. Due to magnified harmonic levels, the cables may be subjected to the voltage stress and corona, which can lead to dielectric failure.

Additionally, the presence of harmonics may cause metering and instrumentation devices to produce erroneous results. In power system equipment such as switchgears, harmonic currents increase heating and losses, thereby reducing steady state current carrying capacity and shortening the life of insulating components. Fuses also suffer de-rating because of the heat generated by the harmonics during 'normal' operation.

The IEEE recommended practices and harmonic control guidelines [3] limit the harmonic contents and the distortions caused by them in the waveform to a certain level. The distortion level is gauged in terms of total harmonic distortion (THD), defined as,

$$THD = \frac{\sqrt{V_{RMS}{}^2 - V_1{}^2}}{V_1} * 100 \tag{2.1}$$

Where, V_{RMS} is the root mean square value of the total voltage waveform, comprising all the harmonics including the fundamental frequency component. Whereas, V_1 is the root mean square value of the fundamental components of total voltage.

The distortion limits recommended by IEEE 519 standard are listed in Table 2.1. The limits are applicable only at the point of common coupling (PCC) of the utility and plant interface. The limits are recommended to be used as system design values for the "worst case" for normal operation. Normal operation is the operating condition lasting longer than an hour. For shorter periods, such as during start-ups or unusual conditions, the limits may be exceeded by 50%.

Table 2.1: Voltage distortion limits

Bus Voltage at Point of Common Coupling (PCC)	Individual Voltage Distortion (%)	Total Harmonic Distortion (%)
69 kV and below	3.0	5.0
69.001 kV through 161 kV	1.5	2.5
161.001 kV and above	1.0	1.5

2.3   Role of Power Electronics in Improving Quality of AC Grid Power

Power electronics, which is the major contributor to the troublesome line-side interactions in the form of reactive currents and harmonics, can also provide solution for removing such effects. The prospects of using a power electronics based system to address the power quality issues promise to change the landscape of future power systems in terms of generation, transmission and distribution, operation and control. The ever increasing interest in these applications can be attributed to the several factors as listed below [4]:

1. Availability of power semiconductor devices with high power ratings capable of switching fast lead to better conversion efficiency and high power density.

2. Growing awareness of power quality issues and stricter norms set forth by the utility companies and regulatory authorities to control harmonic pollution and EMC effects.

3. Continual use of existing transmission system capacity for increased power transfer without compromising transmission system stability and reliability.

4. Need for effective control of power flow in a deregulated environment.

5. Increased emphasis on decentralized generation with renewable energy sources to avoid transmission line congestion.

Many types of utility applications based on power electronics controllers are being envisaged. These include active and reactive power flow control, system stability, improving power quality by eliminating harmonics, improving transmission efficiency, and protection.

Thus, power quality solutions comprising reactive compensation, compensation for the non-active currents, harmonic compensation, or active filtering is one of the many significant areas of utility applications for these controllers, summarily referred to as flexible ac transmission system (FACTS) controllers. The different types of FACTS controllers and the principle of operation is reviewed briefly in the following subsections.

2.3.1 Flexible AC Transmission Systems (FACTS) Operating Principle

In existing ac transmission networks, limitations on constructing new power lines has led to several ways to increase power transmission capability without sacrificing the stability requirements. Power flow on a transmission line connecting two ac systems is given by,

$$P = \frac{E_1 E_2}{X} \sin \delta \qquad\qquad (2.2)$$

Where E_1 and E_2 are magnitudes at the two ends of transmission line, X is the line reactance, and δ is the angle between the two bus voltages. Equation 2.2 shows that power flow on a transmission line depends on the voltage magnitude E_1 and E_2, the line reactance X, and the power angle δ. FACTS devices based on phase-controlled thyristors or active switches such as IGBTs can be used to rapidly control one or more of above three quantities.

The term, FACTS devices, can be formally defined as a collection of power converters and controllers that can be applied individually or in coordination with others to control – series impedance, shunt impedance, current, voltage, phase angle, oscillation damping. By controlling one or all these quantities, FACTS devices enable transmission system to be operated closer to its thermal limit without decreasing the system's reliability in addition to providing improved quality power. Depending on whether they are connected in shunt or series, the FACTS devices can be categorized as shunt-connected and series-connected controllers [5].

2.3.2 Shunt-Connected Controllers

Typically, the shunt-connected controllers draw or supply reactive power from a bus, thus causing the bus voltage to change due to the internal system reactance. Some of the popular shunt controllers are described below [6].

Static synchronous compensator (STATCOM) is a shunt-connected static VAR compensator, which can control its output current (inductive/capacitive) independent of

19

the ac system voltage variations. It uses self commutated (active) switches like IGBTs, GTOs, or IGCTs. It may or may not need large energy storage capacity depending on what active and/or reactive power compensation is desired.

Static VAR compensator (SVC) is another type of power compensator, whose output is adjusted to exchange capacitive or inductive current so as to maintain bus voltage constant. SVC is based on devices without turn-off capability, like thyristors. SVC functions as a shunt-connected controlled reactive admittance. Some popular SVC configurations are thyristor controlled reactor (TCR), thyristor switched reactor (TSR), and thyristor switched capacitor (TSC). The TCR has an effective inductive reactance which is varied by firing angle control of the thyristor valve. The effective inductive reactance of a TSR, on the other hand, is varied in step-wise manner by full or zero conduction of the thyristor vale. In case of a TSC, the effective capacitive reactance is varied in a step-wise manner by full or full conduction of the thyristor valve.

2.3.3 Series-Connected Controllers

These types of devices are connected in series with a transmission line, thereby, changing the effective transmission line reactance. This feature allows series-connected controllers to control the flow of power through the transmission line. Various forms of such devices include static synchronous series compensator (SSSC), thyristor controlled or switched series capacitor (TCSC/TSSC), and thyristor controlled or switched series inductor (TCSR/TSSR).
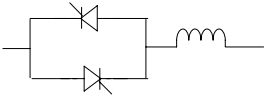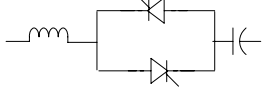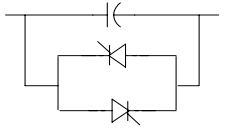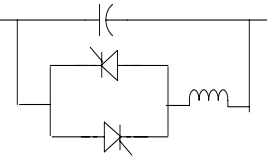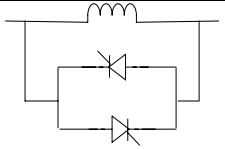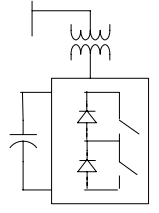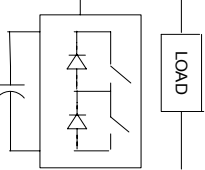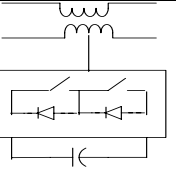
The output of SSSC is in quadrature with the line current, and is controlled independently of the line current. The SSSC decreases the overall reactive voltage drop

across the transmission line and controls flow of electric power. The SSSC may include transiently rated energy storage to compensate temporarily an additional real power component. The TCSC varies its effective capacitive reactance smoothly by firing angle control of the thyristor valve. Alternately, the effective capacitive reactance of a TSSC is varied in step-wise manner, by full or zero conduction of the thyristor vale. Similarly in case of a TCSR and TSSR, the effective reactance is varied smoothly and in a step-wise manner respectively.

Table 2.2 summarizes the above discussion on different types of controllers, their respective circuit schematic, system functions, and control principle [5]. The active front-end induction motor drive analyzed in this thesis work falls under the category of static synchronous compensator (STATCOM). From power quality point of view, it is basically a shunt-connected static VAR compensator which can control its output current (inductive/capacitive) independent of the ac system voltage variations or load. It needs a temporary energy storage element in the form of a dc-link capacitor to effectively supply the desired power compensation while driving the mechanical load connected to the induction motor.

After establishing different methods of compensation, it will be worthwhile to know exactly how much and which component of the source power needs to be compensated. In other words we need to establish the reference commands for the power controllers discussed above. The instantaneous power definitions presented in the next section explain how to choose compensation references.

Table 2.2: A summary of FACTS controllers' configurations

Controller	Circuit configuration	System functions	Control principle
TCR/TSC - Thyristor Controlled or Switched Reactor		• Regulate voltage • Improve stability	VAR control by varying L in the shunt connection
TCC/TSC – Thyristor Controlled or Switched Capacitor		• Regulate voltage & compensate VAR • Improve stability	VAR control by varying C in the shunt connection
TSSC – Thyristor Switched Series Capacitor		• Control power flow • Improve stability	Power and VAR control through varying C.
TCSR – Thyristor Controlled Series Capacitor		• Control power flow • Improve stability • Limit fault current	Power and VAR control through varying C & L in shunt connection
TCSR – Thyristor Controlled Series Reactor		• Limit fault current	Current control by inserting L in series.
STATCOM Static Synchronous Compensator		• Regulate voltage & compensate VAR • Improve stability	VAR control through current control in shunt connection
Active Filter (Shunt Connected)		• Harmonic current filtering	Inject canceling harmonic current into the source
SSSC – Static Series Synchronous Compensator		• Control power flow • Improve stability	VAR control through series voltage control.

2.4 Generating Reference Currents Using Instantaneous Power *p-q* Theory

For single-phase and three-phase power systems with sinusoidal voltages and sinusoidal currents, the quantities such as active power, reactive power, active current, reactive current, and power factor are based on the average concept [7]. For compensating the non-active currents, however, instantaneous power and current definitions are required. Akagi et al [8] have introduced an interesting theory of instantaneous power in three-phase circuits, without zero sequence currents. The theory is also popularly referred to as *p-q* theory. The concept establishes an effective method to compensate instantaneous components of active and reactive power of the three-phase system.

This work is widely regarded as a classical theoretical research and is one of the most cited references in the field of reactive power compensation and active filtering [2]. Since, it is also the basis for generating reference commands for active compensator presented in this thesis, the brief summary of the instantaneous power *p-q* theory is presented below. The three-phase, three-wire system is shown in Figure 2.1. The three-phase voltages and currents are transformed to *d-q* coordinates as shown below.

$$\begin{bmatrix} e_q \\ e_d \\ e_0 \end{bmatrix} = \sqrt{\frac{2}{3}} \cdot \begin{bmatrix} 1 & -1/2 & -1/2 \\ 0 & \sqrt{3}/2 & -\sqrt{3}/2 \\ 1/\sqrt{2} & 1/\sqrt{2} & 1/\sqrt{2} \end{bmatrix} \begin{bmatrix} e_a \\ e_b \\ e_c \end{bmatrix} \tag{2.3}$$

$$\begin{bmatrix} i_q \\ i_d \\ i_0 \end{bmatrix} = \sqrt{\frac{2}{3}} \cdot \begin{bmatrix} 1 & -1/2 & -1/2 \\ 0 & \sqrt{3}/2 & -\sqrt{3}/2 \\ 1/\sqrt{2} & 1/\sqrt{2} & 1/\sqrt{2} \end{bmatrix} \begin{bmatrix} i_a \\ i_b \\ i_c \end{bmatrix} \tag{2.4}$$
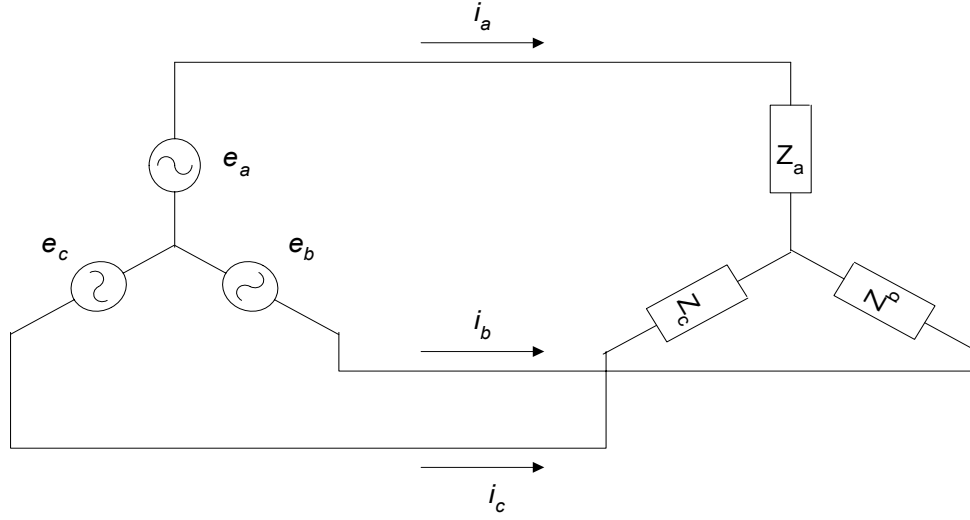
Figure 2.1 Three-phase three-wire system

For balanced voltages $e_1 + e_2 + e_3 = 0$. Thus e_0 equals to zero. For balanced currents, i_0 equals to zero as well.

The transformation matrix C_1 and its inverse matrix C_1^{-1} are defined as,

$$C_1 = \sqrt{\frac{2}{3}} \cdot \begin{bmatrix} 1 & -1/2 & -1/2 \\ 0 & \sqrt{3}/2 & -\sqrt{3}/2 \\ 1/\sqrt{2} & 1/\sqrt{2} & 1/\sqrt{2} \end{bmatrix}, \; C_1^{-1} = \sqrt{\frac{3}{2}} \cdot \begin{bmatrix} 2/3 & 0 & \sqrt{2}/3 \\ -1/3 & 1/\sqrt{3} & \sqrt{2}/3 \\ -1/3 & -1/\sqrt{3} & \sqrt{2}/3 \end{bmatrix}$$

Using the matrices C_1 and C_1^{-1} we can do following coordinate transformation

$$\begin{bmatrix} i_q \\ i_d \\ i_0 \end{bmatrix} = C \cdot \begin{bmatrix} i_a \\ i_b \\ i_c \end{bmatrix}, \; \begin{bmatrix} i_a \\ i_b \\ i_c \end{bmatrix} = C_1^{-1} \cdot \begin{bmatrix} i_q \\ i_d \\ i_0 \end{bmatrix}, \text{ and } \begin{bmatrix} e_a \\ e_b \\ e_c \end{bmatrix} = C_1^{-1} \cdot \begin{bmatrix} e_q \\ e_d \\ e_0 \end{bmatrix}$$

Note, C_1 and C_1^{-1} are orthogonal matrices, so that,

$$C_1^{\mathrm{T}} C_1 = C_1 C_1^{\mathrm{T}} = (C_1^{-1})^{\mathrm{T}} C_1^{-1} = C_1^{-1} (C_1^{-1})^{\mathrm{T}} = I \tag{2.5}$$

Where, I represent an identity matrix.

24

The instantaneous active power, p, in *a-b-c* coordinates is defined by,

$$p = e_a i_a + e_b i_b + e_c i_c = \begin{bmatrix} e_a & e_b & e_c \end{bmatrix} \cdot \begin{bmatrix} i_a \\ i_b \\ i_c \end{bmatrix} \tag{2.6}$$

Converting voltages and currents in *d-q* coordinates, we can write,

$$p = \begin{bmatrix} e_q & e_d & e_0 \end{bmatrix} \cdot \begin{bmatrix} i_q \\ i_d \\ i_0 \end{bmatrix}$$

$$p = e_q i_q + e_d i_d \tag{2.7}$$

In the similar way, an instantaneous reactive power q is defined as [9],

$$q = e_q i_d - e_d i_q \tag{2.8}$$

Note that, p, as shown in Equation 2.7 is an instantaneous active power, because it is defined as the sum of the product of the instantaneous voltage and instantaneous current in the same phase. So, p has dimension of Watt (W). On the contrary, the expression for q contains the product of instantaneous voltage in one phase and instantaneous current in another phase. Therefore, q cannot have dimension of W, instead, a new dimension called as "imaginary watt" will be used [2].

Combining Equation 2.7 and 2.8, we can write,

$$\begin{bmatrix} p \\ q \end{bmatrix} = \begin{bmatrix} e_q & e_d \\ -e_d & e_q \end{bmatrix} \cdot \begin{bmatrix} i_q \\ i_d \end{bmatrix}$$

Alternatively, currents in *d-q* coordinates can be expressed as:

$$\begin{bmatrix} i_q \\ i_d \end{bmatrix} = \begin{bmatrix} e_q & e_d \\ -e_d & e_q \end{bmatrix}^{-1} \cdot \begin{bmatrix} p \\ q \end{bmatrix} \tag{2.9}$$

Equation 2.9 can be rewritten as,

$$\begin{bmatrix} i_q \\ i_d \end{bmatrix} = \frac{1}{e_q^2 + e_d^2} \cdot \begin{bmatrix} e_q & -e_d \\ e_d & e_q \end{bmatrix} \cdot \begin{bmatrix} p \\ 0 \end{bmatrix} + \frac{1}{e_q^2 + e_d^2} \cdot \begin{bmatrix} e_q & -e_d \\ e_d & e_q \end{bmatrix} \cdot \begin{bmatrix} 0 \\ q \end{bmatrix}$$

$$\begin{bmatrix} i_q \\ i_d \end{bmatrix} = \begin{bmatrix} i_{q\_p} \\ i_{d\_p} \end{bmatrix} + \begin{bmatrix} i_{q\_q} \\ i_{d\_q} \end{bmatrix} \tag{2.10}$$

Where, the p and q components of q-axis and d-axis currents are given by,

$$i_{q\_p} = \frac{e_q \cdot p}{e_q^2 + e_d^2} \; ; \; i_{d\_p} = \frac{e_d \cdot p}{e_q^2 + e_d^2} \tag{2.11}$$

And

$$i_{q\_q} = \frac{-e_d \cdot q}{e_q^2 + e_d^2} \; ; \; i_{d\_q} = \frac{e_q \cdot q}{e_q^2 + e_d^2} \tag{2.12}$$

Next, the instantaneous <u>active power</u> in terms of q-axis power p_q, and d-axis power p_d, is given by,

$$p = e_q i_q + e_d i_d = p_q + p_d \tag{2.13}$$

$$\begin{bmatrix} p_q \\ p_d \end{bmatrix} = \begin{bmatrix} e_q i_q \\ e_d i_d \end{bmatrix} = \begin{bmatrix} e_q i_{q\_p} \\ e_d i_{d\_p} \end{bmatrix} + \begin{bmatrix} e_q i_{q\_q} \\ e_d i_{d\_q} \end{bmatrix} \tag{2.14}$$

The two components of instantaneous <u>active power</u> in Equation 2.14 are referred to as,

$$\begin{bmatrix} p_q \\ p_d \end{bmatrix} = \begin{bmatrix} p_{q\_p} \\ p_{d\_p} \end{bmatrix} + \begin{bmatrix} p_{q\_q} \\ p_{d\_q} \end{bmatrix} \tag{2.15}$$

Also note that,

$$p_{q\_p} + p_{d\_p} = e_q i_{q\_p} + e_d i_{d\_p} = e_q i_q + e_d i_d = p_L = p \tag{2.16}$$

$$p_{q\_q} + p_{d\_q} = e_q i_{q\_q} + e_d i_{d\_q} = 0 = p_R \tag{2.17}$$

As can be seen, p_L ($e_q i_q + e_d i_d$) is the net power delivered to the load while, p_R is the ripple power oscillating between source and load, such that net p_R is zero.

In similar fashion, we can also write instantaneous <u>reactive power</u> in *d-q* coordinates as,

$$q = e_q i_d - e_d i_q$$

$$\begin{bmatrix} q_q \\ q_d \end{bmatrix} = \begin{bmatrix} e_q i_d \\ -e_d i_q \end{bmatrix} = \begin{bmatrix} e_q i_{d\_p} \\ -e_d i_{q\_p} \end{bmatrix} + \begin{bmatrix} e_q i_{d\_q} \\ -e_d i_{q\_q} \end{bmatrix} \tag{2.18}$$

The two components of instantaneous <u>reactive power</u> in above equation are referred to as,

$$\begin{bmatrix} q_q \\ q_d \end{bmatrix} = \begin{bmatrix} q_{q\_p} \\ q_{d\_p} \end{bmatrix} + \begin{bmatrix} q_{q\_q} \\ q_{d\_q} \end{bmatrix} \tag{2.19}$$

Note here that,

$$q_{q\_p} + q_{d\_p} = e_q i_{d\_p} - e_d i_{q\_p} = 0 = q_R \tag{2.20}$$

$$q_{q\_q} + q_{d\_q} = e_q i_{d\_q} - e_d i_{q\_q} = q = q_L \tag{2.22}$$

Equations 2.15 through 2.17 and Equations 2.19 through 2.22 lead to the following interesting interpretations of instantaneous real and imaginary power [9].

- The instantaneous <u>active power</u> has two components, p_L and p_R. p_L is the active power delivered to the load. While, p_R is the ripple power which oscillates between source and load, such that average p_R is zero.

- Similarly, the instantaneous <u>reactive power</u> can be split in two components, q_L and q_R. q_L is the reactive power delivered to the load. While, q_R is the ripple power which oscillates between source and load, such that average q_R is zero.

- The *p-q* theory reveals exactly which components of real and reactive power flow

to the load and which oscillates between source and load. As required by the utility, the particular power/current components can be compensated.

- Thus a shunt active compensator **without energy-storage element** can be used to compensate a ripple component of reactive power, which is flowing to-and-from between source and load.

- On the other hand, the ripple component of the active power, which is the result of harmonic currents, can be compensated by a shunt active filter **with energy-storage element**.

The *p-q* theory, however, does not take into account zero-sequence currents. A generalized theory of instantaneous active and reactive power proposed by Peng et al [10] define instantaneous real and reactive power for all scenarios such as, sinusoidal or non-sinusoidal, and balanced or unbalanced three-phase systems, with or without zero-sequence currents and/or voltages.

Based on above generalized power definitions, reactive power compensation references are generated for the active front-end drive simulations presented in this thesis.

2.5 Comparison between Traditional Drives and Active Front-End Drives

The discussion so far in this chapter leads us to a couple of interesting scenarios. First, the presence of non-linear loads in a power system has been significantly increased, and because of their ability to control electric power precisely and efficiently, the widespread use of power electronics converters is indispensable. Secondly, utilities are

increasing concern about the non-linear currents in power system, resulting into stricter harmonic and power quality standards. This situation calls for alternative solutions in the form of various compensation techniques. Depending on the compensation objective, different topologies as discussed in section 2.3 can be used.

For large variable speed drives such as those used in mining excavators, the huge influx of non-linear currents, seriously affect the power quality at the point of common coupling. To ensure power grid compatibility, a reactive compensator such as a capacitor bank or a STATCOM device is required for such installations. Alternatively, an induction motor drive with an active front-end can be used. It can achieve powerful dynamic performance, while providing exceptional compatibility with the line in terms of power factor and total harmonic distortion. Figure 2.2 shows the two schemes.
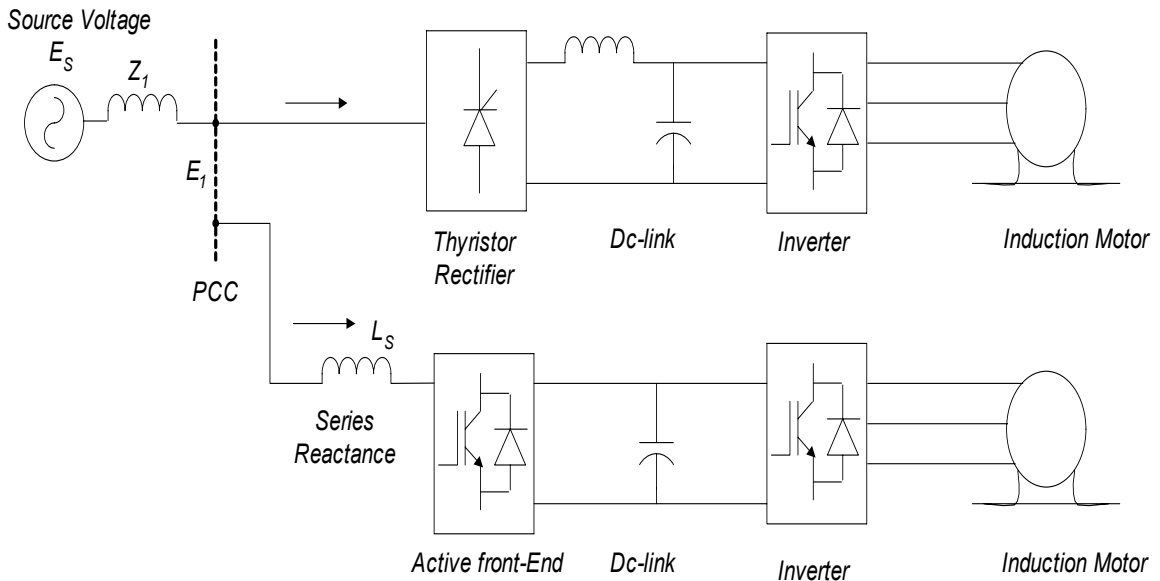
Figure 2.2 Comparison between phase-controlled and active front-end rectifiers

2.5.1 Traditional Interface with the Power Grid

As can be seen in Figure 2.2 a rectifier consists of a standard phase-controlled thyristor. The drive typically operates near its full load at all the time. The line-side rectifier controls need to provide a stable dc-link voltage under all line and load conditions or drive performance may suffer.

Maintaining a stable dc-link voltage in the presence of wide power swings is difficult for phase-controlled thyristors because of the poor power factor to the line. Thus, when the distribution system voltage is weak, the voltage available for rectification is also reduced resulting in poor time response. The poor power factor and limited time response of phase-controlled rectifiers require a large amount of capacitance in the dc-link to minimize the voltage fluctuations seen by the inverter [11].

2.5.2 Improved Power Grid Interface with Active Front-End Inverter

The use of high power IGBTs in active front-end inverter (AFE) topology as shown in Figure 2.2 eliminates the shortcomings of traditional rectifier front ends. The active front end boosts the line voltage to a dc-link voltage higher than normally produced with a diode bridge. It takes an advantage of the network's inherent reactance to increase dc-link voltage greater than the peak of the line-to-line supply voltage. The line reactance is a disadvantage in a phase-controlled rectifier resulting in voltage notching.

The system can be designed to operate with sufficient control margins so that the desired dc-link voltage can be maintained, even in the presence of large dips in the

incoming line voltage. The current flow between the line and the active rectifier is directly dependent on the voltage difference between line voltage and PWM voltage generated by the active rectifier. This voltage difference is applied across the line reactance. Adjusting the magnitude and phase of this voltage gives the active rectifier continuous control over the current amplitude and phase in all four quadrants of operation.

The controller regulates the dc-link voltage by maintaining the balance of active power supplied by the rectifier and the active power required by the inverter/load. At the same time, the controller can independently control flow of reactive power allowing unity power factor at the primary of the transformer or at any other given point in the network, like the point of common coupling that feeds the rectifier. This helps in improving the voltage regulations and overall efficiency.

However, there is a limit on the amount of power that can be transferred to or from the grid. The voltage ratio between the line voltage peak and dc-link voltage imposes this limit [11]. Additionally, the current rating of active front-end rectifier imposes constraints on both the active and reactive power to be transferred to and from the power grid. To find out the limits, first the system model is required which is presented in Chapter 3.

2.6   Chapter Summary

In this chapter, a background material on reactive power compensation and power electronics controllers used in utility applications was presented. Power quality standards and IEEE guidelines on harmonic distortion were also discussed.

A brief review of FACTS devices, their respective circuit configuration, system function and operating principle was presented. Further, the instantaneous active and reactive power theory was discussed. The power definitions provided by *p-q* theory are the basis of compensation commands generated for the active drive. The benefits of using active drive were discussed by comparing it with traditional drive with phase-controlled rectifiers. In the next chapter the mathematical model for active drive is derived. Based on this mathematical model, a control approach is formulated in Chapter 4.

3 System Modeling

3.1 Chapter Overview

In the previous chapter, the need for compensating non-active currents and a detailed review of the compensation methods using power electronic devices were discussed. The theoretical background on instantaneous power definitions was also presented. In this chapter, a dynamic *d-q* model, needed for faster transient response of an active front end converter will be derived. Later in this chapter, the power loss model to estimate the total heat dissipation in a front-end rectifier will be introduced.

In Section 3.2, the system configuration for using active drive as a shunt compensator will be presented. The compensation characteristics and the steady-state controllability of an active drive will be discussed here. Section 3.3 will introduce the *d-q* theory of transforming three-phase parameters to equivalent two-phase rotating coordinate system. In Section 3.4 the *d-q* theory will be applied to the system differential equations to derive the dynamic *d-q* model. To provide desired reactive power compensation, the active and reactive power measurements in *d-q* coordinates are required. These power definitions will be presented in Section 3.5.

In Section 3.6 the power loss model to estimate conduction and switching losses in IGBTs and anti-parallel diodes used in the front-end rectifier will be presented. The total heat dissipation estimated using the power loss model can be used in designing an appropriate thermal system.

3.2   System Configuration

Consider a simplified power system shown in Figure 3.1. It is assumed that the system voltage E_S is purely sinusoidal. E_1 and E_2 are the intermediate line voltages which are not sinusoidal, but are distorted at varying degrees. V_{pwm} is the voltage generated by the active front-end converter, while Z_1 and Z_2 are transmission line impedances. L_S is the series reactance of an active drive used for boost operation.

The non-linear load, shown in figure, draws currents with active and non-active components. If the non-active currents are not compensated, it will result in source voltage distortion. The role of an active front-end converter, in this situation, is to supply the non-active currents needed to keep total harmonic distortion (THD) at the desired level. At the same time, the converter must draw real current to feed its own load which is induction motor.
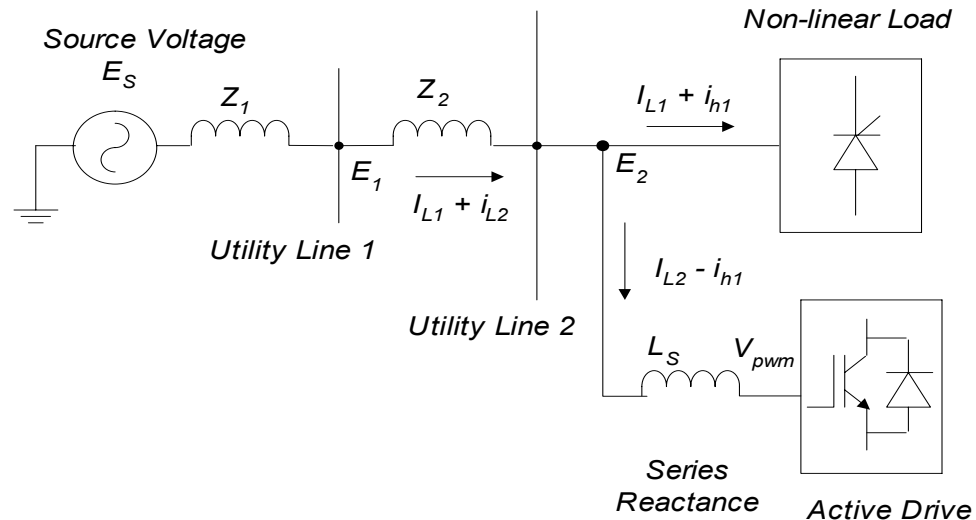
Figure 3.1 A simplified power system

34

The fundamental real current drawn by the active drive depends on the application. In applications like mine hoists, the drive draws the real power from utility to feed the continuously varying mine load. In other applications such as, an induction motor connected to an external energy source like a wind powered generator or a micro-turbine, the inverter may feed net real power back into the network.

3.2.1 Compensation Characteristics of an Active Drive

As illustrated in Figure 3.1, the active front-end converter represents a shunt-connected synchronous voltage source (STATCOM), previously described in Chapter 2. The active drive can be viewed as a shunt compensator with an energy storage element in the form of a dc-link capacitor. Due to energy storage capability, the active drive has several beneficial features, which are used to maintain desired power grid compatibility. These features are listed below.

- The maximum attainable compensating current of an active drive is limited only by the current ratings of the active switches and by the chosen ratio of peak line voltage to dc-link voltage. The active drive can maintain the maximum VAR compensation and the desired dc-link voltage, even in the presence of large dips in the incoming line voltage [11].

- The active front-end converter can be operated over its full current range even at the low line voltage levels. Sometime line voltages as low as 20% of the rated can also be tolerated.

- Operation over full current range help increase the stability margin in case of a fault, and thus improves overall transient stability.

- The response time of an active front-end converter for compensation purposes can be as fast as a fraction of a half cycle ($\sim$ 10ms) [12]. For thyristor controlled reactors, the dynamic response can be as slow as 5 to 6 cycles. Later in Chapter 5, the compensator response to the step input is plotted to illustrate this.

- The decoupled control strategy allows the compensator to exchange reactive as well as real power to and from the ac system. The two power exchanges are mutually exclusive.

- Due to real power exchange capability, the compensator can be used for power oscillation damping.

3.2.2 Steady-State Control

The steady state characteristics as well as differential equations describing the dynamics of the front-end rectifier can be obtained independent of an inverter and motor load. This is because the dc-link voltage can be viewed as a voltage source, if V_{dc} is maintained constant for the full operating range. The inverter is thus connected to the voltage source, whose terminal voltage V_{dc}, remains unaffected by any normal inverter-motor operation.

Furthermore, as shown in Figure 3.2, the rectifier can also be viewed as connected to the voltage source V_{dc}. Thus, the rectifier is able to control magnitude and phase of PWM voltages V_{abc} irrespective of line voltages E_{123}.
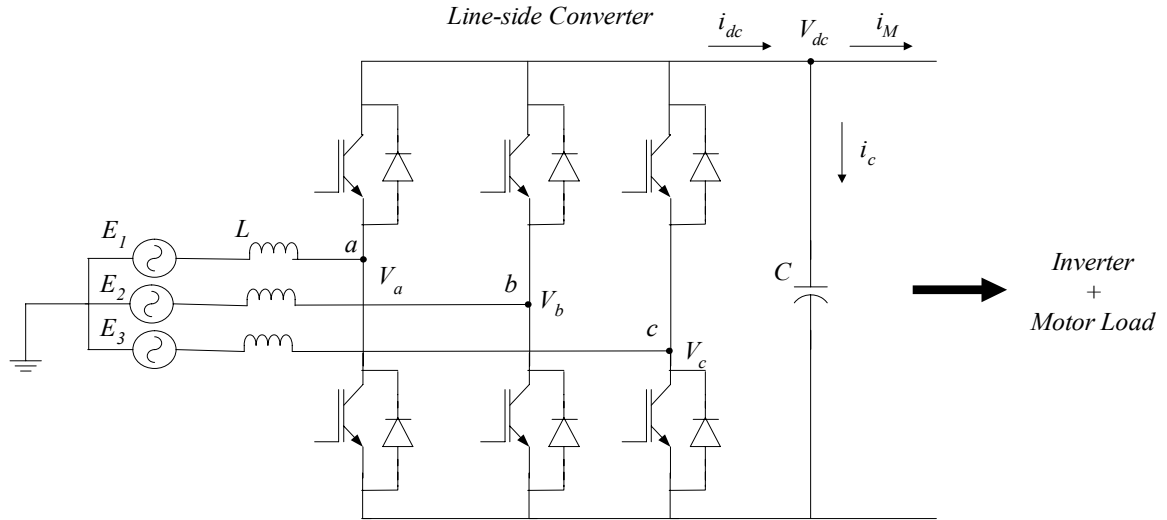
Figure3.2 A voltage source rectifier

The system is an exact replica of the inverter-motor system. The PWM voltages, V_{abc}, are now excitation voltages similar to the motor terminal voltages. The source voltages E_{123} can be compared to the motor counter emf voltages. Whereas, line inductance is similar to the motor leakage reactance!

During steady state, the system operation can be described using the phasor diagram shown in Figure 3.3. As explained earlier in Chapter 1, the real and reactive power are represented by,

$$P = 3E_S \cdot \frac{V \sin \delta}{\omega L} \tag{3.1}$$

$$Q = 3E_S \cdot \frac{V \cos \delta - E_S}{\omega L} \tag{3.2}$$

Equations 3.1 and 3.2 suggest that an active rectifier can generate a desired, fixed valued reactive power while supplying the variable real power demanded by the motor.
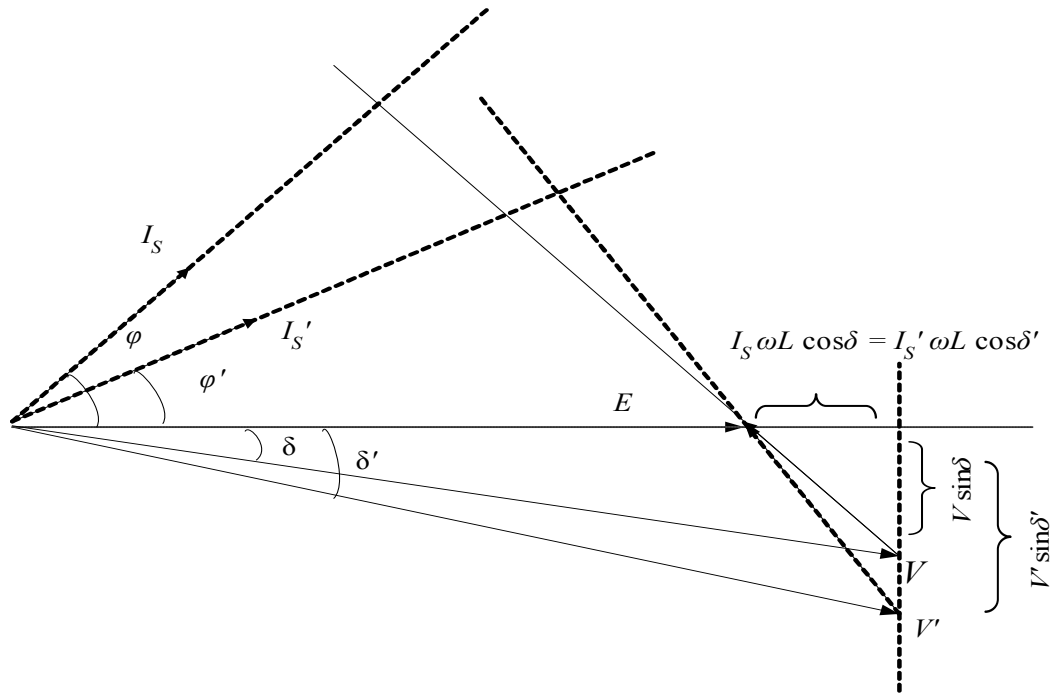
Figure 3.3 Steady-state control of PWM rectifier

As shown in Figure 3.3, this can be done by keeping "$V\cos\delta$" constant and varying "$V\sin\delta$". Thus by controlling the magnitude and phase rectifier voltage V, the steady state control of active and reactive power is possible. However, the equations fail to explain simultaneous control over real and reactive power, which is required for a dynamic operation of an active drive.

Secondly, an important prerequisite for an active drive operation is a constant dc-link voltage, V_{dc}. A variable dc-link will introduce undesirable fluctuations in the magnitude and phase of PWM voltages generated by the rectifier. It will cause the active and reactive currents drawn by the rectifier to vary from the desired values. This will further introduce additional noise in the dc-link voltage, since these line currents charge and discharge the dc capacitor. To solve this non-linearity and at the same time achieve

fast dynamic response, an effective control scheme is needed.

The voltage source rectifier connected to the utility can be effectively controlled using the field oriented approach, same as used for controlling the voltage source inverter feeding an induction motor [13]. The rotating reference frame *d-q* theory is first used to obtain a dynamic *d-q* model of a line side converter. The dynamic *d-q* model is then used to implement field oriented control. The *d-q* theory is introduced in the next section.

3.3   The *d-q* Theory

A system of three-phase, sinusoidal, time-varying voltages can be represented by an equivalent two-phase system. Consider a balanced, three-phase, Y-connected voltages, E_1, E_2, E_3, which are 120 electrical degrees apart. Consider a stationary, two- axis coordinate system, where the *q*-axis is aligned with E_1, and *d*-axis is orthogonal to the *q*-axis. The three-phase voltages have component on both the *q* and *d* axes. The *q* and *d* axis components can be expressed as,

$$E_{qs} = E_1 - E_2 \cos 60 - E_3 \cos 60 = E_1 - \frac{E_2}{2} - \frac{E_3}{2} \tag{3.3}$$

$$E_{ds} = 0 + E_2 \cos 30 - E_3 \cos 30 = E_2 \sqrt{\frac{3}{2}} - E_3 \sqrt{\frac{3}{2}} \tag{3.4}$$

In matrix form,

$$\begin{bmatrix} E_{qs} \\ E_{ds} \\ E_{0s} \end{bmatrix} = \begin{bmatrix} 1 & -1/2 & -1/2 \\ 0 & \sqrt{3}/2 & -\sqrt{3}/2 \\ 1/\sqrt{2} & 1/\sqrt{2} & 1/\sqrt{2} \end{bmatrix} \begin{bmatrix} E_1 \\ E_2 \\ E_3 \end{bmatrix} \tag{3.5}$$

However, in order that the two coordinate systems are equivalent, the instantaneous power in both the coordinate systems should be equal.

$$P_{dq} = P_{123} \tag{3.6}$$

where P_{123} is power in three-phase circuit, and P_{dq} is power in equivalent two-phase system. To meet this requirement, the transformation matrix needs to be multiplied by a factor of $\sqrt{2/3}$.

The new transformation matrix, C_1, is,

$$C_1 = \sqrt{\frac{2}{3}} \cdot \begin{bmatrix} 1 & -1/2 & -1/2 \\ 0 & \sqrt{3}/2 & -\sqrt{3}/2 \\ 1/\sqrt{2} & 1/\sqrt{2} & 1/\sqrt{2} \end{bmatrix}, \; C_1^{-1} = \sqrt{\frac{3}{2}} \cdot \begin{bmatrix} 2/3 & 0 & \sqrt{2}/3 \\ -1/3 & 1/\sqrt{3} & \sqrt{2}/3 \\ -1/3 & -1/\sqrt{3} & \sqrt{2}/3 \end{bmatrix} \tag{3.7}$$

The Equation 3.5 is rewritten as,

$$\begin{bmatrix} E_{qs} \\ E_{ds} \\ E_{0s} \end{bmatrix} = \sqrt{\frac{2}{3}} \cdot \begin{bmatrix} 1 & -1/2 & -1/2 \\ 0 & \sqrt{3}/2 & -\sqrt{3}/2 \\ 1/\sqrt{2} & 1/\sqrt{2} & 1/\sqrt{2} \end{bmatrix} \begin{bmatrix} E_1 \\ E_2 \\ E_3 \end{bmatrix} \tag{3.8}$$

Note that parameters E_{qs}, E_{ds} in two-phase stationary reference frame are still time-varying. Because most of the electric circuits are associated with inductances, the time varying parameters such as sinusoidal currents and voltages tends to make the system model complex, and system response is often sluggish.

R. H. Park proposed in 1920 [1] to transform these variables to a fictitious reference frame rotating at some angular speed. If this speed of rotation is the same as the angular frequency of time-varying parameters, then all the parameters in this reference frame become time invariant or dc quantities. Because the effect of inductances associated with varying currents and voltages is removed, the system model is relatively simple and system response can be sufficiently fast.

Figure 3.4 and 3.5 illustrate Park's transformation.
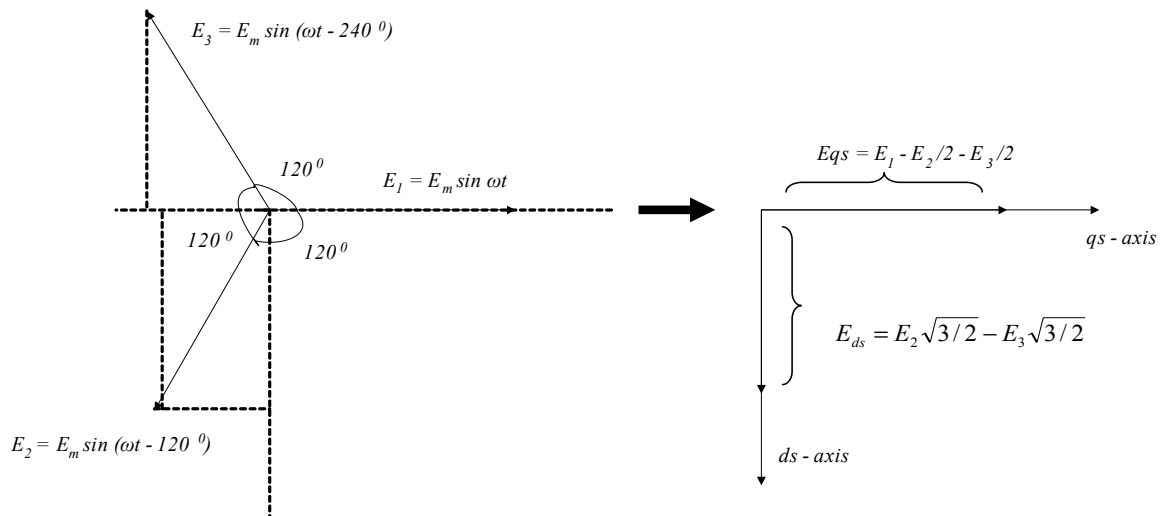
Figure 3.4 Three-phase to two-phase transformation
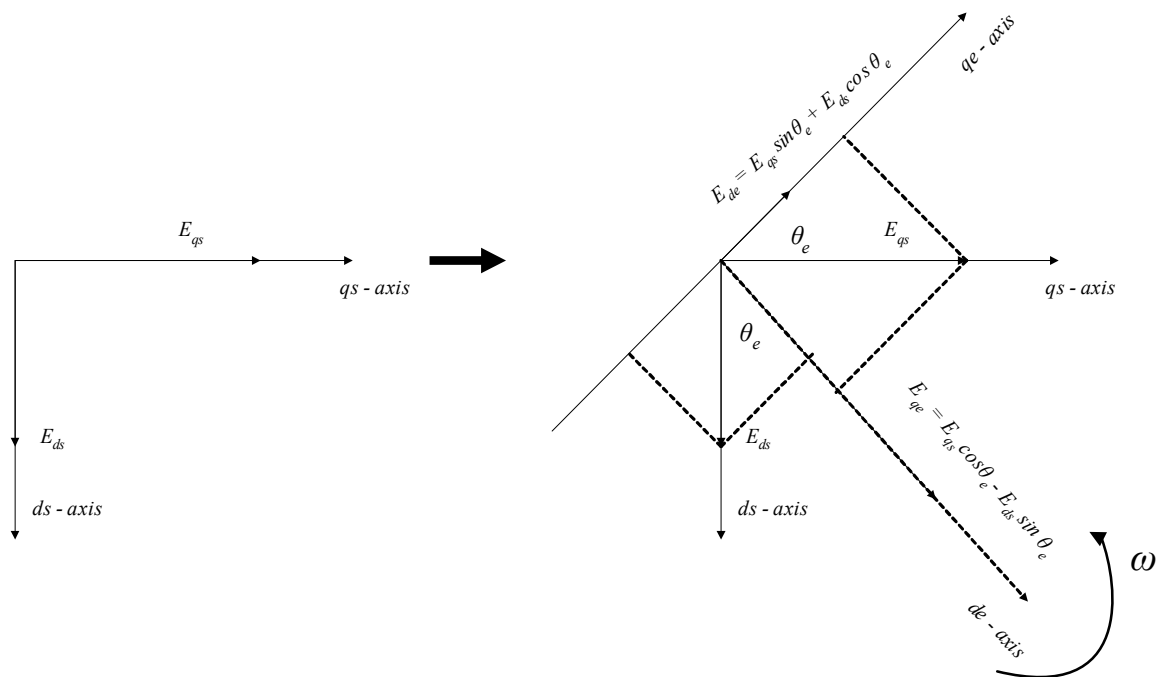
Figure 3.5 Stationary to rotary reference frame, Park's transformation

The orthogonal axes *de* and *qe* are rotating at an angular speed of ω_e. The θ_e is the angular displacement such that,

$$\omega_e = \frac{d\theta_e}{dt} \tag{3.9}$$

The new variables in *de-qe* reference frame are,

$$\begin{bmatrix} E_{qe} \\ E_{de} \end{bmatrix} = \begin{bmatrix} \cos\theta_e & -\sin\theta_e \\ \sin\theta_e & \cos\theta_e \end{bmatrix} \begin{bmatrix} E_{qs} \\ E_{ds} \end{bmatrix} \tag{3.10}$$

The Park's transformation matrix is referred to as C_2,

$$C_2 = \begin{bmatrix} \cos\theta_e & -\sin\theta_e \\ \sin\theta_e & \cos\theta_e \end{bmatrix} ; \quad C_2^{-1} = \begin{bmatrix} \cos\theta_e & \sin\theta_e \\ -\sin\theta_e & \cos\theta_e \end{bmatrix} \tag{3.11}$$

Note that, both the matrices C_1 and C_2 are orthogonal matrices such that,

$$C_1^T C_1 = C_1 C_1^T = I \text{ and } C_2^T C_2 = C_2 C_2^T = I \tag{3.12}$$

where *I* represents an identity matrix.

3.4   Dynamic *d-q* Model

Figure 3.6 shows source voltages E_1, E_2, E_3 as line-to-neutral voltages for each of the three phases. The phase voltages and line currents i_1, i_2, and i_3 are given by,

$$E_1 = E_m \sin\omega t ; \qquad\qquad i_1 = i_m \sin(\omega t + \varphi)$$

$$E_2 = E_m \sin(\omega t - 120); \qquad\qquad i_2 = i_m \sin(\omega t - 120 + \varphi) \tag{3.13}$$

$$E_3 = E_m \sin(\omega t - 240); \qquad\qquad i_3 = i_m \sin(\omega t - 240 + \varphi)$$

The currents lead the source voltages by angle φ. E_m is the maximum line-to-neutral voltage, while i_m is the peak line current.
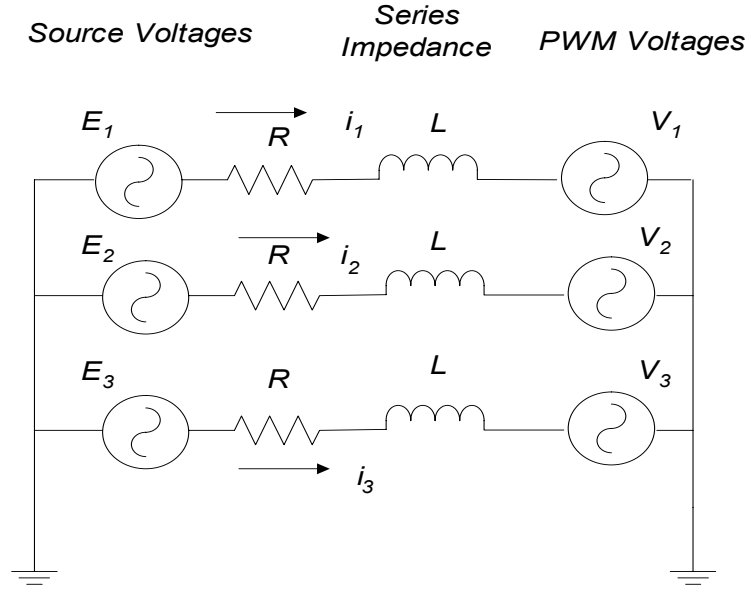
Figure 3.6 Circuit representation of system mathematical model

3.4.1 Deriving the *d-q* Model

The dynamic equations for each phase can be written as,

$$E_1 = L \cdot \frac{di_1}{dt} + R \cdot i_1 + V_{ao}$$

$$E_2 = L \cdot \frac{di_2}{dt} + R \cdot i_2 + V_{bo} \qquad (3.14)$$

$$E_3 = L \cdot \frac{di_3}{dt} + R \cdot i_3 + V_{co}$$

In matrix form, Equation 3.14 can be written as,

$$\begin{bmatrix} E_1 \\ E_2 \\ E_3 \end{bmatrix} = L \frac{d}{dt} \begin{bmatrix} i_1 \\ i_2 \\ i_3 \end{bmatrix} + R \begin{bmatrix} i_1 \\ i_2 \\ i_3 \end{bmatrix} + \begin{bmatrix} V_{ao} \\ V_{bo} \\ V_{co} \end{bmatrix} \qquad (3.15)$$

Using transformation matrix C_1, we can write,

$$\begin{bmatrix} i_{qs} \\ i_{ds} \\ i_{0s} \end{bmatrix} = C_1 \begin{bmatrix} i_1 \\ i_2 \\ i_3 \end{bmatrix}, \text{ and } \begin{bmatrix} E_{qs} \\ E_{ds} \\ E_{0s} \end{bmatrix} = C_1 \begin{bmatrix} E_1 \\ E_2 \\ E_3 \end{bmatrix}, \text{ and } \begin{bmatrix} V_{qs} \\ V_{ds} \\ V_{0s} \end{bmatrix} = C_1 \begin{bmatrix} V_{ao} \\ V_{bo} \\ V_{co} \end{bmatrix} \tag{3.16}$$

Pre-multiplying Equation 3.15 by C_1,

$$C_1 \begin{bmatrix} E_1 \\ E_2 \\ E_3 \end{bmatrix} = L \frac{d}{dt} (C_1 \begin{bmatrix} i_1 \\ i_2 \\ i_3 \end{bmatrix}) + RC_1 \begin{bmatrix} i_1 \\ i_2 \\ i_3 \end{bmatrix} + C_1 \begin{bmatrix} V_{ao} \\ V_{bo} \\ V_{co} \end{bmatrix},$$

Since C_1 is a constant, it can be taken inside the derivative term.

$$\begin{bmatrix} E_{qs} \\ E_{ds} \end{bmatrix} = L \frac{d}{dt} \begin{bmatrix} i_{qs} \\ i_{ds} \end{bmatrix} + R \begin{bmatrix} i_{qs} \\ i_{ds} \end{bmatrix} + \begin{bmatrix} V_{qs} \\ V_{ds} \end{bmatrix} \tag{3.17}$$

Equation 3.17 represents dynamic model in stationary reference frame.

Using second transformation matrix, C_2, we can write,

$$\begin{bmatrix} i_{qe} \\ i_{de} \end{bmatrix} = C_2 \begin{bmatrix} i_{qs} \\ i_{ds} \end{bmatrix}, \text{ and } \begin{bmatrix} i_{qs} \\ i_{ds} \end{bmatrix} = C_2^{-1} \begin{bmatrix} i_{qe} \\ i_{de} \end{bmatrix} \tag{3.18}$$

Pre-multiplying Equation 3.17 by C_2 and using Equation 3.18,

$$C_2 \begin{bmatrix} E_{qs} \\ E_{ds} \end{bmatrix} = LC_2 \frac{d}{dt} (C_2^{-1} \begin{bmatrix} i_{qe} \\ i_{de} \end{bmatrix}) + RC_2 \begin{bmatrix} i_{qs} \\ i_{ds} \end{bmatrix} + C_2 \begin{bmatrix} V_{qs} \\ V_{ds} \end{bmatrix}$$

$$\begin{bmatrix} E_{qe} \\ E_{de} \end{bmatrix} = LC_2 \left\{ \frac{d}{dt} (C_2^{-1}) \right\} \begin{bmatrix} i_{qe} \\ i_{de} \end{bmatrix} + LC_2 C_2^{-1} \frac{d}{dt} \left\{ \begin{bmatrix} i_{qs} \\ i_{ds} \end{bmatrix} \right\} + R \begin{bmatrix} i_{qe} \\ i_{de} \end{bmatrix} + \begin{bmatrix} V_{qe} \\ V_{de} \end{bmatrix}$$

Putting the value of C_2, and differentiating with respect to time,

$$\begin{bmatrix} E_{qe} \\ E_{de} \end{bmatrix} = L \begin{bmatrix} \cos\theta_e & -\sin\theta_e \\ \sin\theta_e & \cos\theta_e \end{bmatrix} \left\{ \frac{d}{dt} \begin{bmatrix} \cos\theta_e & \sin\theta_e \\ -\sin\theta_e & \cos\theta_e \end{bmatrix} \right\} \begin{bmatrix} i_{qe} \\ i_{de} \end{bmatrix} + L \cdot I \frac{d}{dt} \begin{bmatrix} i_{qe} \\ i_{de} \end{bmatrix} + R \begin{bmatrix} i_{qe} \\ i_{de} \end{bmatrix} + \begin{bmatrix} V_{qe} \\ V_{de} \end{bmatrix}$$

44

$$\begin{bmatrix} E_{qe} \\ E_{de} \end{bmatrix} = L \begin{bmatrix} \cos\theta_e & -\sin\theta_e \\ \sin\theta_e & \cos\theta_e \end{bmatrix} \begin{bmatrix} -\omega\sin\theta_e & \omega\cos\theta_e \\ -\omega\cos\theta_e & -\omega\sin\theta_e \end{bmatrix} \begin{bmatrix} i_{qe} \\ i_{de} \end{bmatrix} + L \frac{d}{dt} \begin{bmatrix} i_{qe} \\ i_{de} \end{bmatrix} + R \begin{bmatrix} i_{qe} \\ i_{de} \end{bmatrix} + \begin{bmatrix} V_{qe} \\ V_{de} \end{bmatrix}$$

$$\begin{bmatrix} E_{qe} \\ E_{de} \end{bmatrix} = \omega L \begin{bmatrix} 0 & 1 \\ -1 & 0 \end{bmatrix} \begin{bmatrix} i_{qe} \\ i_{de} \end{bmatrix} + L \frac{d}{dt} \begin{bmatrix} i_{qe} \\ i_{de} \end{bmatrix} + R \begin{bmatrix} i_{qe} \\ i_{de} \end{bmatrix} + \begin{bmatrix} V_{qe} \\ V_{de} \end{bmatrix} \tag{3.19}$$

where $\omega = d\theta_e/dt$. Expanding Equation 3.19,

$$E_{qe} = L \frac{di_{qe}}{dt} + \omega L i_{de} + R i_{qe} + V_{qe} \tag{3.20}$$

$$E_{de} = L \frac{di_{de}}{dt} - \omega L i_{qe} + R i_{de} + V_{de} \tag{3.21}$$

Equations 3.20 and 3.21 represent the dynamic *d-q* model of an active front end inverter in a reference frame rotating at an angular speed of ω. In this model ω, i_{qe}, i_{de} E_{qe}, and E_{de} are state variables while V_{qe} and V_{de} are the inputs.

Note that although the i_{qe} and i_{de} components of line currents are orthogonal to each other, they are not perfectly decoupled. The dynamics of i_{qe} and i_{de} interfere with each other. Based on this dynamic model an effective method of control, one in which the two current components are decoupled is proposed in Chapter 4.

3.4.2 Selecting the Rotating Coordinate System

A better insight into the dynamic behavior of the system is obtained by choosing a rotating system of coordinates, where the steady state oscillations disappear. For the dynamic model described in Equations 3.20 and 3.21, the pulse-width-modulated rectifier voltages serve as actuating voltages, while the line voltages assume the role similar to that of rotor induced voltages in induction motor [13]. The PWM voltages control the line

current so that desired power factor with respect to the line voltages can be achieved. A suitable choice of coordinate system in this case is the one defined by the line voltages.

A moving coordinate frame formed by the sinusoidal line voltages is shown in Figure 3.7. The two-phase voltages are represented by,

$$E_{qe} = E_{qs} \cos\theta_e - E_{ds} \sin\theta_e$$

$$E_{de} = E_{qs} \sin\theta_e + E_{ds} \cos\theta_e$$

E_{qe} and E_{de} are the projections of the E_{qs} and E_{ds} components on q and d axis respectively.

The angular speed of rotation of the moving coordinates, ω, is given by,

$$\omega = \frac{d\theta_e}{dt}$$

As illustrated in Figure 3.7, select θ_e such that, $E_{qe} = 0$. The E_{qs} and E_{ds} components of source voltage thus form a right angle triangle so as to give,

$$\tan\theta_e = \frac{E_{qs}}{E_{ds}}.$$

This choice helps to track θ_e by expressing θ_e in terms of E_{qs} and E_{ds} as below,

$$\cos\theta_e = \frac{E_{ds}}{\sqrt{E_{qs}^2 + E_{ds}^2}}, \text{ and } \sin\theta_e = \frac{E_{qs}}{\sqrt{E_{qs}^2 + E_{ds}^2}}$$

$\sin\theta_e$ and $\cos\theta_e$ are used to rotate parameters at an angular speed of $\omega = \frac{d\theta_e}{dt}$.

Since θ_e is the angular displacement of the source voltages, the above approach ensures correct tracking of supply frequency even if it is varying and not constant.
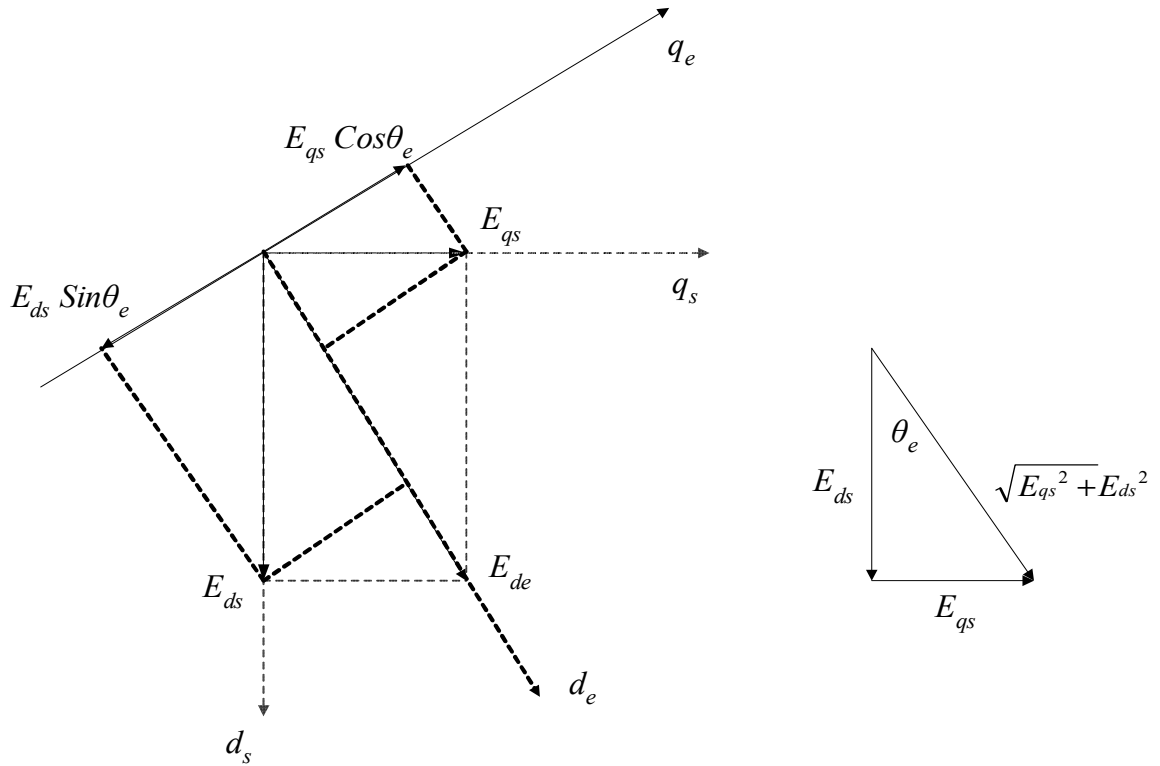
Figure 3.7 Tracking θ_e

3.5 Power Definitions in *d-q* Coordinate System

Using the system dynamic model established in previous sections, the control of line currents is carried out in a moving reference frame so that the feedback signals are dc quantities. This suggests that the current and/or power reference commands also need to be defined in a rotating reference frame. For this purpose the instantaneous active and reactive power in moving coordinate frame are defined below.

Refereeing to the generalized instantaneous power theory [10], the instantaneous active power P in three-phase coordinates is defined by,

$$P = E_1 i_1 + E_2 i_2 + E_3 i_3$$

where E_1, E_2, E_3 are the source phase-to-neutral voltages, and i_1, i_2, i_3 are the line currents.

In matrix form we can write,

$$P = \begin{bmatrix} E_1 & E_2 & E_3 \end{bmatrix} \cdot \begin{bmatrix} i_1 \\ i_2 \\ i_3 \end{bmatrix}$$

Converting the parameters to two-phase moving coordinates using transformation matrices C_1 and C_2,

$$P = \left\{ C_1^{-1} C_2^{-1} \begin{bmatrix} E_{qe} \\ E_{de} \end{bmatrix} \right\}^T \left\{ C_1^{-1} C_2^{-1} \begin{bmatrix} i_{qe} \\ i_{de} \end{bmatrix} \right\}$$

$$P = \begin{bmatrix} E_{qe} \\ E_{de} \end{bmatrix}^T (C_2^{-1})^T (C_1^{-1})^T C_1^{-1} C_2^{-1} \begin{bmatrix} i_{qe} \\ i_{de} \end{bmatrix}$$

Since C_1 and C_2 are orthogonal, $(C_1^{-1})^T C_1^{-1} = I$ and $(C_2^{-1})^T C_2^{-1} = I$

$$P = \begin{bmatrix} E_{qe} & E_{de} \end{bmatrix} \cdot \begin{bmatrix} i_{qe} \\ i_{de} \end{bmatrix} = E_{qe} \cdot i_{qe} + E_{de} \cdot i_{de}$$

As explained in previous section, E_{qe} is maintained equal to 0 at all the times, resulting in,

$$P = E_{de} \cdot i_{de} \tag{3.22}$$

In the same manner, according to the generalized instantaneous power theory [11], the reactive power in three-phase coordinates is given by,

$$Q = E_{123} \times i_{123} = \begin{bmatrix} Q_1 \\ Q_2 \\ Q_3 \end{bmatrix} = \begin{bmatrix} \begin{vmatrix} E_2 & E_3 \\ i_2 & i_3 \end{vmatrix} \\ \begin{vmatrix} E_3 & E_1 \\ i_3 & i_1 \end{vmatrix} \\ \begin{vmatrix} E_1 & E_2 \\ i_1 & i_2 \end{vmatrix} \end{bmatrix}$$

$$Q_{123} = (C_1^{-1} E_{dqs}) \times (C_1^{-1} i_{dqs}) = C_1^{-1} (E_{dqs} \times i_{dqs})$$

$$Q_{dqs} = (E_{dqs} \times i_{dqs}) = E_{qs} i_{ds} - E_{ds} i_{qs}$$

This is an expression for reactive power in two-phase stationary frame for a balanced three phase system. In d-q moving coordinates, the expression is given by,

$$Q_{dqe} = E_{qe} i_{de} - E_{de} i_{qe}$$

Recall that E_{qe} is always maintained to zero value.

$$Q_{dqe} = -E_{de} i_{qe} \tag{3.23}$$

Equation 3.23 shows that for a positive i_{qe}, Q_{dqe} is negative, implying that the active rectifier is feeding the reactive power back to the source. Alternatively for a negative i_{qe}, the Q_{dqe} is positive, resulting in net inflow of reactive power from source to the load.

3.6 Active Rectifier Power Loss Modeling

The control scheme based on the dynamic model presented in the previous section is used to determine the current and voltage ratings of an active rectifier for a given motor load and compensation requirements. Further, to analyze the system performance an

effective loss model of an active rectifier is necessary. The loss model will help estimate power loss, evaluate the efficiency, and do thermal analysis.

The heat generated as a result of power loss must be conducted away from the power chips and into the environment using a heatsink. If an appropriate thermal management system is not used, the power devices will overheat which could result in failure [14]. The loss model can also be used for comparing the power loss vis-à-vis phase-controlled rectifier.

3.6.1 Estimating Power Loss

The first step in thermal design is the estimation of total power loss. In an active rectifier using IGBTs, the two most important sources of power dissipation are conduction losses and switching losses. Conduction losses are the losses that occur while the IGBT is on and conducting current. The total power dissipation during conduction is computed by multiplying the on-state saturation voltage by the on-state current. In PWM applications, the conduction loss should be multiplied by the duty factor to obtain the average power dissipated.

The switching loss is the power dissipated during the turn-on and turn-off switching transitions. The most accurate method of determining switching losses is to plot the I_c and V_{ce} waveforms during the switching transition. Multiply the waveforms point by point and get instantaneous power waveform. The area under the power waveform is the switching energy expressed in watt-seconds/pulse. In addition to the IGBT losses, the feedback diode conduction and switching losses also needs to be considered.

3.6.2 Conduction Loss Model

The switches used in simulation are ideal switches with no forward voltage drop and so no power loss is associated with them. But, the switches still carry the rated current. To estimate conduction losses in an IGBT, the device on-state saturation voltage is required along with the on-state current.

Once the IGBT is selected based on voltage and current ratings, the corresponding collector-emitter saturation voltage characteristics are used to calculate the conduction losses. Figure 3.8 shows collector-emitter saturation voltage versus collector current curve for a 1200 V, 100 A IGBT manufactured by POWEREX Inc. This curve is modeled in MATLAB using a 2nd order curve fitting technique. Given a current, the real time saturation voltage can be obtained from the curve. Thus accurate estimation of the conduction loss is possible [15].

The conduction losses in fast recovery diode are estimated in a similar manner by first finalizing the diode ratings. The diode forward characteristics shown in Figure 3.9 are then modeled in MATLAB. The diode current is measured and voltage drop across the diode for a given variable current can be estimated from the device forward characteristics. The conduction loss is obtained by multiplying current with the resulting voltage, and then averaged within one cycle.

The total conduction loss is given by,

$$P_C = P_{cond\_diode} + P_{cond\_IGBT} \tag{3.24}$$

where P_{cond_diode} and P_{cond_IGBT} are average conduction losses for fast recovery diode and IGBT respectively.

COLLECTOR-EMITTER SATURATION VOLTAGE CHARACTERISTICS (TYPICAL)

$V_{GE} = 15V$
$T_j = 25°C$
$T_j = 125°C$

X-axis: COLLECTOR-CURRENT, I_C, (AMPERES)
Y-axis: COLLECTOR-EMITTER SATURATION VOLTAGE, $V_{CE(sat)}$, (VOLTS)
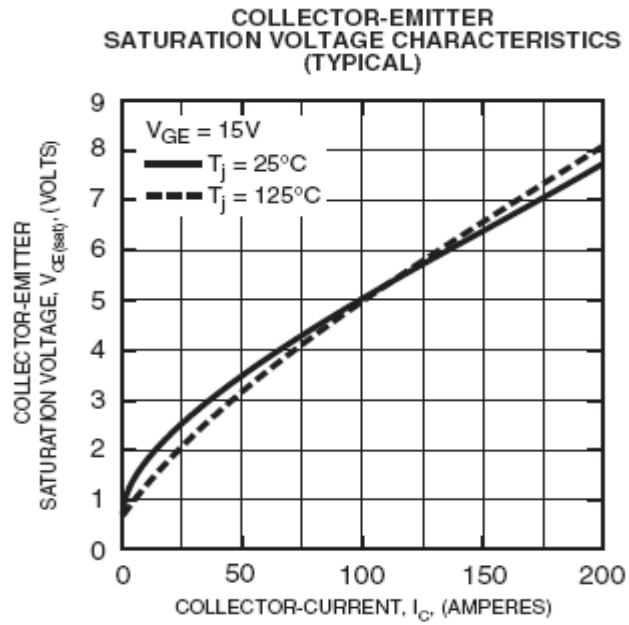
Figure 3.8 Saturation voltage characteristics for a 1200 V, 100 A IGBT

MAXIMUM ON-STATE CHARACTERISTICS

$T_j = 25°C$

X-axis: INSTANTANEOUS ON-STATE CURRENT, I_{FM}, (AMPERES)
Y-axis: INSTANTANEOUS ON-STATE VOLTAGE, V_{FM}, (VOLTS)
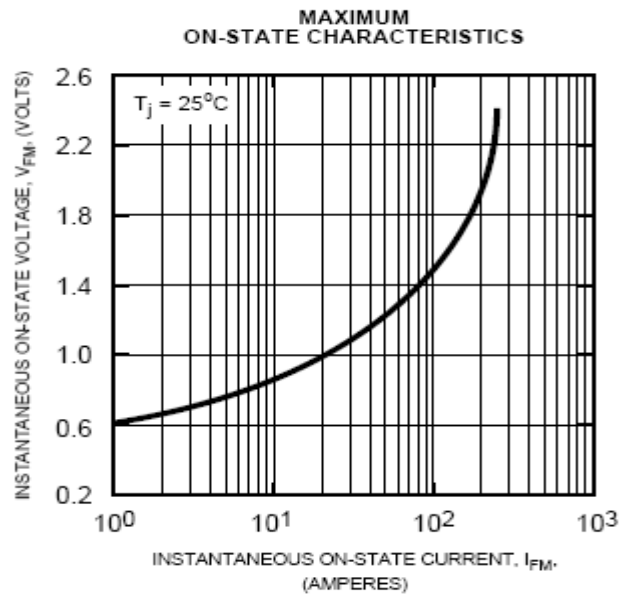
Figure 3.9 Forward voltage characteristics for a 1200 V, 100 A diode

52

3.6.3 Switching Loss Model

To estimate the total switching loss, IGBT switch-on and switch-off losses as well as diode reverse recovery losses are considered. However, as the switches used in the simulation are ideal, the turn-on and turn-off times are almost instantaneous. In this case, switching losses are calculated based on the amount of current to be turned on and off.

To calculate switching losses in an IGBT, the device switching loss versus collector current characteristics shown in Figure 3.10 are used. This curve is modeled in MTALAB using a 2nd order curve fitting technique. Further, the reverse recovery loss in a diode for a given collector current is calculated by [14],

$$P_{RR} = 0.25 * I_{RR} * t_{RR} * V_{CE(pk)} * f_{sw}$$ (3.25)

where I_{RR} is diode peak recovery current, t_{RR} is reverse recovery time; $V_{CE(pk)}$ is the peak voltage across diode at the recovery; and f_{sw} is the switching frequency. The values for I_{RR} and t_{RR} can be obtained from the reverse recovery curves shown in Figure 3.11.

The total switching losses are associated with circuit operating conditions. So, we cannot simply add the IGBT switching losses and diode recovery loss to get the total switching loss in the circuit. Consider that the IGBT is turned-on when the collector current is negative. This means the diode is freewheeling. There is no switching loss because the device is at zero potential. Now consider the switch-off operation. If the collector current is positive, there will be certain switching-off loss associated with the IGBT. However, if the collector current is negative, then anti-parallel diode is carrying the load current and not IGBT [15]. In this case the switching loss is basically the diode reverse recovery loss computed using Equation 3.25.
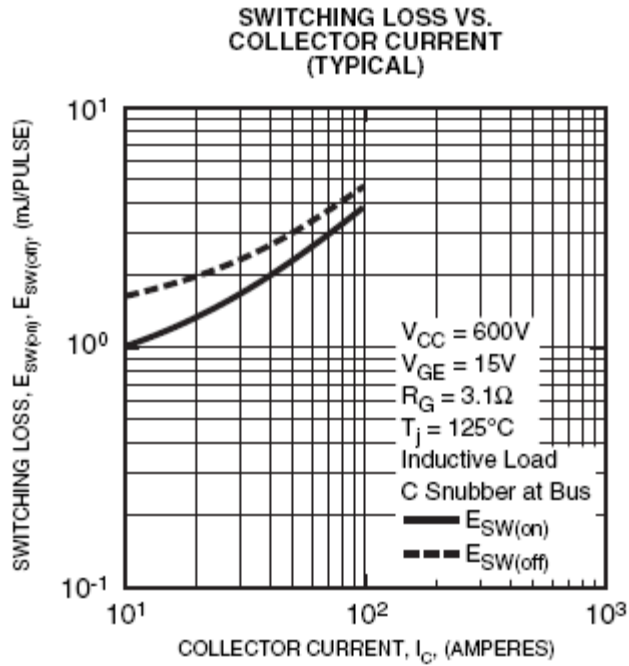
Figure 3.10 Switching energy characteristics for a 1200 V, 100 A IGBT
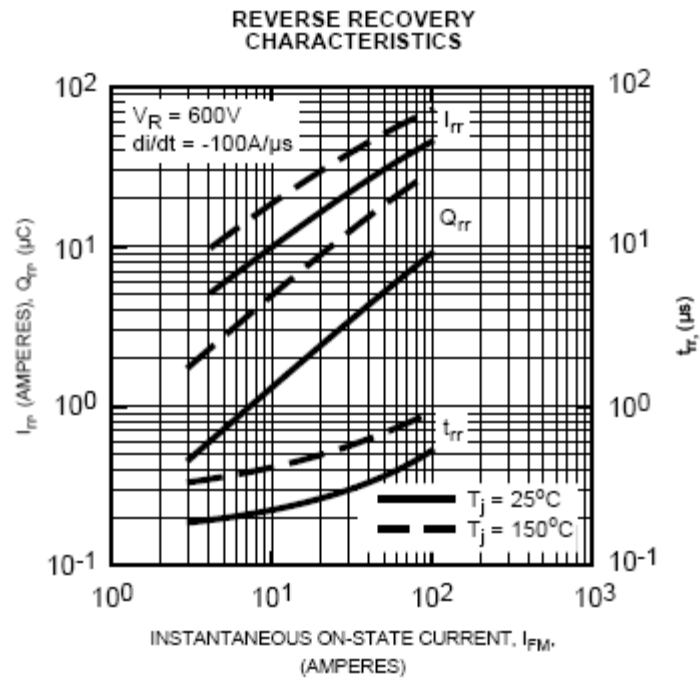
Figure 3.11 Reverse recovery characteristics for a 1200 V, 100 A diode

Based on this discussion the switching loss estimation algorithm is programmed in SIMULINK. Using switching loss algorithm along with the switching energy and reverse recovery plots mentioned earlier, the total switching loss can be calculated as,

$$P_{SW} = P_{SWon\_IGBT} + P_{SWoff\_IGBT} + P_{RR\_diode} \qquad (3.26)$$

where P_{SWon_IGBT} and P_{SWoff_IGBT} are the IGBT switching on and off losses. And P_{RR_diode} is the reverse recovery loss for antiparallel diode.

Finally the total heat dissipation associated with each half leg of an active rectifier is calculated as below,

$$P_L = (P_{cond\_diode} + P_{cond\_IGBT}) + (P_{SWon\_IGBT} + P_{SWoff\_IGBT} + P_{RR\_diode}) \qquad (3.27)$$

3.7   Chapter Summary

In this chapter, several topics were discussed. The system configuration for using an active motor drive as a shunt compensator was introduced. The various features of active drive useful for compensation objective were listed. Further limitations of steady state control to produce better transient performance were discussed. This underlined the need for using decoupling control based on *d-q* theory.

The details of *d-q* theory were then introduced. The system dynamic model was obtained using *d-q* theory. The different transformation matrices used to transform three-phase coordinates to two-phase stationary and moving frame were introduced. Since the control will be carried out in moving *d-q* coordinates the power definitions in *d-q* coordinates are required, which were introduced next. Finally, for evaluating the system efficiency and comparing it vis-à-vis diode rectifier front end, the power loss model was

presented. The loss model was based on device characteristics curves provided in the device datasheet and also circuit operating condition.

The dynamic model presented in this chapter provides the building block for determining suitable control strategies to achieve better transient performance of the active front end induction motor drive. The control scheme is introduced in Chapter 5.

4   Active Front-End Motor Drive Control

4.1   Chapter Overview

In the previous chapter, the mathematical model of an active rectifier describing the dynamic behavior of the active rectifier was presented. Additionally a power loss model to estimate the heat dissipation in a rectifier module was also discussed. The purpose of this chapter is to present a suitable approach for controlling the rectifier dynamics. Apart from the front-end rectifier, the load-side inverter and induction motor are also part of the system configuration. The second half of the chapter is devoted to discussions on the mathematical model and field oriented control of induction motor.

In Section 4.2 the ac side per-phase equivalent circuit and dc side equivalent circuit of the line-side converter will be discussed. The equivalent circuits are based on the system differential equations. In Section 4.3 a high gain feedback controller for controlling line currents will be introduced. A scheme for estimating angular frequency of source voltages in real time will also be discussed in this section. In Section 4.4 an input-output linearization controller to counteract the dc-link variations will be presented.

For achieving better transient performance a feed-forward controller will be presented in Section 4.5. In Section 4.6, the complete control scheme and parameter measurements will be discussed. In Section 4.7 a mathematical model of an induction machine will be introduced. Further, a classical field-oriented controlled for induction motor will be discussed.

4.2   Dynamic Equations for an Active Front-End Converter

For the purpose of fast response, the control is carried out in the *d-q* reference frame. This type of control is referred to as '*field-oriented*' control. The starting point of the control is the system of non-linear differential equations which characterizes its behavior. As derived previously, the dynamics of an active front-end converter are given by a system of differential equations stated below,

$$L\frac{di_{qe}}{dt} = E_{qe} - \omega L i_{de} - R i_{qe} - V_{qe} \tag{4.1}$$

$$L\frac{di_{de}}{dt} = E_{de} + \omega L i_{qe} - R i_{de} - V_{de} \tag{4.2}$$

The differential equation governing dc-link voltage also needs to be added to the above set of system equations to completely define system dynamics.

$$C\frac{dV_{dc}}{dt} = i_{dc} - i_M \tag{4.3}$$

where, i_{dc} is the total dc-link current supplied by the rectifier, while i_M is the load-side dc current which is the result of induction motor operation. The i_{dc} and i_M currents are shown in Figure 4.1. Figure 4.2 and 4.3 show ac and dc side equivalent circuits respectively.

The dc current, i_M, can be viewed as a noise in dc-link voltage V_{dc} [13]. A positive i_M (motoring-mode) will discharge the dc-link, while a negative i_M (regeneration-mode) will charge the dc-link to a higher potential. If the dc-link current i_{dc} supplied by the line-side converter equals to i_M, then we have,

$$C\frac{dV_{dc}}{dt} = 0.$$
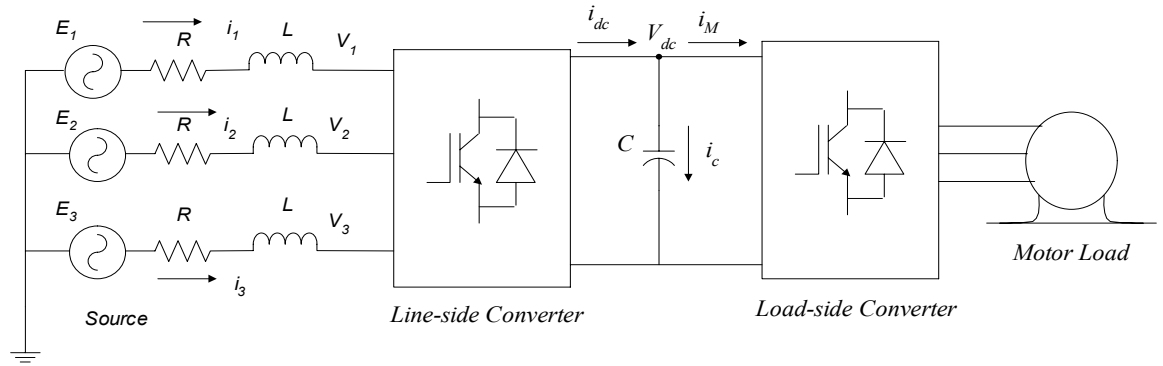
In other words, dc-link voltage remains constant.

58

Figure 4.1 DC-link dynamics controlled by line-side converter
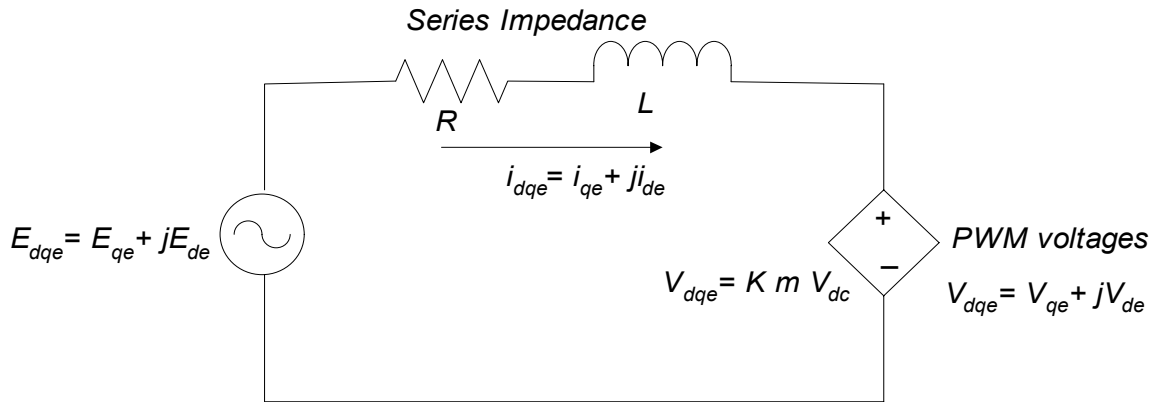
Figure 4.2 AC-side per-phase equivalent circuit
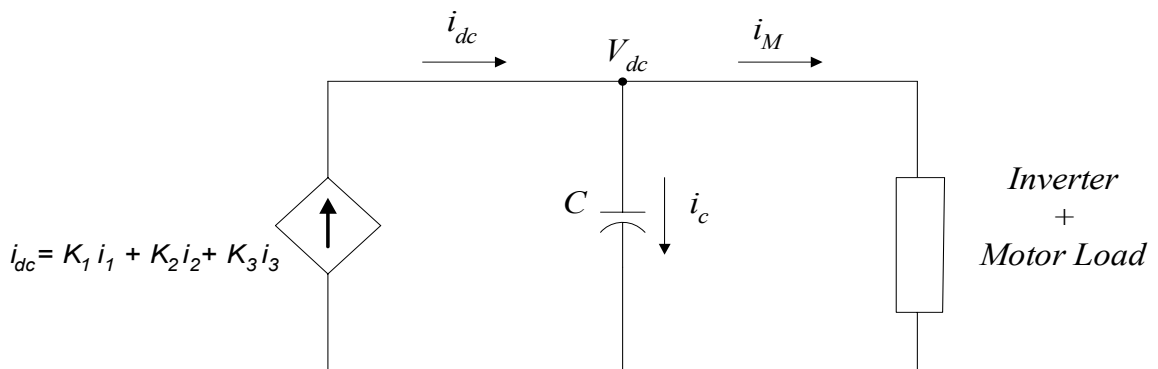
Figure 4.3 DC-side equivalent circuit of an active drive

In Equation 4.1, the terms E_{qe} and E_{de} are computed from source voltages, E_1, E_2, and E_3. Since line voltages are known, the angular frequency, ω, can be easily estimated. The PWM voltages V_{qe} and V_{de} are the two inputs to the system which are generated using the sine-triangle PWM controller. L_S and R represent series impedance.

Figure 4.2 illustrates ac-side per-phase equivalent circuit representation of Equation 4.1. V_{dqe} appears as a controlled voltage-source which is a function of a modulation index and dc-link voltage V_{dc}. On the other hand, Figure 4.3 shows dc-side equivalent circuit representation of Equation 4.2. The dc-link current, i_{dc}, appears as a current source, which controls the capacitor voltage while supplying the current required by the motor load [16].

4.3   Control of Active Drive

The above discussion sets up the non-linear control problem. The system to be controlled is basically multiple-input-multiple-output (MIMO) type system. The PWM voltage commands, V_{qe} and V_{de}, are the two inputs to the system. The resultant i_{qe}, and i_{de} currents are the output of the system.

These two output currents are utilized for two different purposes. The i_{qe} component is assigned to produce the desired reactive power ($Q = -E_{de}i_{qe}$). Thus, i_{qe} is considered as a reactive compensation command. Further, the real component of line currents is required to maintain constant voltage across dc-link capacitor, and also to drive a physical load connected to the motor. Thus, i_{de} is assigned to supply the desired real power ($P = E_{de}i_{de}$) to the system.

The control problem is to choose V_{qe} and V_{de} in such a way as to force i_{qe} and i_{de} to track the respective reactive and real power reference trajectories.

4.3.1 Feed-Back Control

The suitable control strategy for the above mentioned non-linear system is the one which effectively eliminates the coupling between the two current components. This is done by forcing the system into current-command mode using high gain feedback. Firstly, the current reference commands need to be generated.

To ensure constant dc-link voltage, the PI control loop is applied to the dc-link voltage error, resulting in the current reference command, $i_{de}*$. The dc current, i_M, fed to the load through an inverter is added to $i_{de}*$ to form a new current reference command as,

$$i_{de}^{*} = K_{dI}^{'} \int (V_{dc\_ref} - V_{dc}) dt + K_{dP}^{'} (V_{dc\_ref} - V_{dc}) + i_M \tag{4.4}$$

Secondly, the reactive power compensation algorithm will generate a second current reference command $i_{qe}*$. The PI controllers shown in Figure 4.4 are then applied directly to the error between current reference and actual values, as shown below.

$$V_{de}^{*} = K_{dI} \int (i_{de}^{*} - i_{de}) dt + K_{dP} (i_{de}^{*} - i_{de}) \tag{4.5}$$

$$V_{qe}^{*} = K_{qI} \int (i_{qe}^{*} - i_{qe}) dt + K_{qP} (i_{qe}^{*} - i_{qe}) \tag{4.6}$$

By appropriately choosing the gains of the PI controllers, i_{qe} and i_{de} can be made to track $i_{qe}*$ and $i_{qe}*$ respectively. Consequently the new references, V_{de}^{*} and V_{de}^{*} for the PWM controller are generated. The PWM controller, if not saturated, will produce a switching pattern such that desired active and reactive power can be provided.

61
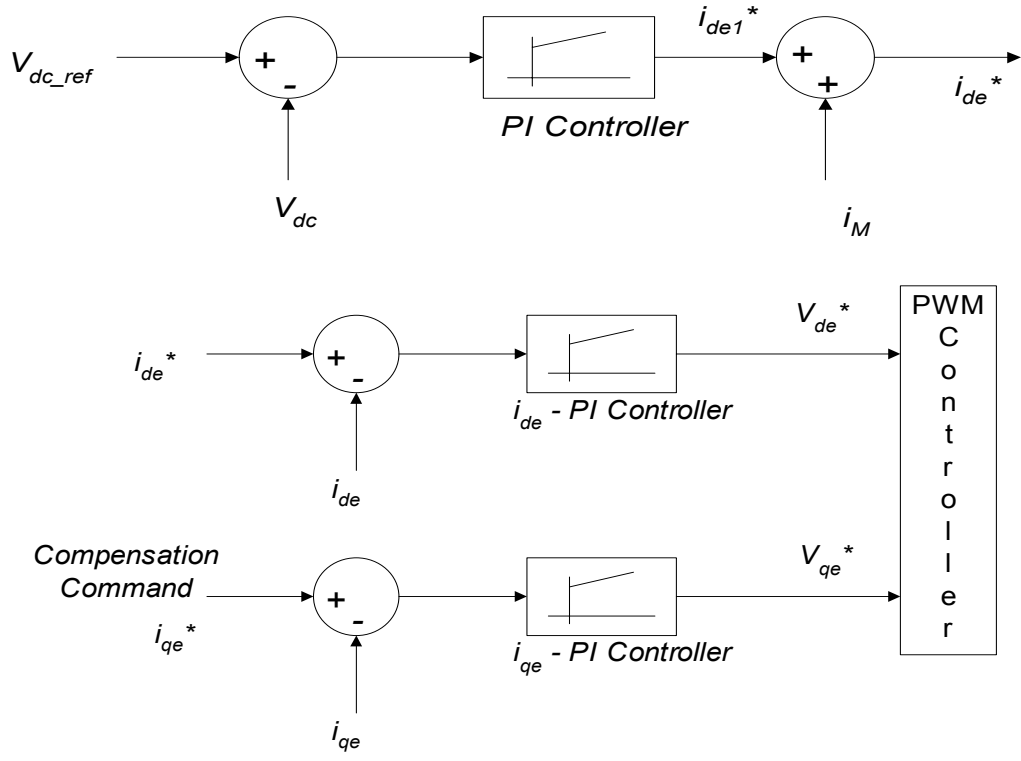
Figure 4.4 High-gain feedback controller for line-side converter

4.3.2 Estimating Angular Frequency of Source Voltages

A suitable choice of coordinate system, defined by the source voltages, is made in Chapter 3 to achieve better transient performance. The three-phase source voltages, separated by 120 electrical degrees, rotate at an angular speed of ω radians per second. Since the control is carried out in moving coordinates, all the variables must be converted to the moving coordinate system, rotating at an exact same angular speed of ω rad/ sec.

The source voltage frequency usually remains unchanged during normal operation of the power system. However, even a small variation in ω will cause error in all the parameters that are transformed into the rotating coordinate system. This will result in

erroneous feedback and consequently affect the performance of the system. For this reason, the supply frequency needs to be tracked and continuously estimated in real time.

Recall, for a given supply frequency, we choose *d-q* axes such that E_{qe} component always remains zero. Now if the supply frequency changes, E_{qe} will no longer be zero. The error in E_{qe} can be minimized by a PI controller to track ω in real-time as,

$$\omega = K_I \int (0 - E_{qe}) dt + K_P (0 - E_{qe}) \tag{4.7}$$

The new angular displacement θ_e, is then given by,

$$\theta_e = \int \omega \cdot dt \tag{4.8}$$

By choosing appropriate gains for the PI controller the variations in supply frequency can be tracked accurately. This is illustrated in Fig 4.5
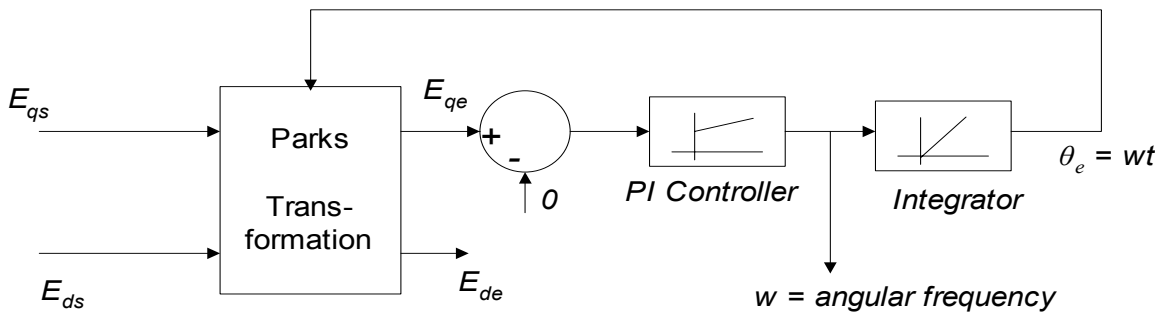
Figure 4.5 Supply voltage frequency estimation

4.4   Input-Output Linearization Control

For a relatively constant V_{dc}, the field oriented high-gain feedback control scheme, explained in the previous section, removes the coupling effect. In other words, the current equations are decoupled, and the equations are linear as long as dc-link voltage is constant. Recall the system dynamic equations,

$$L\frac{di_{qe}}{dt} = E_{qe} - \omega L i_{de} - R i_{qe} - V_{qe}$$

$$L\frac{di_{de}}{dt} = E_{de} + \omega L i_{qe} - R i_{de} - V_{de} \qquad (4.9)$$

$$C\frac{dV_{dc}}{dt} = i_{dc} - i_M$$

The PWM voltages V_{qe} and V_{de} can be represented in terms of modulation index and dc-link voltage as,

$$V_{qe} = G \cdot M_{qe} \cdot V_{dc} \qquad (4.10)$$

$$V_{de} = G \cdot M_{de} \cdot V_{dc} \qquad (4.11)$$

Where G is the PWM controller gain and M_{qe} and M_{de} are modulating vectors in d-q coordinates. For large variations in dc-link voltage; however, the equations are no longer linear. This situation arises when the motor load changes suddenly or during high acceleration and decelerations (regeneration) of motor shaft.

During dc-link variations, the i_{de} current reference varies as a function of V_{dc}. The dynamics of i_{de} then interfere with the dynamics of i_{qe}, resulting into unsatisfactory performance. This coupling of currents can be effectively eliminated by considering an input-output linearization controller.

In dynamic equations (4.9), V_{qe} and V_{de} are the inputs, controlled in such a way as to generate desired currents. Now define new variables V_{qe}' and V_{de}' such that,

$$V_{qe}' = V_{qe} - E_{qe} + \omega L i_{de} + i_{qe} R \tag{4.12}$$

$$V_{de}' = V_{de} - E_{de} - \omega L i_{qe} + i_{de} R \tag{4.13}$$

So that the new system dynamic equations become,

$$L\frac{di_{qe}}{dt} = -V_{qe}' \tag{4.14}$$

$$L\frac{di_{de}}{dt} = -V_{de}' \tag{4.15}$$

In equations 4.14-4.15, the dynamics of i_{de} and i_{qe} are decoupled. The high gain feedback controller is then applied to these currents to generate new voltage commands.

The final voltage commands however, should account for the substitution made in equations 4.12 and 4.13. Thus new voltage references are given by [12], [17]:

$$V_{qe}^* = V_{qe}'^* + E_{qe} - \omega L i_{de} - i_{qe} R \tag{4.16}$$

$$V_{de}^* = V_{de}'^* + E_{de} + \omega L i_{qe} - i_{de} R \tag{4.17}$$

4.5   Feed-Forward Compensation

The linearization controller explained in the previous section decouples the two current controllers effectively, and allows the system operation during variable dc-link. However, the system still suffers from slow response.

Refer to the Figure 4.1 again, and consider following sequence of events. If the motor load changes suddenly, dc current i_M will rise sharply, resulting in a dip in dc-link voltage. The linearization controller now tries to restore the dc-link voltage back to its reference value. If the rate of rise of dc current i_M is faster than rate of restoration of dc-link voltage, the V_{dc} will continue to decrease until it reaches zero potential. Alternatively, the rate of rise of i_M can be restricted to avoid considerable decrease in dc-link voltage. In other words the system time response would be slow.

A better dynamic response is achieved by employing feed-forward compensation [18]. The power required to generate the desired electromagnetic torque is measured in the dc-link using dc voltage and current sensors. This power needs to be supplied from the source. Thus, the feed-forward compensation current i_{d_f} can be obtained from [17],

$$i_{d\_f} = K_1 \cdot \frac{V_{dc} i_{dc}}{E_{de}} \tag{4.18}$$

where, E_{de} is source voltage and K_1 is proportional gain in feed-forward loop. K_1 is allowed to vary to maintain the stability in the current loop, and it is also dependent on line voltage fluctuations.

Figure 4.6 illustrates feed-forward compensation with input-output linearization controller.

4.6   Complete Control Scheme for Active Front-End Converter

Based on above discussions the complete control scheme for control of active front-end converter is implemented using two ac voltage sensors, three line current sensors, one dc current sensor, and one dc voltage sensor

66
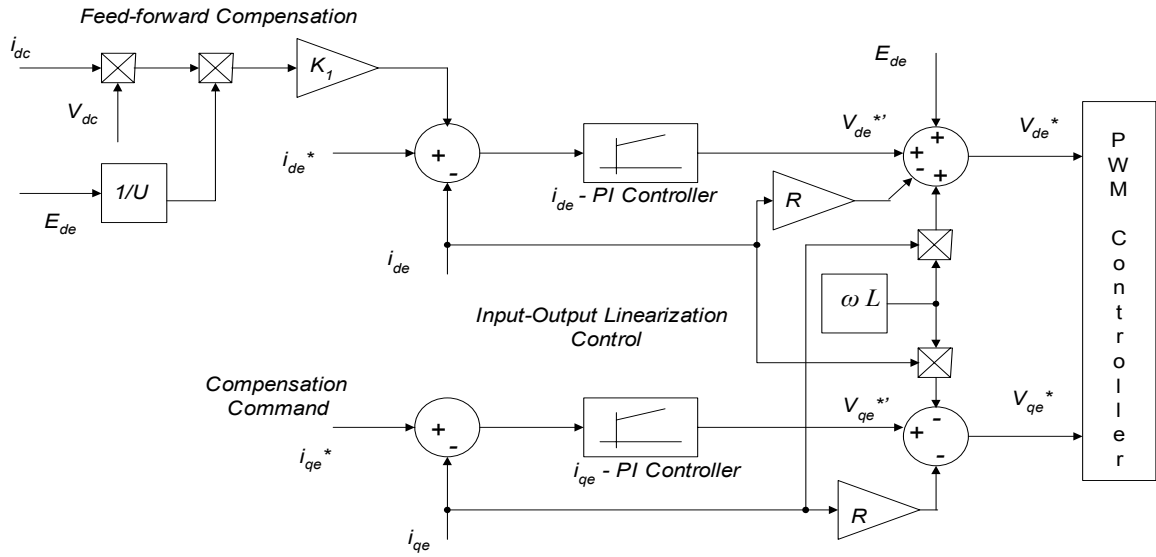
Figure 4.6 Feed-forward compensation for input-output linearization controller

Figure 4.7 illustrates the control of front-end converter. The two ac voltage sensors are connected to the source voltage. From these line sensors, the three source voltages (phase-neutral) are available for use. These voltages are further transformed into equivalent two-phase moving coordinates E_{qe} and E_{de}. The de-qe axes are aligned such that the E_{qe} component of the source voltages always remains at zero value.

The next step is to generate current references. The i_{de} reference is formed as a function of dc-link voltage variations and feed-forward compensation. The dc current i_M, is measured by the dc current sensor placed on load-side of the capacitor. The i_{qe} reference current is generated from the reactive power compensation command. In current-command control mode, the actual currents i_{qe} and i_{de} are forced to follow the reference commands using high-gain feedback and input-output linearization controller.
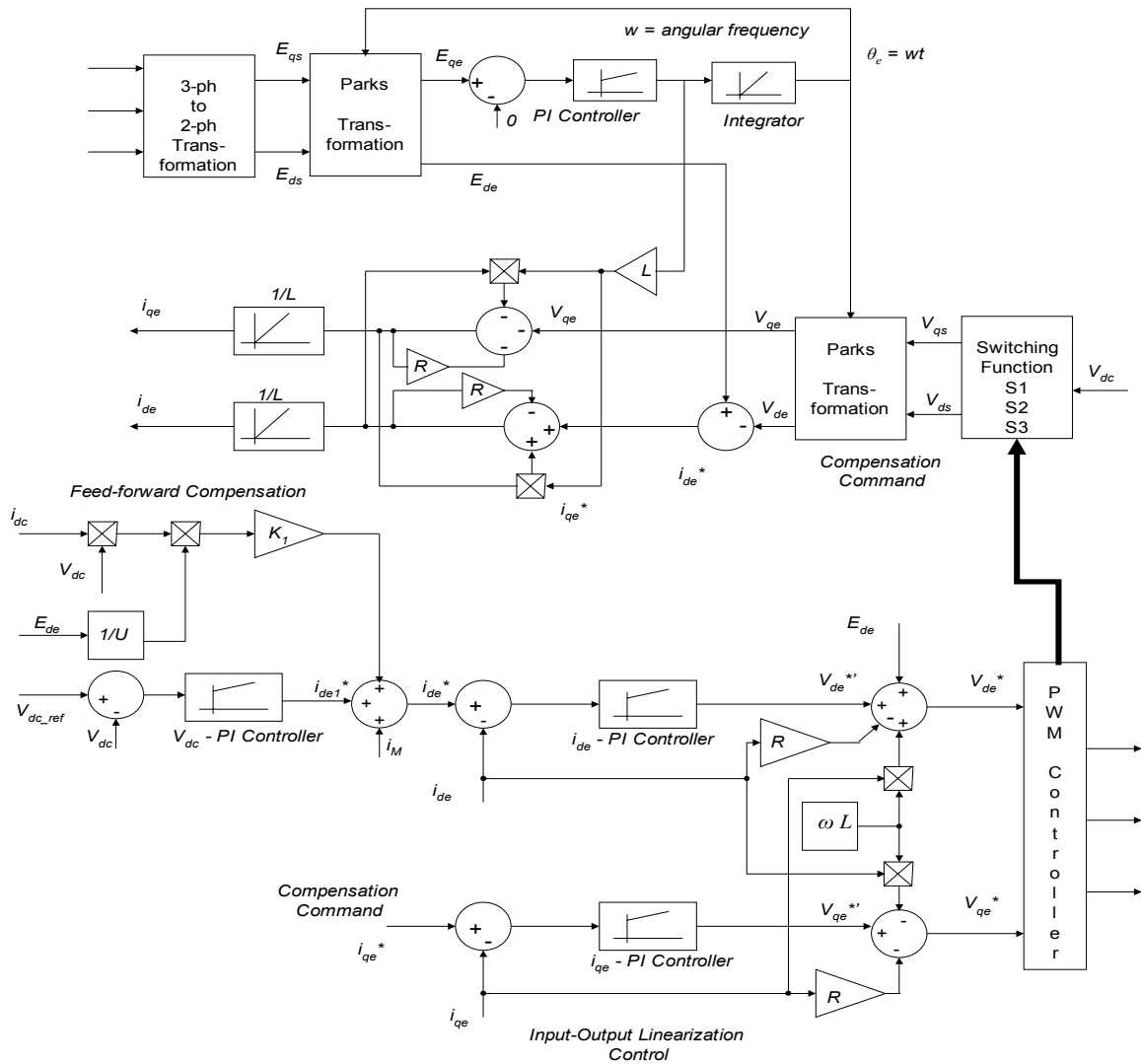
Figure 4.7 Complete control scheme for front-end converter

The new input for the system, V_{qe} and V_{de}, are fed to PWM controller to provide required switching pulses using either sine-triangle or space-vector PWM algorithm. The instantaneous values of currents i_{qe} and i_{de}, can be measured using three current sensors. Alternatively, they are estimated using the system dynamic model shown in Equation 4.9. In the model, L, ω, E_{qe} and E_{de} are all known; V_{qe} and V_{de} are unknown. The instantaneous values of PWM voltages are estimated from the switching signals to IGBT devices, and the dc-link voltage as shown below,

$$V_{qs} = \frac{V_{dc}}{4}(2S_1 - S_2 - S_3) \tag{4.19}$$

And

$$V_{ds} = \frac{V_{dc}}{4}\sqrt{3} \cdot (S_2 - S_3) \tag{4.20}$$

where S_1, S_2, S_3 are integer variables which cannot assume any values other than +1 and -1.

When the IGBT in the upper half of the first leg of the rectifier-bridge is switched on, + V_{dc} is connected to the phase-1 of the supply. Thus, S_1 assumes value equal to 1. When this IGBT is switched off, - V_{dc} is connected to the phase-1 of the supply. Thus, S_1 assumes value equal to -1. In the same manner S_2 and S_3 assume value equal to either 1 or -1. This approach measures instantaneous values of PWM voltages without needing to employ three current sensors.

4.7   Induction Motor Control

The field of induction motor control is well established today. The major challenges in controlling induction motors are: non-linear system dynamics, inability to measure control variables such as rotor flux and rotor current physically, and the motor parameters variations with heating such as variations in rotor resistance value. Taking these challenges into account, the universally accepted approach for controlling an induction motor is the field-oriented approach also referred to as vector control [19].

The field-oriented control deals with rewriting the system dynamic equations in a moving coordinate system that is rotating with the rotor flux vector. In this new coordinate system, the dynamics in motor torque and speed becomes linear, provided the rotor flux magnitude is kept constant. For a variable rotor flux, an input-output linearization controller is used that decouples the speed and rotor flux magnitude.

4.7.1   Induction Motor Dynamic Model

For field oriented control, the new coordinate system rotates with the rotor flux. Since rotor flux or rotor currents are not available for measurements, the rotor flux is estimated using a flux observer. The rotor flux linkages in a two-phase stationary reference frame are expressed as [19],

$$\frac{d\psi_{Ra}}{dt} = -\frac{R_R}{L_R}\psi_{Ra} - n_p\omega\psi_{Rb} + \frac{R_R}{L_R}M \cdot i_{Sa} \qquad (4.21)$$

$$\frac{d\psi_{Rb}}{dt} = -\frac{R_R}{L_R}\psi_{Rb} + n_p\omega\psi_{Ra} + \frac{R_R}{L_R}M \cdot i_{Sb} \qquad (4.22)$$

where, ψ_{Ra} and ψ_{Rb} are rotor flux linkages, n_p is number of pole-pairs of induction motor, M is coefficient of mutual inductance between stator and rotor windings, R_R and L_R are rotor resistance and leakage reactance respectively. ω is the speed of rotation of rotor. i_{Sa} and i_{Sb} are the line currents in stationary two-phase coordinates.

The motor currents can be measured using current sensors, which are then transformed to equivalent two-phase values i_{Sa} and i_{Sb}. A simple way to estimate rotor flux linkages is then to solve Equations 4.21 and 4.22. Once rotor flux linkages are known, the angular position in the moving coordinate system can be defined as,

$$\rho = \tan^{-1}(\frac{\psi_{Rb}}{\psi_{Ra}}) \tag{4.23}$$

$$\psi_d = \sqrt{\psi_{Ra}^2 + \psi_{Rb}^2} \tag{4.24}$$

where ψ_d is called the magnitude of rotor flux linkage and ρ is the angle of rotor field flux. The motor currents and voltages are then rewritten in the moving coordinate system as,

$$\begin{bmatrix} i_d \\ i_q \end{bmatrix} = \begin{bmatrix} \cos\rho & \sin\rho \\ -\sin\rho & \cos\rho \end{bmatrix} \begin{bmatrix} i_{Sa} \\ i_{Sb} \end{bmatrix}; \begin{bmatrix} V_d \\ V_q \end{bmatrix} = \begin{bmatrix} \cos\rho & \sin\rho \\ -\sin\rho & \cos\rho \end{bmatrix} \begin{bmatrix} V_{Sa} \\ V_{Sb} \end{bmatrix} \tag{4.25}$$

where V_{Sa} and V_{Sb} are motor terminal voltages in an equivalent two-phase stationary reference frame. i_d, i_q and V_d, V_q are the motor currents and terminal voltages in the moving reference frame, along d and q axis respectively.

Using the above mentioned coordinate transformation, a mathematical model of an induction motor with state variables expressed in moving coordinates is given by, [19]

71

$$\frac{d\theta}{dt} = \omega \tag{4.26}$$

$$\frac{d\omega}{dt} = \mu\psi_d i_q - (\frac{D}{J})\cdot\omega - \frac{T_L}{J} \tag{4.27}$$

$$\frac{d\psi_d}{dt} = -\frac{R_R}{L_R}\psi_d + \frac{R_R}{L_R}M\cdot i_d \tag{4.28}$$

$$\frac{di_d}{dt} = -\gamma\cdot i_d + \frac{R_R}{L_R}(\frac{M}{\sigma\cdot L_R L_S})\cdot\psi_d + n_p\omega\cdot i_q + \frac{R_R}{L_R}\frac{M\cdot i_q^2}{\psi_d} + \frac{V_d}{\sigma\cdot L_S} \tag{4.29}$$

$$\frac{di_q}{dt} = -\gamma\cdot i_q - (\frac{M}{\sigma\cdot L_R L_S})n_p\omega\cdot\psi_d - n_p\omega\cdot i_d - \frac{R_R}{L_R}\frac{M\cdot i_q i_d}{\psi_d} + \frac{V_q}{\sigma\cdot L_S} \tag{4.30}$$

where ω is the angular velocity of the rotor, $\frac{d\omega}{dt}$ is angular acceleration, J is moment of

inertia of the rotor, T_L is load torque, and D is coefficient of friction. The electromagnetic

torque developed is thus given by, $T_e = J\mu\psi_d i_q$. R_S and L_S are stator resistance and

leakage reactance respectively, while the motor constants are defined as,

$$\gamma = (\frac{M^2 R_R}{\sigma\cdot L_R^2 L_S}) + \frac{R_S}{\sigma\cdot L_S} \text{ and } \mu = (\frac{n_p M}{JL_R}). \tag{4.31}$$

This model is then used to develop an effective method of control.

4.7.2 Feed-Back Control

The effect of non-linear terms appearing in the dynamic model is eliminated using

the high-gain feedback. For this, the first step is to find the current references. Desired

rotor acceleration and load torque will decide how much electromagnetic torque needs to

produced. The current reference i_q* can be assigned to generate required electromagnetic

torque. Secondly, as explained before, for the torque and speed dynamics to remain linear, ψ_d should be kept constant. The second current command, $i_d{}^*$, can be assigned the job of keeping ψ_d constant. The two current references are then given by,

$$i_q{}^* = \left\{ K_0 \int (\omega_{ref} - \omega) dt + K_1 (\omega_{ref} - \omega) + \frac{D}{J} \omega \right\} / \mu \psi_{d0} \tag{4.32}$$

$$i_d{}^* = K_{\psi I} \int (\psi_{d0} - \psi_d) dt + K_{\psi P} (\psi_{d0} - \psi_d) + i_{d0} \tag{4.33}$$

These new inputs $i_q{}^*$ and $i_d{}^*$ are then given PI controllers to produce required motor terminal voltage references as below,

$$V_d{}^* = K_{dI} \int (i_d{}^* - i_d) dt + K_{dP} (i_d{}^* - i_d) \tag{4.34}$$

$$V_q{}^* = K_{qI} \int (i_q{}^* - i_q) dt + K_{qP} (i_q{}^* - i_q) \tag{4.35}$$

By proper choice of proportion and integral gains, i_d an i_q can be forced to track their corresponding references. The resultant $V_d{}^*$ and $V_q{}^*$ commands are given to the inverter PWM controller, to produce required switching pulses for the IGBTs.

The new motor terminal voltages, thus generated, will produce the electromagnetic torque, essential to drive the load at desired acceleration. At the same time the motor terminal voltages are such that the rotor flux magnitude is maintained constant. The complete motor control scheme is illustrated in Figure 4.8.

4.8   Chapter Summary

In this chapter, the control methods for a front-end converter and an induction motor were examined. The system dynamics on ac side and dc-side were discussed with the help of equivalent circuit representations.
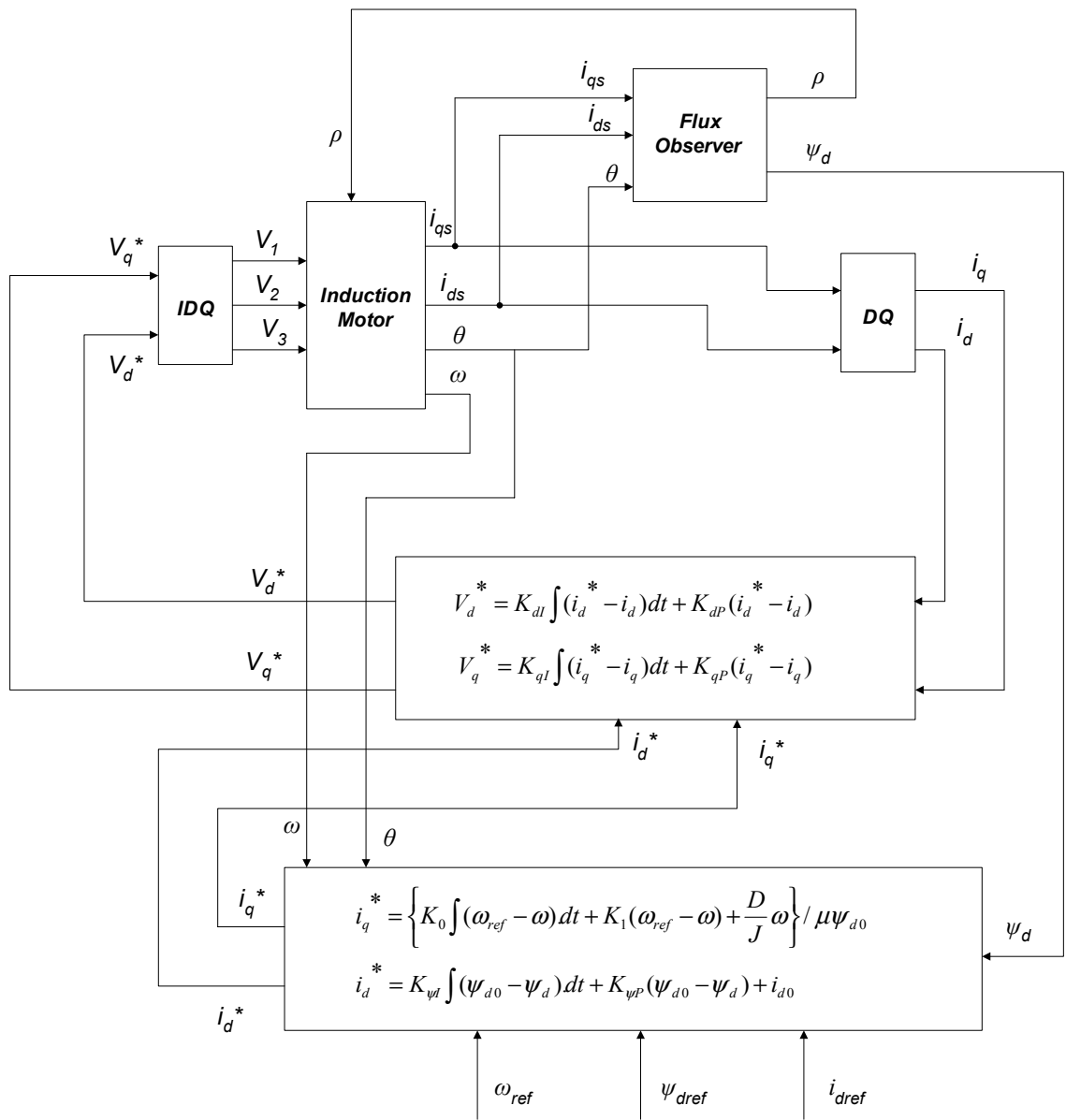
Figure 4.8 Block diagram of motor controller

The feedback control strategy for the front-end converter was introduced next. Tracking the angular frequency of supply voltages was also discussed. Further, input-output linearization controller was introduced to obtain satisfactory system performance under varying dc-link voltage. For better transient performance a feed-forward compensation loop was added to the linearization controller. The advantages of feed-forward compensation were discussed. A block diagram of the complete control scheme was presented, and various inputs and outputs to the system were discussed. Further, the induction motor dynamic model was analyzed. The field-oriented control of induction motor with high-gain feedback was discussed.

The control strategies to achieve better transient performance discussed in this chapter are used in next chapter to simulate various scenarios.

5 Simulation Results

5.1 Chapter Overview

The previous two chapters introduced the theory behind the research presented in this thesis. In this chapter, the simulation results will be presented. In Section 5.2, a methodology used in the research will be presented. The steps performed in simulating the various modes of operation and in evaluating the system performance will be listed. In Section 5.3 the simulation set-up and the software configuration will be discussed.

In Section 5.4, the active drive operation with and without motor load will be simulated. The different features of an active drive, such as variable power factor and better control over dc-link voltage will be verified. In Section 5.5, the drive performance will be analyzed in detail. The simulation data will be used to address design issues, such as device rating, power loss, power quality, and thermal management system. Further, the drive will be simulated to define limits on the amount of reactive power that can be compensated.

5.2 Methodology used in Research

To evaluate the performance of active front-end drive by accurate simulations and to establish the limits on amount of reactive power that can be compensated was the main objective behind this work. The application targeted was a 50 hp induction motor driving a conveyor load and supplying maximum possible VARs to the utility.

The broad task was organized into three major tasks:

- Present theoretical modeling and effective control strategy.

- Accurately simulate system modes of operation.

- Analyze system performance from point of view of device ratings, power losses, and power quality.

The first step dealt with deriving the mathematical model of front-end converter connected to the utility. The *d-q* theory presented in Chapter 3 was used to derive the system model. Further, the different control principles suitable for independently controlling real and reactive power supplied to or consumed by the drive were presented in Chapter 4. Based on these discussions a comprehensive control scheme was developed. The remaining two tasks, outlined above, are elaborated in this chapter.

5.2.1 Steps Performed in Simulating System Modes of Operation

The simulations to demonstrate different modes of operation were divided in two stages. During the first stage, the load-side inverter and the induction motor was disconnected from the rest of the system. The front-end converter was then controlled to provide unity, leading, and lagging power factor to the utility, while dc-link variations were monitored. The magnitude of dc-link ripples and the step response to the reactive power command were used to gauge the effectiveness of the control scheme.

Once the stability of the controllers and satisfactory system response was ascertained, the load-side inverter and motor load were connected to the dc-link. In the second stage, different operating scenarios were simulated. These include unity power factor operation and reactive compensation during motor acceleration and deceleration.

5.2.2 Steps Performed in Analyzing System Performance

The task here was to use the modeling and simulations to analyze the drive performance for a given application. The application under consideration was: active front-end induction motor drive providing reactive power compensation to the utility. The analysis was carried out with regard to:

1. Determining device voltage and current ratings.

2. Amount of reactive compensation possible under different load conditions.

3. Device power losses and thermal design considerations.

4. Power quality issues such as total harmonic distortion (THD), during VAR compensation.

First, the application specifications such as motor power rating and line-side power specification were determined. Appropriate dc-link voltage, capacitor and line-side inductance were chosen. The electrical parameters of the induction motor were identified. Accordingly, the motor field-oriented controller was carefully tuned to provide satisfactory variable speed operation. The induction motor was accelerated to the full load, while line-side power factor was maintained at unity.

The currents carried by the devices and the voltage waveforms across the devices were analyzed to determine the ratings of IGBTs and anti-parallel diodes. Once the switches were selected, the characteristic curves of the respective switches were modeled to estimate the total power loss. The line-side power factor was maintained at unity and the motor load was varied in steps. The total harmonic distortion of line currents and power losses in active front-end converter were plotted.

Further, the reactive compensation command and the motor load were increased in steps in such a way that peak line current remained below the rated value. The maximum VAR compensated at each step thus defined the limit on amount of reactive power that can be compensated to the source. These limits are valid for a given ratio of dc-link voltage to the line voltage peak, and the current rating of the active switches. To ascertain the power quality at the line-side, total harmonic distortion of line currents was calculated in each step.

5.3 Simulation Set-up

Two three-phase, two-level converters were needed to implement the active drive configuration. One of the converters was connected to the three-phase, wye-connected source while, other was operated as a load-side inverter. The power electronics switches employed in the simulations were ideal IGBTs, with no forward voltage drop and almost instantaneous switching times.

The PSIM software package from Powersim Inc. was used to implement the active drive configuration with motor load. Figure 5.1 shows the complete circuit schematic. The complete hardware and sensors were implemented in PSIM. Secondly, Simulink, an extension to MATLAB, was used to implement the control functions. The "Simcoupler" module, provided by PSIM was used to interface control and power signals between PSIM and Simulink. Thus hardware configuration was separated from the system control functions. The simulation step-size in Simulink and PSIM was chosen to be 1 μs for better results. All the reference commands for desired operation and various control functions were generated in Simulink. Figure 5.2 illustrates the Simulink model.

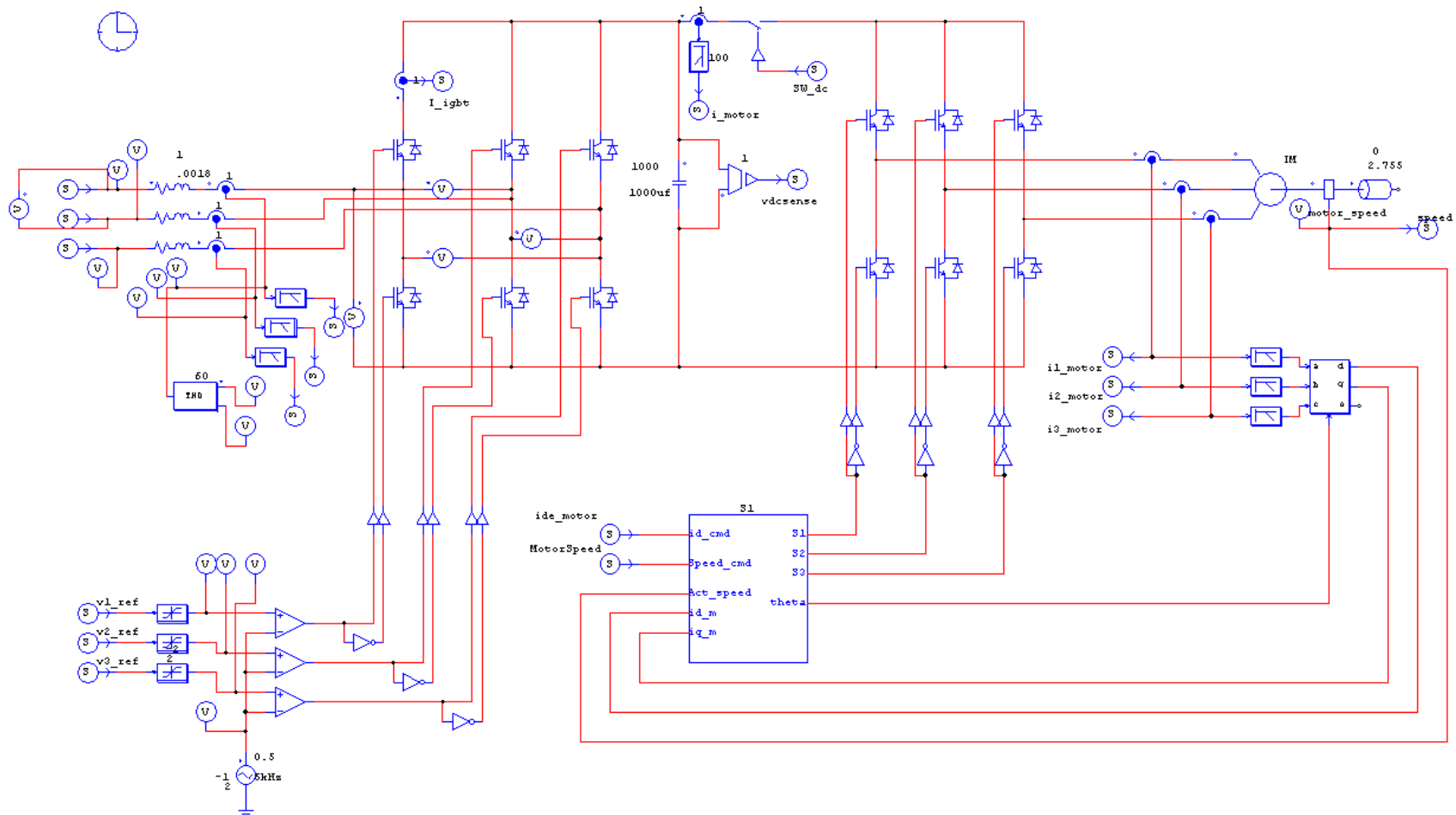**Field-Oriented Control of Active Front-End Induction Motor Drive**

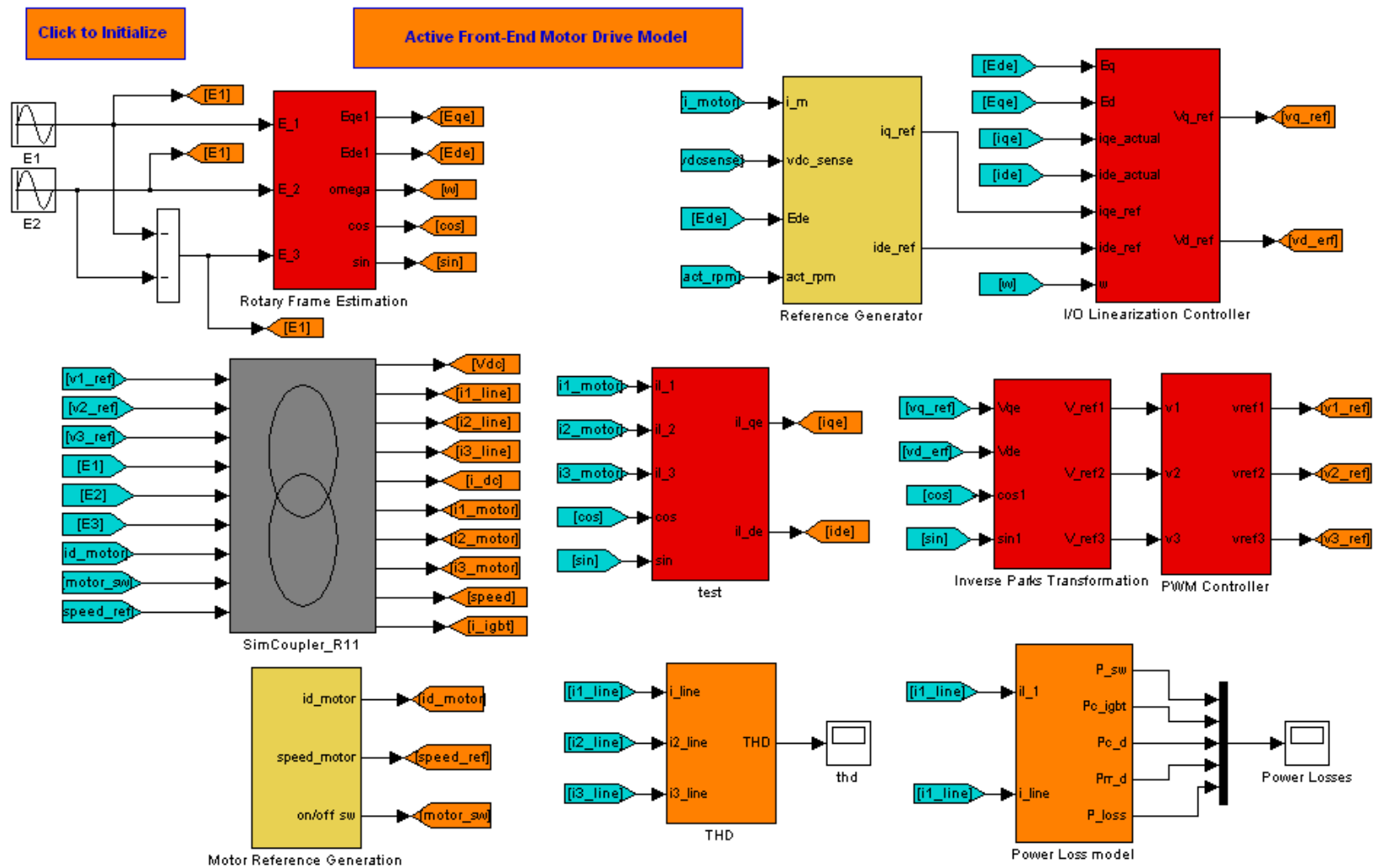**Figure 5.1** The hardware configuration

80

Figure 5.2 SIMULINK model for active front-end drive control

81

5.4   Demonstrating System Modes of Operation

As mentioned before, two scenarios were considered to simulate different modes of operation. In the first case, there was no motor load connected to the dc-link while in the second case, the motor was operating at full load. The front-end converter was connected to the three-phase, wye-connected, 110 V (line-to-line), 60 Hz supply. The series inductance was chosen to be 10 mH. The dc-link voltage was maintained constant at 500 V to provide sufficient margin for current control. The dc capacitor was 700 μF.

5.4.1 Without Motor Load

In *d-q* coordinates the reactive power is given by,

$$Q = E_{de} \cdot i_{qe} \tag{5.1}$$

Since the sign of E_{de} is chosen to be negative, a positive valued i_{qe} results in leading line currents while, a negative valued i_{qe} causes lagging line currents. Figure 5.3 shows the i_{qe} component of line current following the step change in reference command. Accordingly, the line-side power factor changes from unity to leading and then lagging. This is shown in Figure 5.4. Note the time response to step change in compensation command. The transition from leading to lagging reactive current took only a few milliseconds. Figure 5.5 shows the effect of compensation on dc-link voltage. The maximum ripple magnitude was found to be 5 V, which is 1% of total dc-link voltage (500 V). The i_{de} current reference changes according to the dc-link voltage variations so that the dc-link voltage ripple can be kept to the minimum value. Figure 5.6 shows the i_{de} component of line current tracking the reference.
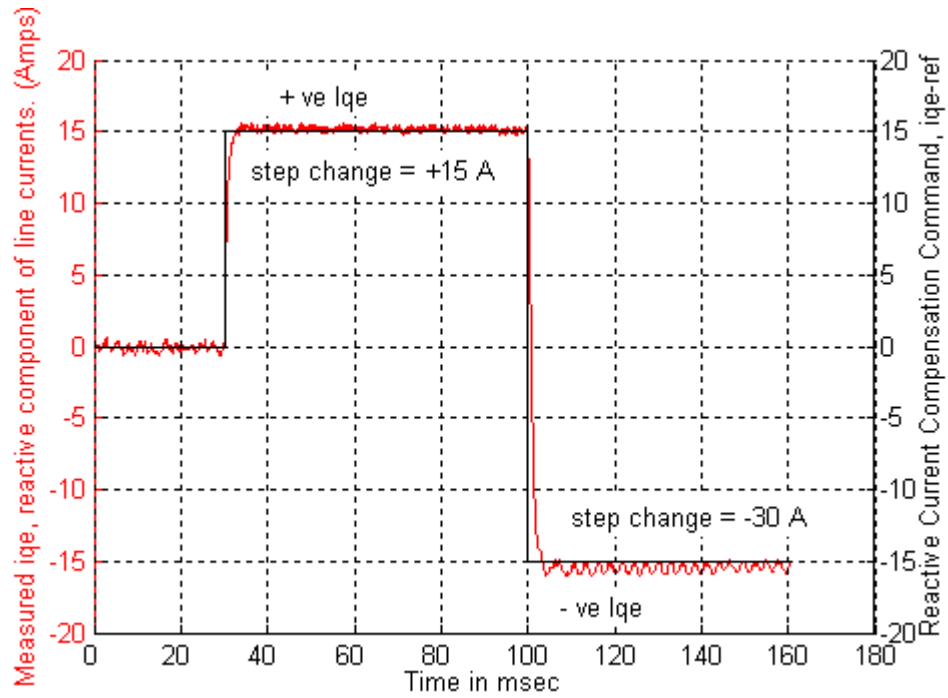
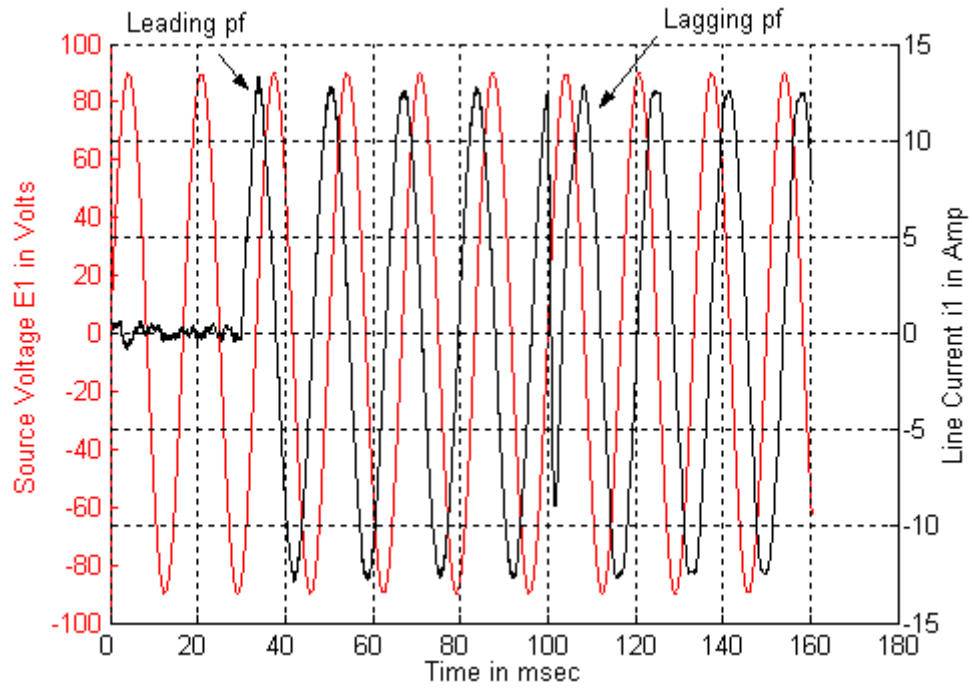**Figure 5.3** i_{qe} component of line current tracking the compensation command
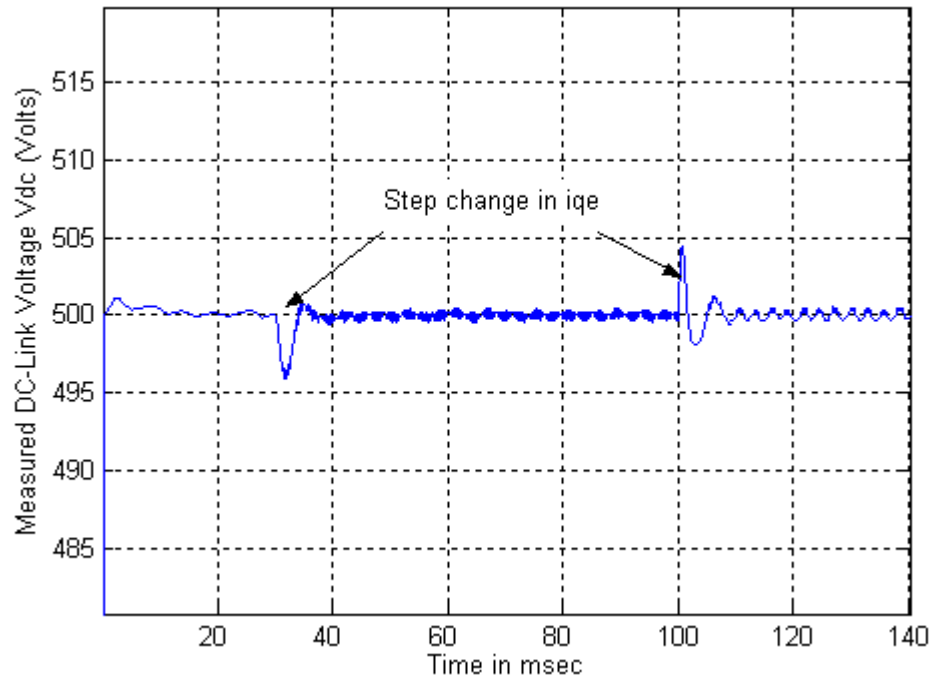

Figure 5.4 Reversal of line current

83

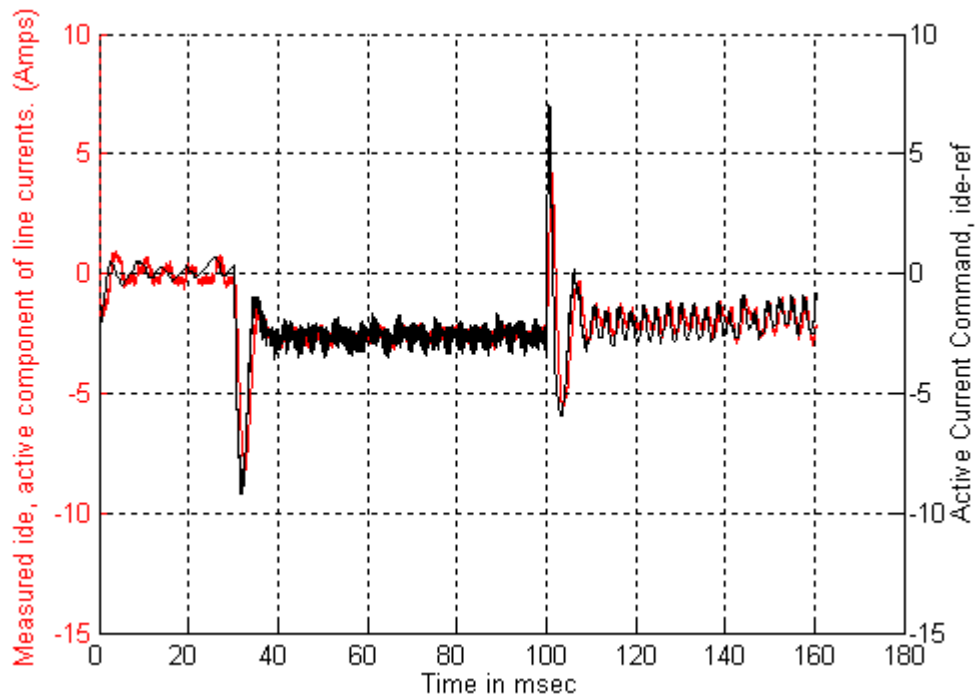**Figure 5.5** DC-link variations during compensation

Figure 5.6 i_{de} tracking the reference to maintain constant V_{dc}

84

One important feature of an active-front end rectifier is the better control over dc-link voltage. The step response of the dc-link controller to the step-change in dc-link voltage reference, shown in Figure 5.7, demonstrates this feature. As can be seen, it took a little more than one cycle (20 ms) for the V_{dc} to reach to the new reference value.

The change in dc-link reference resulted in brief active current component for charging the dc-link capacitor, while the reactive current component remained nearly undisturbed. Figure 5.8 shows active and reactive current components. As can be seen, the decoupling control was clearly effective.

The ability of the active front-end converter to smoothly control the dc-link voltage can be used in improving efficiency of large power motor drives. Traditionally the variable output power from motor drive is achieved by varying the modulation index and keeping the dc-link voltage constant. As pointed out in [20], the amplitude of modulation index affects the amount of current that flows through active devices in two-level PWM inverter. Consequently, at low modulation indices the power loss in the inverter is considerably high when compared to output power resulting in low efficiency. The active rectifier, on the other hand, can provide variable output power by controlling the dc-link voltage to keep the modulation index close to one.

Further, the percentage core losses in an induction motor are minimized when the inverter is operating at modulation index close to one [21]. In this case an active front-end converter can improve the overall efficiency of the motor by varying the dc-link voltage and allowing the load-side inverter to be operated at higher modulation indices. The choice of variable dc-link operation is not available for the rectifier with phase-controlled thyristors, due to the complexity of control and slow dynamic response [21].
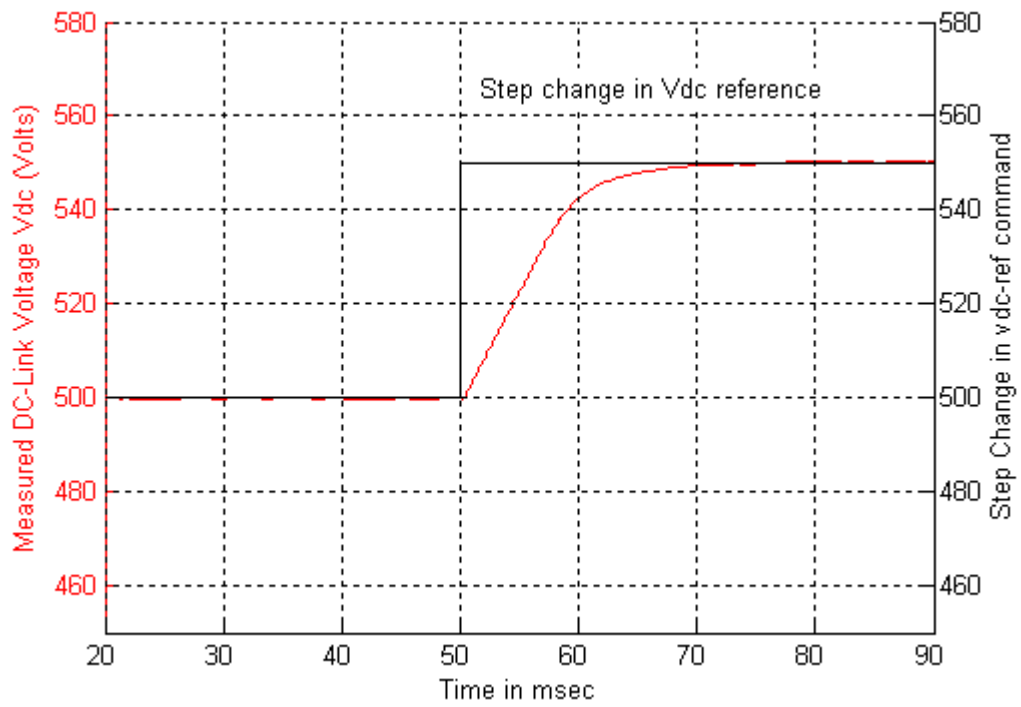
85

Fig 5.7 Step response of dc-link voltage controller
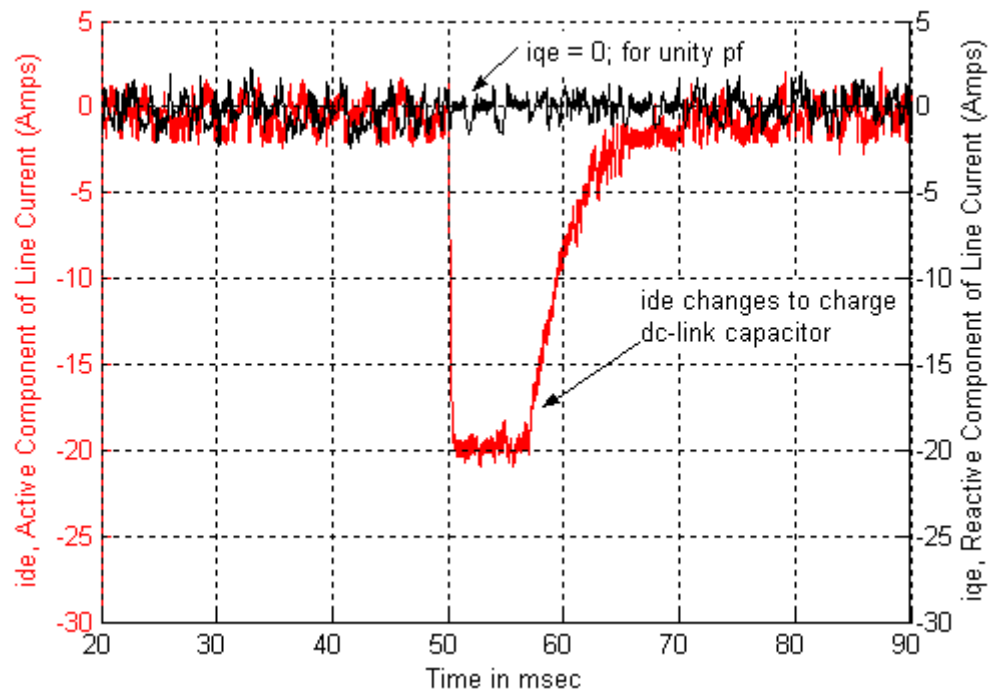

Fig 5.8 Decoupled control of active and reactive current components

5.4.2 With Motor Load

The effectiveness of decoupling control also needs to be proven when operating under full motor load. This was done by connecting the load-side inverter to a 110 V, 3 hp, 6-pole induction motor. The motor fed a conveyor type load. The torque for the conveyor load varies linearly with angular speed of rotation.

Since the motor will be used for a variable speed operation, the speed reference, ω, was set as an input to the motor controller. For the rectifier controller, i_{qe} reference was set to provide desired reactive compensation during motor acceleration, deceleration, and constant speed operation. The motor load was 40 Nm.

Figure 5.9 shows the speed command for motor controller and the reactive compensation reference for the rectifier controller. The motor was first accelerated to a speed of 120 rpm (revolutions per minute) in 0.5 seconds. The compensation started during constant speed operation at time, t = 0.6 seconds. At time, t = 0.7 seconds, the motor began decelerating.

Figure 5.10 illustrates line current at unity power factor and later at leading power factor with respect to the line voltage. As can be seen in Figure 5.11, the i_{qe} component of line current followed the reactive compensation reference while, i_{de} component provided real power required for acceleration and deceleration. The two current components remained unaffected by each other, thereby illustrating independent control over real and reactive power. The actual currents drawn by the motor are shown in Figure 5.12 emphasizing healthy operation of motor.
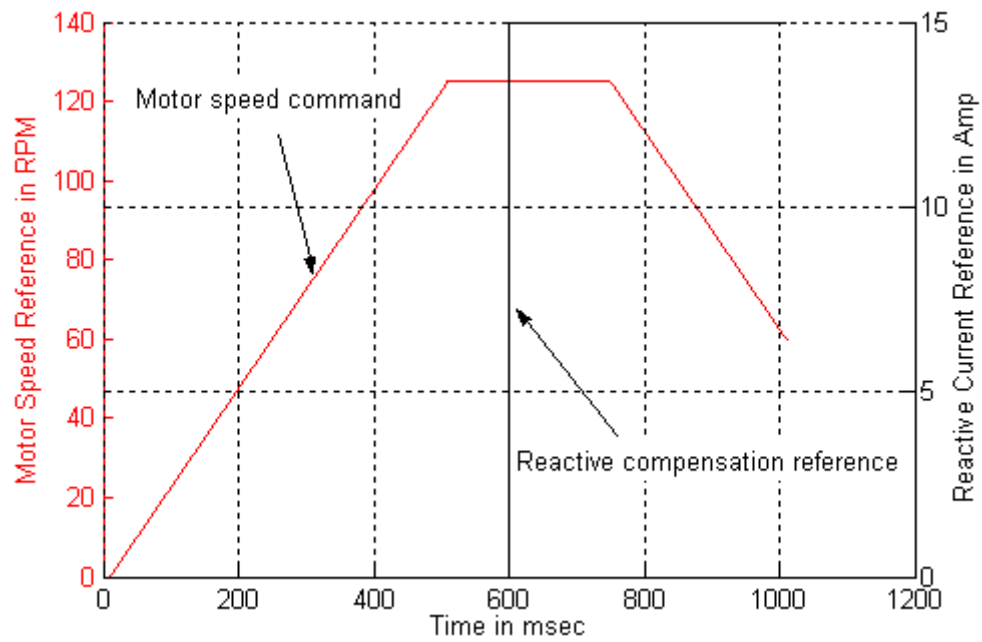
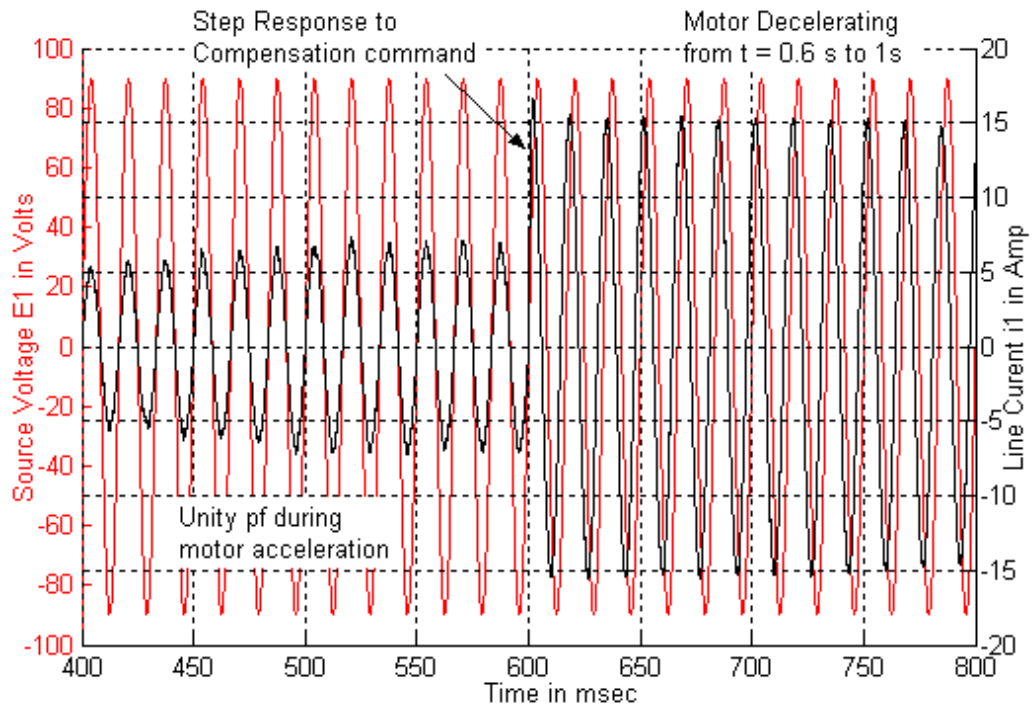**Figure 5.9** Reactive compensation and Motor Speed commands

Figure 5.10 Unity and leading power factor at the source

88
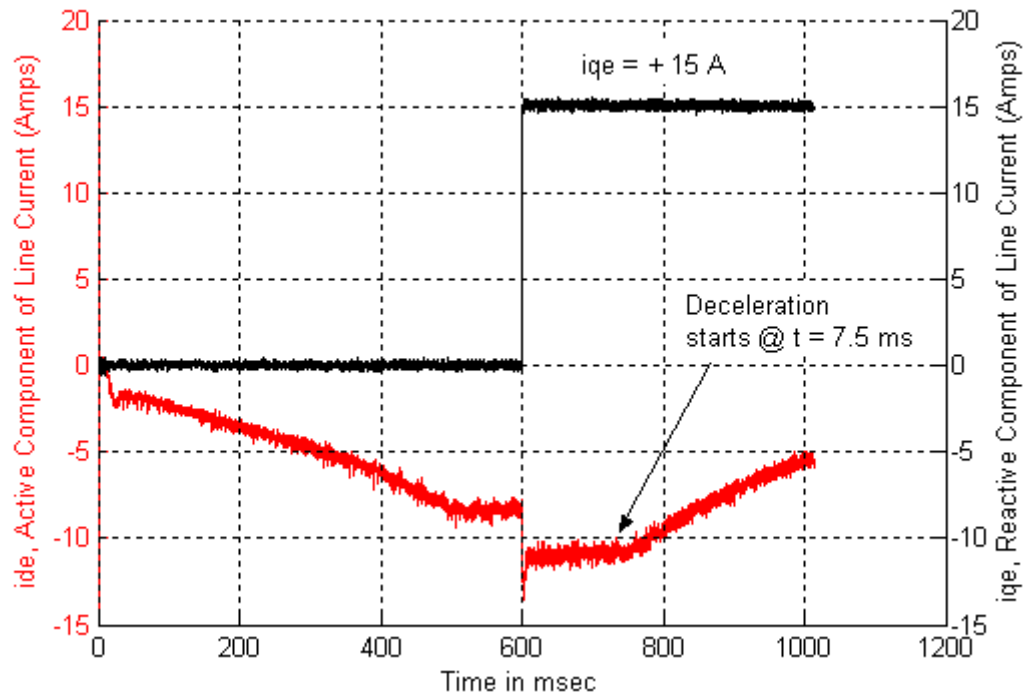
Figure 5.11 Decoupled control during motoring operation
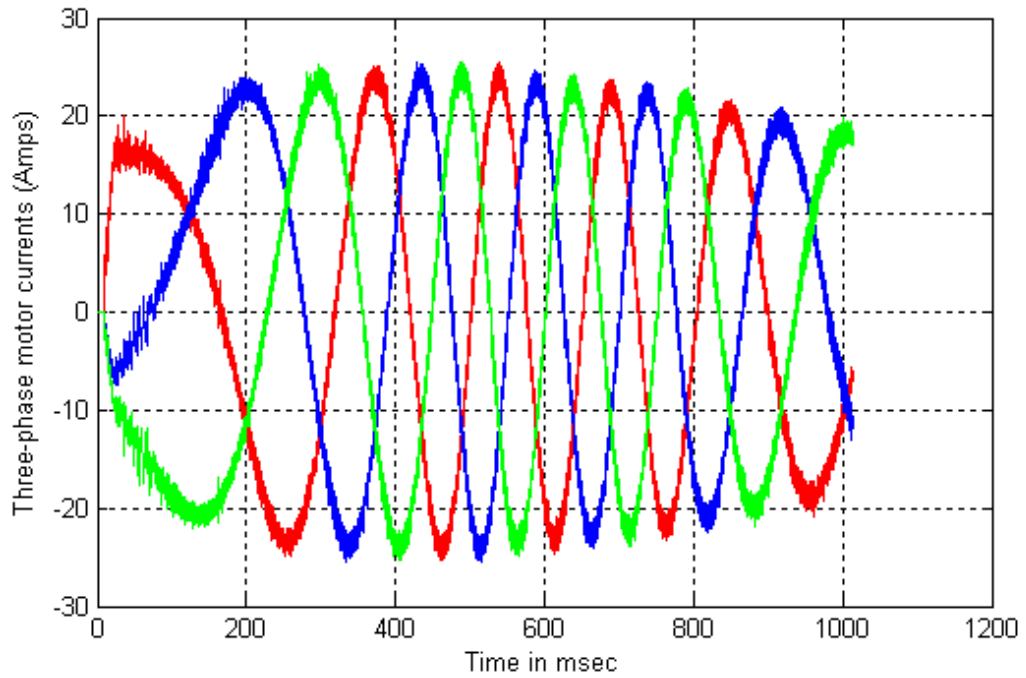
Figure 5.12 Motor currents during the motor acceleration and deceleration

89

5.5   Active Front-End Inverter System Design and Analysis Issues

A 50 hp induction motor was considered to analyze performance of an active front-end drive and to discuss the design issues. First step was to select system parameters such as converter power rating, dc-link voltage, dc capacitance, reactance of line-side inductor. Further, induction motor parameters needed to be identified to achieve satisfactory performance from the field-oriented controller.

5.5.1 System Specifications

The induction motor specifications were: 50 hp, 480 V, 60 Hz, 6-pole, with base speed of 1200 rpm. The mechanical load connected to the motor was conveyor type load. The torque for the conveyor load, T_L is defined by,

$$T_L = K \cdot \omega \text{ Nm} \tag{5.2}$$

where, K is a torque constant and ω is motor speed in radians per second.

The torque constant is chosen to be equal to 2.8 so that the mechanical torque at 1100 rpm would be,

$$T_L = 2.8 * \frac{2\pi}{60} * 1100 = 322.53 \text{ Nm} \tag{5.3}$$

The steady state motor output power would be,

$$P_{mech} = \frac{2\pi}{60} * 1100 * 322.53 = 37.153 \text{ kW} \tag{5.4}$$

Further, the parameters for an equivalent circuit model of the induction motor used in the simulations were:

Stator resistance, $R_s = 0.294 \ \Omega$;

Stator Reactance, L_s = 1.39 mH;

Rotor resistance, R_r = 0.156 Ω;

Rotor Reactance, L_r = 0.74 mH;

Magnetizing Reactance, L_m = 41 mH;

The motor parameters were assumed to be known. In practice however, the equivalent-circuit parameters can be estimated using laboratory tests [22]. The tests generally performed are a dc test, no-load test, and a blocked rotor test. Stator resistance can be found by a dc test. The remaining parameters can be determined by performing the no-load test and blocked-rotor test.

The supply side had a three-phase, wye-connected, 480 V (line-to-line), 60 Hz source. The dc-link voltage needs to be chosen as shown in Equation 5.4, so that the front-end rectifier can generate sinusoidal PWM voltages [1].

$$\sqrt{2} * \frac{E_{ll}}{\sqrt{3}} \leq \frac{V_{dc}}{2} \qquad (5.5)$$

where E_{ll} is line-to-line supply voltage and V_{dc} is dc-link voltage.

A higher V_{dc} is desired, because the voltage ratio between the E_{ll} and V_{dc} imposes a limit on amount of reactive power that can be compensated [11]. However, higher V_{dc} means the active devices have a higher voltage rating. The dc-link voltage is selected to be equal to 1000 V as a trade off between reactive compensation capabilities and the device voltage rating. This choice obviously satisfies the condition laid down by Equation 5.5. The line-side resistance, R, was equal to 1 Ω while, the line reactance, L, was chosen as 10 mH. The dc-link capacitor was selected to be equal to 1000 μF so that dc-link voltage ripples could be kept to the minimum level.

5.5.2 Device Power Rating Considerations

To define device voltage and current ratings, the induction motor needed to be driven at full load. As explained in Chapter 4, the K_P and K_I gains for the field-oriented controller were properly chosen based upon the induction motor parameters. The motor was accelerated to 1100 rpm. The line current was maintained at unity power factor with respect to supply voltage.

The maximum voltage that the IGBT and anti-parallel diode have to block is V_{dc} (1000 V). As a result, the voltage rating of switches in both the front-end converter and line-side inverter was selected to be 20% more than the dc-link voltage i.e. 1200 V. It was later shown that when the motor load was varied in steps and reactive compensation limit set at different levels, the maximum fluctuations in dc-link voltage remained less than 3% (30 V). Thus, the 20% margin in device voltage rating was considered to be sufficient. For any dc-link voltage swings, greater than 15% (150 V) the converter operation would be halted.

The peak current that flows through the switches in front-end converter is the peak line current. Figure 5.13 shows that the peak current of 100 A was carried by IGBT and feedback diode at full load. Consequently, the current rating for the switches was selected to be 150 A, with 50% overcurrent margin. Similarly as seen in Figure 5.14, for a 480 V motor, the peak current to drive a 50 hp load was 85 A. This suggests the same devices used for front-end converter can be used for load-side inverter as well. As a result there is an opportunity for a modular design with simplified assembly and repair.
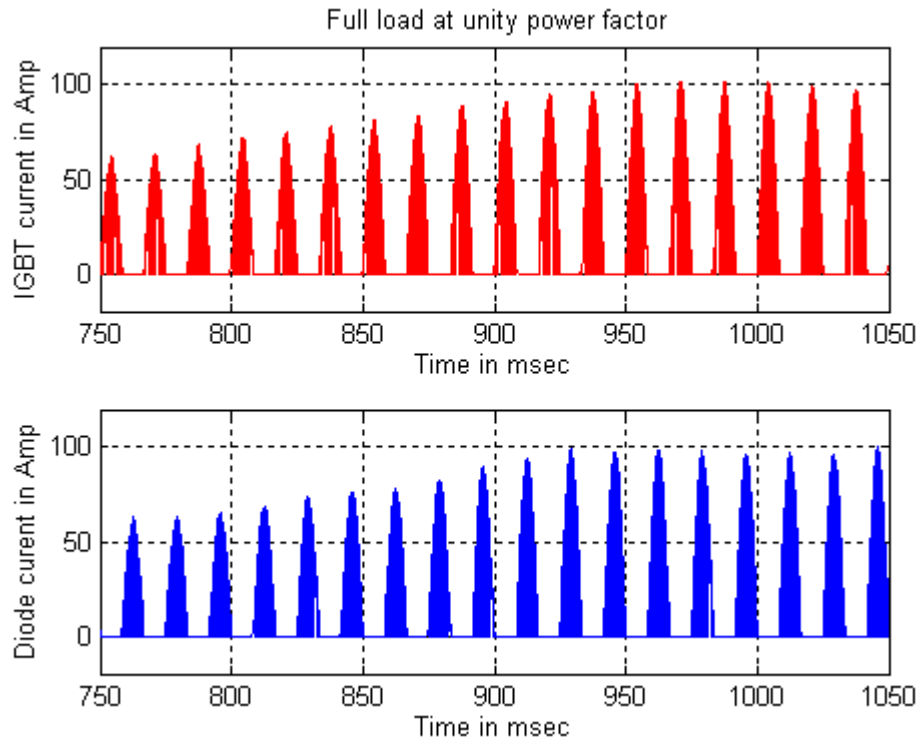
Figure 5.13 Current flowing through IGBT and anti-parallel diode at full motor load
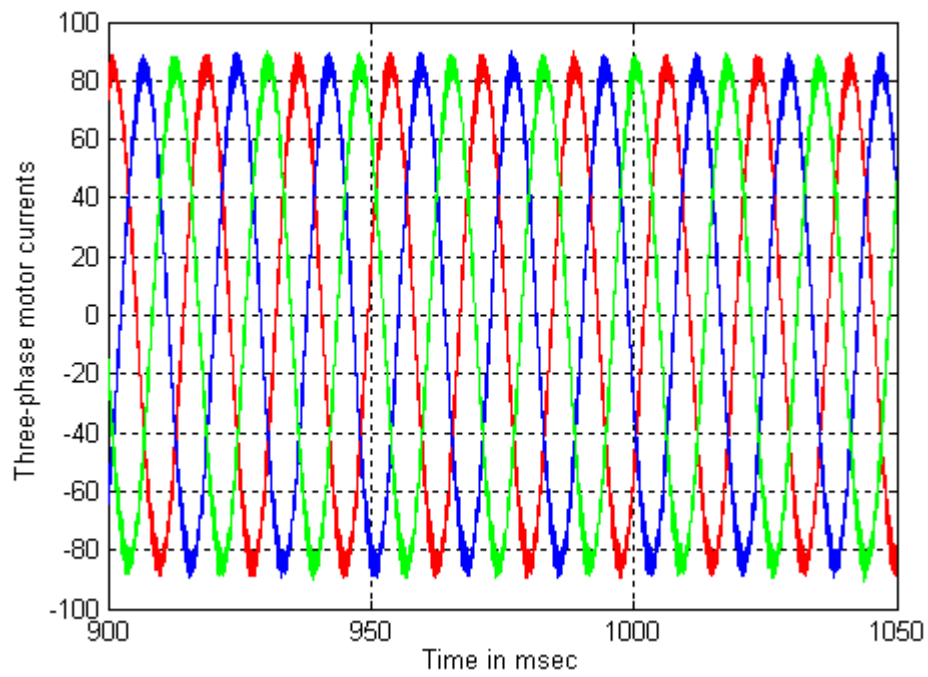
Figure 5.14 Motor currents for 322 Nm load at 1100 rpm (50 hp)

Further, to ensure correctness of simulated values of currents and voltages, a power balance at the source and load side needs to be verified. Accordingly, power at the input and output terminals of motor is given by,

$$P_{in} = \sqrt{3} \cdot V \cdot I \cdot \cos\phi \ \text{ And } \ P_{out} = 2\pi \cdot \frac{N}{60} \cdot T_L \tag{5.6}$$

where, the motor power factor is <u>0.86</u> and the load torque, $T_L =$ <u>322.54</u> Nm.

Thus, the real power at the input and output of the motor is,

$$P_{in} = \sqrt{3} * 480 * \frac{85}{\sqrt{2}} * 0.86 = 42973 \ \text{W} \tag{5.7}$$

$$P_{out} = 2\pi \cdot \frac{1100}{60} \cdot 322.54 = 37153 \ \text{W} \tag{5.8}$$

The motor copper losses, core losses and friction losses accounted for the remaining (P_{in} - P_{out}) 5820 watts. Figure 5.15 shows real and reactive currents.
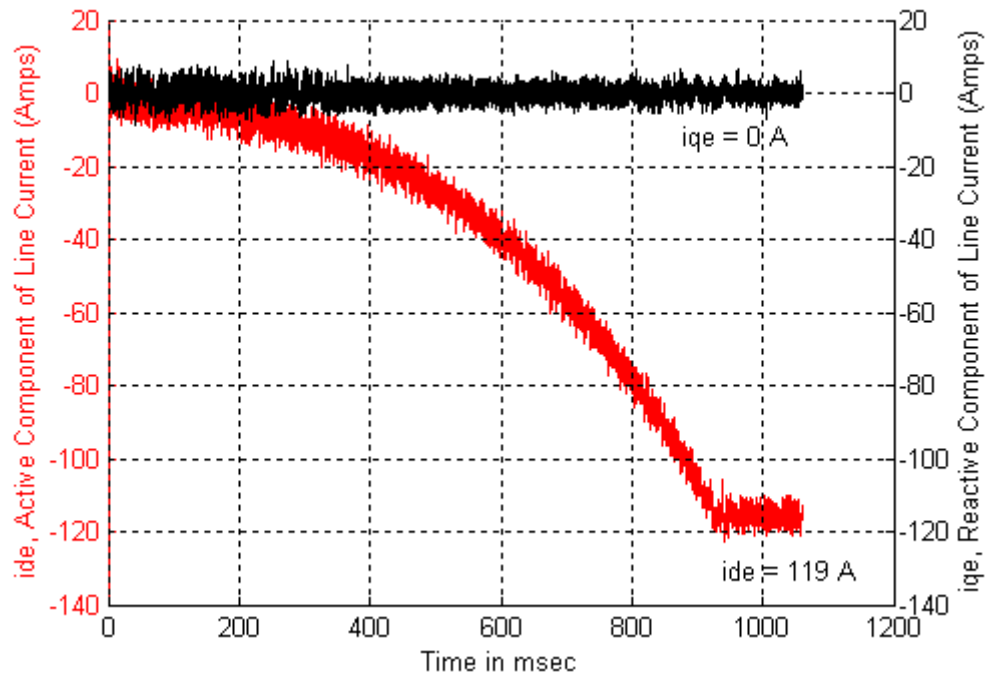
Figure 5.15 Real and reactive current components

94

Similarly power on the supply side can be calculated. Figure 5.15 shows the real component of line current to be equal to 119 A, while the reactive current component is zero. Recall that real and reactive power in *d-q* coordinates are given by,

$$P = \sqrt{3} \cdot E_{ll} I \cos\varphi = E_{de} \cdot i_{de} \tag{5.9}$$

$$Q = \sqrt{3} \cdot E_{ll} I \sin\varphi = E_{de} \cdot i_{qe} \tag{5.10}$$

From Equation 5.9 and 5.10, we can write,

$$\cos\varphi = \frac{i_{de}}{\sqrt{i_{de}^2 + i_{qe}^2}} \tag{5.11}$$

Further, the line-to-line supply voltage, E_{ll}, is given by,

$$E_{ll} = \sqrt{E_{de}^2 + E_{qe}^2} \tag{5.12}$$

Since, $E_{qe} = 0$, the E_{de} component would be 480 V. Thus, the real power supplied by the converter was,

$$P = 480 * 119 = 57120 \text{ W.} \tag{5.13}$$

From Figure 5.13, the peak line current was found to be 98 A. So, for the line side resistance of 1 Ω, the power at the input of the rectifier, P_{rect}, was,

$$P_{rect} = P - 3 \cdot I^2 R = 57120 - 14406 = 42714 \text{ W} \tag{5.14}$$

Because the switches used in the simulation were all ideal devices, there was no power loss in the rectifier, dc-link, or inverter. Thus the power at the input of rectifier should be equal to the power at the input of the motor. From Equation 5.6 and 5.7 we have $P_{rect} \approx P_{in}$ ($42973 \approx 42714$). This illustrates power balance between source and a load. The small difference in P_{rect} and P_{in} is an error in i_{de} and line current measurements.

5.5.3 Thermal Management System Issues

Based on the voltage and current requirements for the front-end converter, the switching device recommended was: 1200 V, 150 A, IGBT module (Module No: CM150DY-24NF) with built in free-wheeling diode, supplied by POWEREX Inc.

The thermal loss model discussed in Chapter 3 was used to estimate power losses. Depending upon how much heat needs to be dissipated, a suitable thermal management system will be recommended. First, the characteristic plots for the selected device were modeled in MATLAB. Figure 5.16 shows IGBT collector-emitter saturation voltage characteristics provided in device datasheet while, Figure 5.17 shows the actual characteristics modeled in MATLAB using curve-fitting techniques. In a similar way, IGBT switching loss characteristics, free-wheeling diode forward, and reverse recovery characteristics were also plotted.

The switching loss curves provided in the device data-sheet assume a common dc-link voltage of 600 V. Moreover, the switching energy is expressed in units of mJ/Pulse. The term, "Pulse", constitutes one period of a switching cycle. So the actual switching losses for a 1000 V dc-link voltage and a switching frequency of 4 kHz were calculated as [15],

$$E_{sw\_on} = E_{sw\_onrated} * f_{sw} * \frac{1000}{600} \text{ W} \tag{5.15}$$

$$E_{sw\_off} = E_{sw\_offrated} * f_{sw} * \frac{1000}{600} \text{ W} \tag{5.16}$$

where, $E_{sw\_onrated}$ and $E_{sw\_offrated}$ are switch-on and switch-off energy losses in mJ per pulse at 600 V.
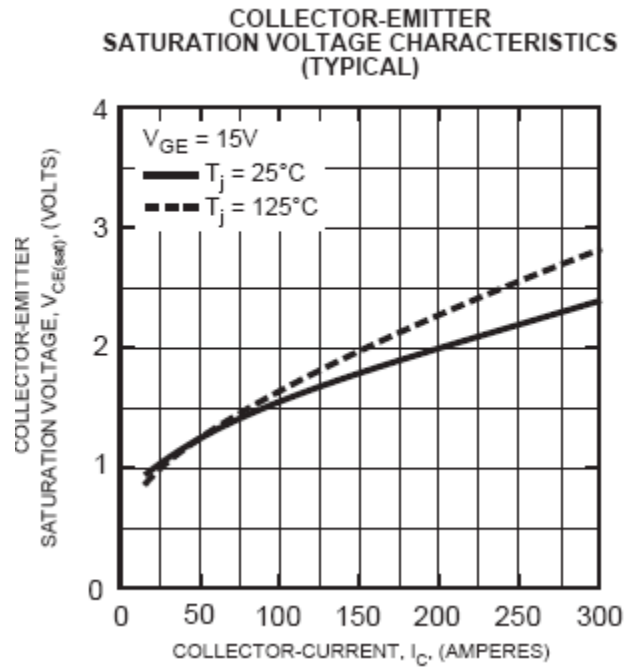
Figure 5.16 IGBT collector-emitter characteristics provided by the device data-sheet
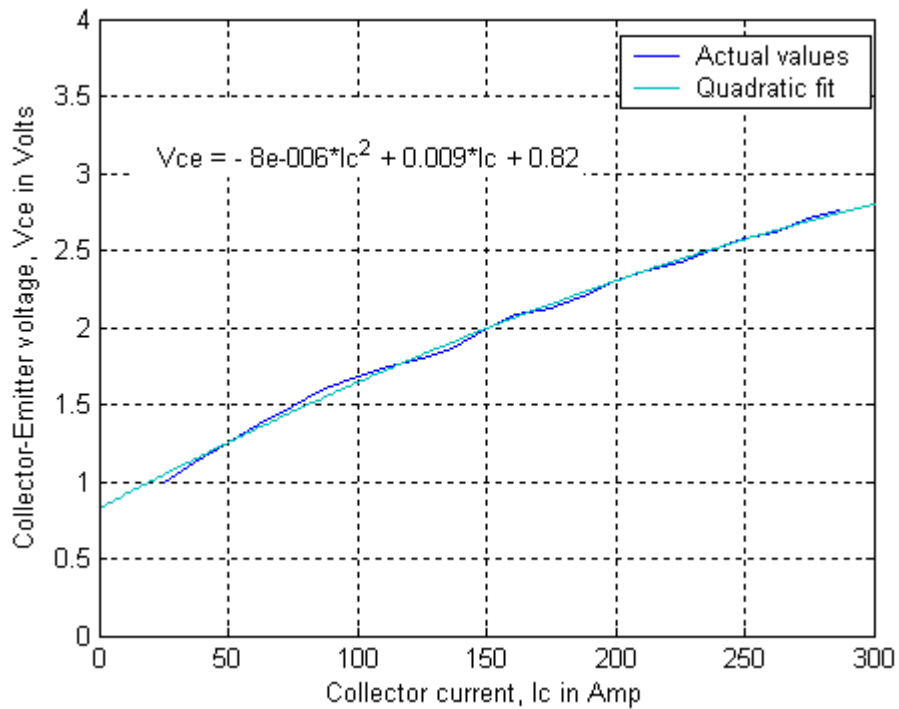

$$Vce = -8e\text{-}006*Ic^2 + 0.009*Ic + 0.82$$

Figure 5.17 IGBT collector-emitter curve modeled in MATLAB

97

To estimate the maximum heat dissipation, the front-end converter was operated to the full capacity at unity power factor. The conduction and switching losses for <u>one IGBT module</u> at the peak line current of 98 A are shown in Figure 5.18. The conduction and reverse recovery losses in the free-wheeling diode are shown in Figure 5.19.

The average total power loss per switching device (IGBT + diode) is given by,

$$P_L = (P_{Cond\_diode} + P_{Cond\_IGBT}) + (P_{SWon\_IGBT} + P_{SWoff\_IGBT} + P_{RR\_diode}) \qquad (5.17)$$

From Figure 5.18 and 5.19, the average power loss per device, P_L, was:

$$P_L = 11 + 32 + 45 + 6 = 94 \text{ W} \qquad (5.18)$$

The amount of heat that can be taken away from the device junction to ambient is given by [23],

$$P_L = \frac{T_j - T_a}{R_{\theta jc} + R_{\theta cs} + R_{\theta sa}} \qquad (5.19)$$

where, $R_{\theta jc}$ is the device junction-to-case thermal resistance, R_{jcs} is the case-to-heat sink thermal resistance, and $R_{\theta sa}$ is the heat sink-to-air thermal resistance. The thermal resistance is expressed as °C/W.

From the device data-sheet, $R_{\theta jc}$ is 0.25 °C/W and R_{jcs} is 0.093 °C/W. The maximum junction temperature recommended is 125 °C. Considering the worst case ambient temperature of 50 °C, we can calculate $R_{\theta sa}$ as,

$$94 = \frac{125 - 50}{0.25 + 0.093 + R_{\theta sa}}; \text{ Thus, } R_{\theta sa} = 0.45 \text{ °C/W} \qquad (5.20)$$

It is not possible to get an appropriate sized heat sink with natural convection which provides $R_{\theta sa}$ as low as 0.45 °C/W [23]. Thus for this application, a heat sink with forced air cooling is recommended.
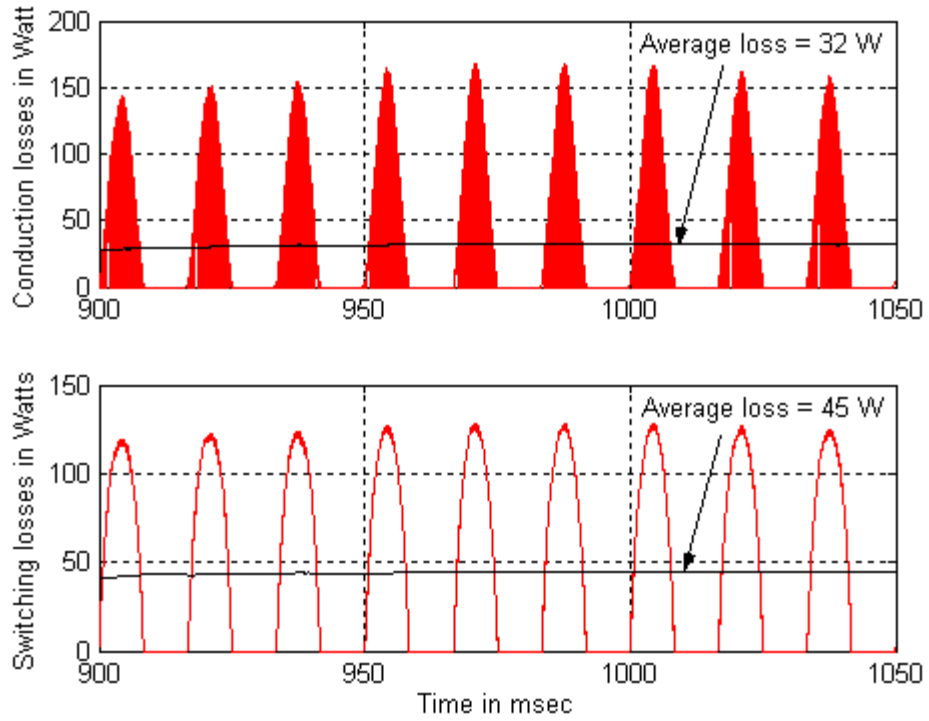
Figure 5.18 IGBT power losses at peak load
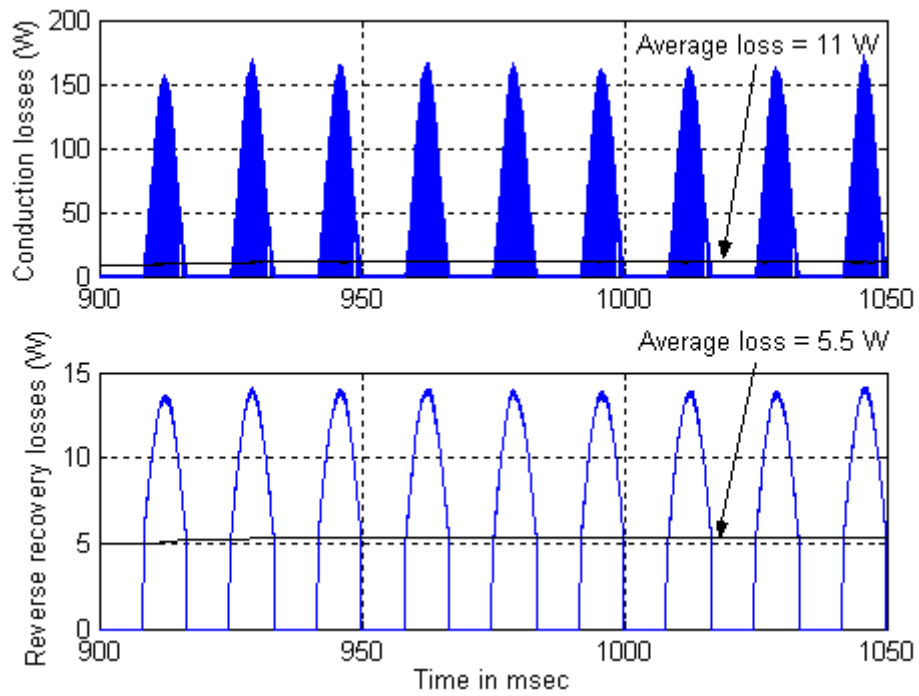
Figure 5.19 Free wheeling diode power losses at peak load

99

5.5.4 Power Quality Considerations

As mentioned before in Chapter 2, the motor drive with an active front-end provides a much improved interface with power grid. By drawing line currents at unity power factor it eliminates the need for installing a reactive compensator. However, the line current distortions still need to be monitored. Because, highly distorted line currents at unity power factor will introduce harmonics in line voltage, thereby affecting the other loads connected to the system.

To monitor power quality, a motor load is changed from full load to no load in steps of 10%. At each step, total harmonic distortion was monitored. Table 5.1 shows line currents, real and reactive power, current THD and power losses for each step. Based on this data, a current THD is plotted against % of motor load as shown in Figure 5.20.
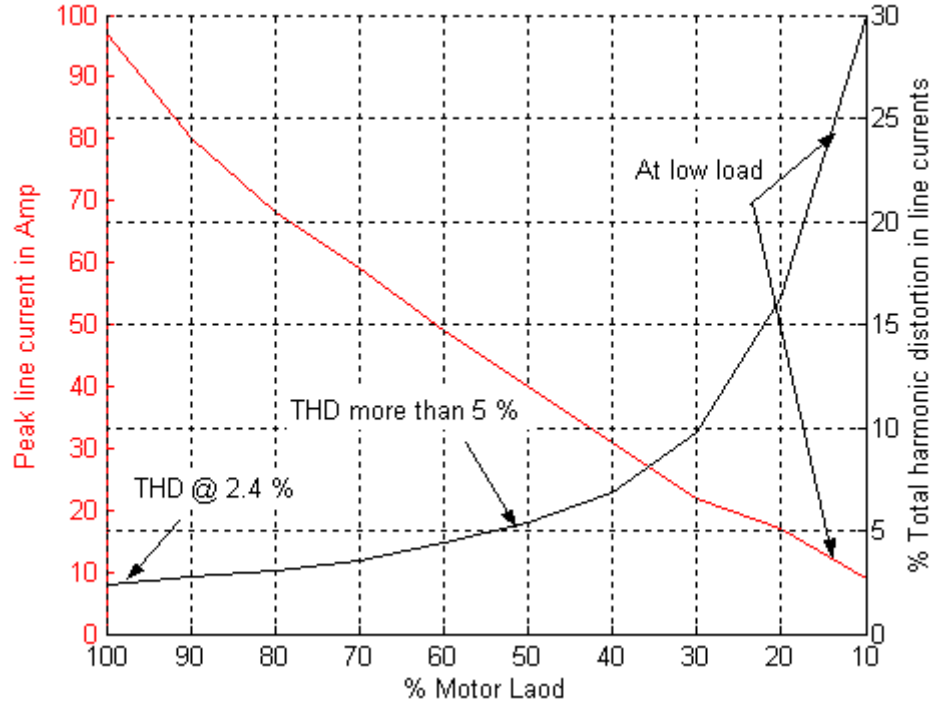
Figure 5.20 Total harmonic distortions in line current at unity power factor

Table 5.1 Drive parameters at different motor loads

Motor Load	I_{de} (A)	I_{qe} (A)	I_line Peak (A)	$E_{de}\,i_{de}$ (kW)	THD in line current (%)	Total Power losses (W)
100%	120	0	97	57.6	2.4	564
90%	99	0	80	47.5	2.5	480
80%	84	0	68	40.3	3.3	420
70%	72	0	59	34.5	3.5	348
60%	58	0	49	27.8	4.5	300
50%	48	0	40	23	5.0	252
40%	37	0	31	17.7	7.0	198
30%	27	0	22	12.9	10.0	150
20%	19	0	17	9.12	16.0	108
10%	10	0	9	4.8	30.0	72

5.5.5 Limits on Reactive Compensation

In this section the amount of reactive power that the active drive can compensate at different load levels is investigated. Again, the motor load was varied from 100% to 10% in ten steps. For each step the reactive compensation command was selected such that the peak line current remained within the rated value of 100 A.

From Equation 5.9 and 5.11 we can write,

$$\sqrt{3}\,\frac{E_{ll} \cdot I}{\sqrt{i_{de}^{\,2} + i_{qe}^{\,2}}} = E_{de} \tag{5.21}$$

where, I is the RMS line current.

Since $E_{ll} = E_{de}$, the line current peak, I_{peak}, is given by,

$$I_{peak} = \frac{\sqrt{3}}{\sqrt{2}} * \sqrt{i_{de}^{\,2} + i_{qe}^{\,2}} \tag{5.22}$$

Note that, for the same motor load, the i_{de} current drawn by the rectifier during reactive compensation will be different from the i_{de} current drawn without reactive compensation. The reason for this is that during reactive compensation the dc-link variations will be different from the variations at unity power factor operation. As a result, more real power in the form of $E_{de} \cdot i_{de}$ will be needed to restrict dc-link variations to the minimum level.

Table 5.2 shows real power, reactive power limits, and the corresponding line current peak value. The table also shows the line current THD, power losses, and maximum change in dc-link voltage, ΔV_{dc} at each step. The total power loss, P_T, was further split into switching loss, P_{sw}, and conduction loss, P_c.

Table 5.2 Drive parameters during reactive compensation at different motor loads

Motor Load	I_{de} (A)	I_{qe} (A)	I_line *peak* (A)	$E_{de}\,i_{de}$ (kW)	Reactive compensation $E_{de}\,i_{qe}$ (kVAR)	Line current THD (%)	DPF at line side	Power Loss (W)	ΔV_{dc} (V)
100%	120	0	98	57.6	0.00	2.34	1.0	570	23
90%	110	50	99.5	52.8	24.00	2.35	0.910	588	21
80%	101	65	99	48.48	31.2	2.45	0.841	582	20
70%	92	78	99	44.16	37.44	2.40	0.763	585	20
60%	84	86	98.5	40.32	41.28	2.45	0.698	570	20
50%	76	95	99.3	36.48	45.6	2.7	0.624	582	15
40%	65	101	98	31.2	48.48	3.15	0.537	588	18
30%	58	106	98.5	27.84	50.88	3.5	0.480	600	20
20%	50	110	99	24.00	52.8	3.7	0.414	594	22
10%	44	115	99.7	21.12	55.2	4.5	0.344	630	25

The peak line current, real power, and the maximum possible reactive power compensation at each load step are shown in Figure 5.21. As can be seen, with increase in motor load, the maximum allowable reactive compensation decreases, so that the peak line current can be kept below rated value.

The front-end converter, when operating at full load at unity power factor, draws 57.6 kW active power. At 90 % motor load, the active power drawn by the front-end converter was 52.8 kW (91.67 %) while, the reactive power compensated was 24 kVAR (41.67 %). Note, that at 90% motor load, the maximum change in dc-link voltage, ΔV_{dc}, was 20 V. Since the power devices used in the simulation were ideal switches with no power loss, all the additional real power (kW) drawn by the front-end converter was utilized for charging the dc-link capacitor, so that ΔV_{dc} could be reduced to zero.
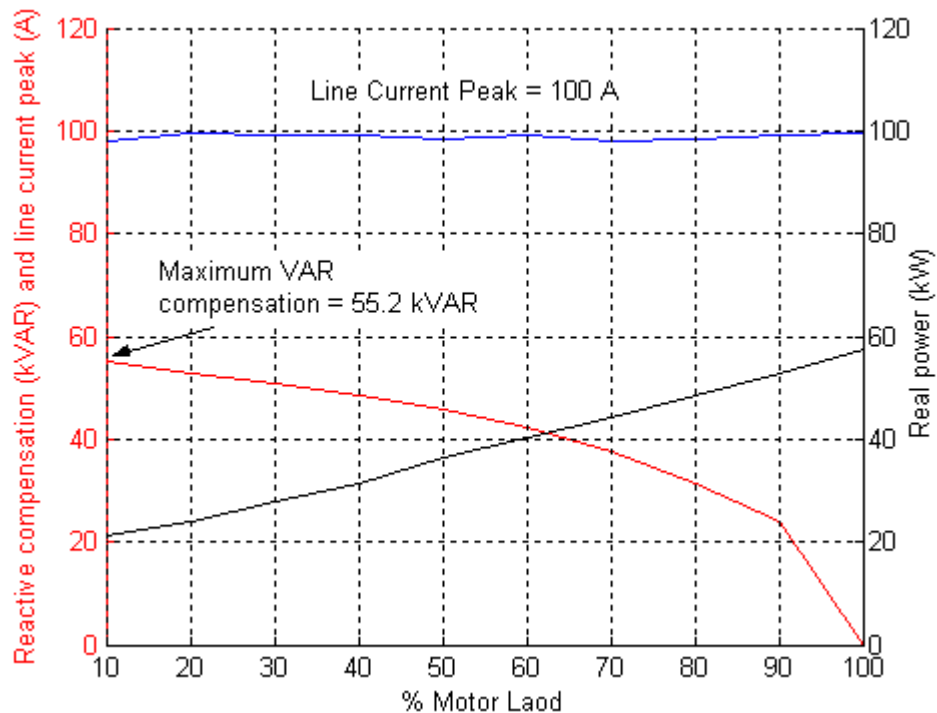

Figure 5.21 Reactive compensation limits for active drive

Figure 5.22 illustrates line current THD at different compensation levels. The maximum distortion, 4.5 %, occurred at 10% load. As motor load increases to its rated value, the i_{de} component of line current becomes dominant. Consequently, the displacement power factor approaches to unity while total harmonic distortion also reduces.

Figure 5.23 shows the total power loss and switching loss along with conduction losses in IGBT and diode. During the load and reactive power changes, the switching loss remained constant. Further, as displacement power factor moves from highly leading towards unity, the IGBT conduction loss increases while, conduction loss in the free-wheeling diode reduces. Consequently, the total power loss also decreases by a small amount.

Further, it can be seen from Table 2.2 that, at all operating conditions, the maximum decrease in the dc-link voltage was about 25 V (< 3%). The less ripple in dc-link means a dc capacitor with lower capacitance can be used.

5.6   Chapter Summary

In this chapter several topics were discussed. A methodology used in the research was presented first. Three main tasks attempted in this research were: theoretical modeling and control of active front-end drive, simulation of system modes of operation, and performance analysis. The simulation setup and software configuration used was then presented.
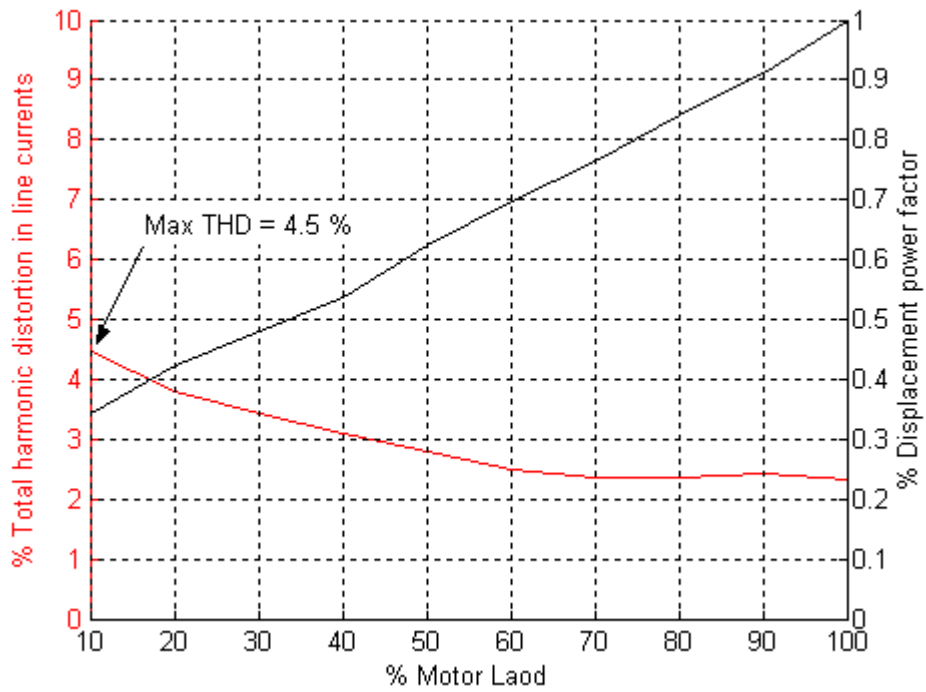
Figure 5.22 Line current THD and displacement power factor during compensation
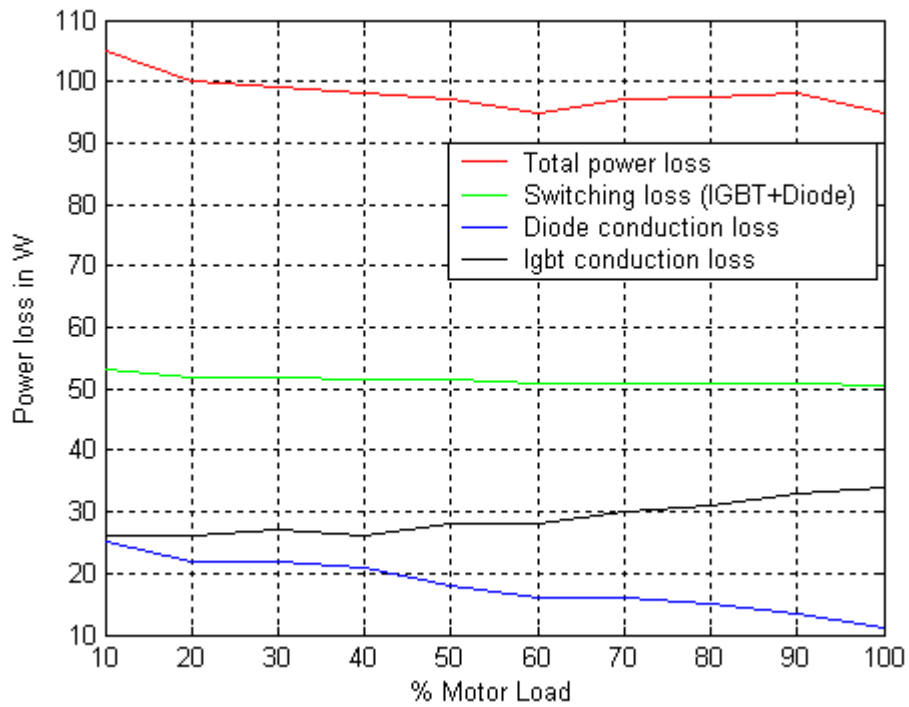
Figure 5.23 Device power losses during compensation

106

Some of the simulation results obtained from active front-end drive operating with and without motor load were then presented. Further, the modes of operation such as variable power factor operation and dynamic control over dc-link voltage were demonstrated. Based on simulation data, several design related issues such as device rating, power loss, power quality, and thermal management system were discussed. In the end, the simulations performed to define reactive compensation limits were discussed.

In the next chapter, a brief summary of the thesis will be given. From this summary, some conclusions regarding the research will be made. Finally, some suggestions on future research will be given.

6   Summary and Conclusions

6.1   Chapter Overview

In this chapter some concluding remarks regarding the research will be provided. In Section 6.2 a brief summary of the thesis will be given. Based on the simulation results presented in Chapter 5, some conclusions regarding the research will be made in Section 6.3. The key features of an active rectifier useful in certain applications were also discussed in this section. Section 6.4 will provide suggestions for possible future research in the area of active front-end drive for VAR compensation and harmonic filtering.

6.2   Thesis Summary

To investigate reactive compensation capabilities of an active front-end drive by accurate simulations was the principal motivation behind this thesis work. The mathematical model of the front-end converter was established. A suitable control strategy for decoupled control of real and reactive power was formulated. The simulations were performed to evaluate system performance. Based on simulation results, the limits on reactive power compensation were established.

Chapter 1 and 2 served to provide an introduction to the active front-end technology used in drives and also some background information regarding the power compensation techniques used in the power system. In Chapter 1, a brief summary of research to be presented in the thesis was first provided. A circuit topology used for reactive power compensation comprising a front-end rectifier, a load-side inverter, and an

induction motor was presented. Further, basic operating principle and modes of operation of active drive were discussed. The research goals and the thesis outline were also presented.

In Chapter 2, a detailed background pertaining to reactive power compensation in the power system and power quality issues such as sources of harmonics and their effects was given. The role of power electronics in improving the ac grid power was reviewed. The interpretations of instantaneous real and reactive power were also discussed. A comparison between traditional drives with phase-controlled rectifiers and drives with active front-ends was presented.

Chapter 3 and 4 discussed theory behind modeling and control of active front-end inverter. In Chapter 3, a dynamic d-q model, needed for a fast transient response of an active drive was derived. Since the control was to be carried out in d-q coordinates, the real and reactive power definitions in d-q coordinates were presented. The compensation characteristics and the steady state controllability of the active front-end converter were also discussed. Further, the power loss model to estimate the conduction and switching losses in IGBTs and free-wheeling diodes was presented. The total heat dissipation estimated from the loss model was used in Chapter 5 to recommend a suitable thermal management system for a high power active drive.

In Chapter 4, an effective approach for controlling the rectifier dynamics was derived. Based on system differential equations, an ac-side per-phase equivalent circuit and a dc-side equivalent circuit models for the front-end converter were introduced. A high gain feedback controller for controlling the magnitude and phase of the line currents was then discussed. A scheme for estimating angular frequency of source voltages in real

time was also discussed.

An input-output linearization controller to effectively decouple the real and reactive current components during the dc-link variations was discussed next. For achieving better transient performance, a feed-forward controller was also presented. In addition to the front-end rectifier, the control of the load-side inverter and induction motor also needed to be discussed. In the later part of Chapter 4, a mathematical model of an induction motor was introduced. Further, a classical field oriented control of induction motor was discussed in detail.

In Chapter 5, the simulation results were presented. The simulation set-up and the software configuration used were discussed first. The steps performed in simulating various modes of operation and in evaluating the system performance were listed as well. The active drive was simulated with and without motor load, and the different key features of the drive, such as variable power factor and better control over dc-link voltage, were demonstrated.

Further, the drive performance was analyzed under different load scenarios to address design issues such as device rating, power loss, power quality, and thermal management system. The simulation data was interpreted to determine the maximum reactive power that can be compensated for a given motor load.

6.3   Conclusions from Research

Compared to conventional AC drives with phase-controlled rectifiers, the active front-end drives provide faster dynamic response, better control over dc-link voltage, and

improved power grid interface with minimum harmonic distortions. The active front-end drives also have integrated line regeneration capability.

This thesis presented a methodic approach to analyze the performance of an active front-end induction motor drive. By establishing the expected performance, technical risks in actual development will be reduced. Further, the research also helps identify the device selection and system design issues prior to the actual design itself.

A controller for the active rectifier was presented which consists of an outer dc-link voltage regulation loop and inner current regulation loop. A faster dynamic response is obtained by including the load power feed-forward compensation.

The decoupled control presented allows independent control over real and reactive power. This makes variable power factor operation possible. The simulation results demonstrated faster time response of the current controllers to the step change in compensation command.

The simulation results also show that the active power drawn by the rectifier is more than the power required to drive the motor load. The additional active power is used to charge a dc-link capacitor. Thus, the maximum reactive compensation depends upon the amount of active motor load as well as the maximum ripple in the dc-link voltage. This compensation limit is valid for a specified ratio of peak line voltage to dc-link voltage, and also for a specified current rating of active switches.

A fast dynamic response of the active rectifier helps regulate the dc-link voltage to a desired value and makes it immune to the load and line variations. The maximum dc-link ripple at different operating conditions was found to be below 3 %. Thus, the dc-link capacitance can be significantly lowered and there is possibility of using film capacitors

instead of expensive electrolytic capacitors [24]. This will result in less number of failures, thereby improving the reliability of the drive measured in terms of the mean-time-between-failures (MTBF).

The current and voltage rating of the active devices used in inverter and rectifier was found to be identical. Thus the same devices and the associated gate drivers can be used for both inverters and rectifiers. This presents an opportunity for modular design, resulting in simplified assembly and repair.

The power loss in switching devices was found to be considerably high. Even with a low switching frequency of 4 kHz, a heat sink with forced cooling system was required. With increase in power rating or switching frequency, the water cooled thermal management system would be necessary to dissipate the extra heat generated. Alternatively, emerging devices such as silicon carbide based IGBTs or MOSFETs with high temperature handling capabilities need to be investigated for such high power applications.

Unlike traditional phase-controlled rectifiers, the active rectifiers do not draw lagging currents from the utility, eliminating the need for additional VAR compensator for high power applications. Secondly, the line current total harmonic distortion at the supply-side was below 5 % even for highly leading power factor. The improved power grid interface argues well for using active front-end rectifier not only for the high power drives, but also for providing utility interface to the distributed energy sources such as micro-turbine generators and wind power generators.

One obvious drawback of the active front-end drives is the high cost on account of extra active devices used in the rectifier. This restricts the use of active front-end

drives for large power applications where the extra cost is justified either by operating at unity power factor, providing integrated line regeneration capabilities, or supplying reactive power compensation to the utility.

6.4   Future Research

One interesting area for the future research would be to extend the capabilities of active drive for harmonic elimination [25]. In the research presented in this thesis, the reference command for reactive power compensation, i_{qe}, was considered to be a dc value. This is because, the sinusoidal line currents with angular frequency of ω, are transformed into the dc quantities in the *d-q* coordinate system rotating at the same angular frequency, ω. Thus the compensation achieved in this case was the fundamental frequency reactive compensation. Alternatively, a new i_{qe} reference can be generated which is the combination of fundamental frequency as well as the harmonic frequency components of line current. By using the same decoupled control principle that was used for VAR compensation, the resultant line currents can be made to eliminate the harmonic components from the source. The active drive thus can also provide harmonic filtering.

Another suggestion for future research concerns dynamically controlling dc-link voltage to keep inverter modulation index close to one. For two level inverters, keeping the amplitude of modulation index close to one reduces the power loss and improves the efficiency [20]. Similarly for induction motor this results into reduced core losses [21]. In future research, this idea of changing the dc-link voltage dynamically to maintain modulation index close to one can be explored.

For the input-output linearization controller used in this research, the exact values of line inductor, resistor and angular frequency are required. The angular frequency is estimated in real time, so it is known accurately. Further, as the voltage drop across the series impedance and the line currents are known, it should be possible to estimate the series inductor and resistor values. The series impedance at the supply side does not change in the same manner as induction motor parameters. However, estimating the series impedance value would eliminate the need to tune the controller for every little change made in system configuration, thus making the controller more robust.

Most often the active front-end drive is considered for high power applications. At such high power ratings the amount of current that can be handled by the IGBTs used in two-level inverter, the dc-link voltage level, and also the switching losses impose a limit on the amount of reactive power that can be compensated. Alternatively, in future research, a cascaded multilevel inverter can be studied for providing reactive compensation while also driving the induction motor load.

6.5   Chapter Summary

The purpose of this chapter was to provide concluding remarks. A brief summary of the thesis was first provided. Following this summary, some conclusions regarding the research were then made. Some topics concerning future research in the area of multilevel inverters were also discussed.

List of References

List of References

[1]   Bimal K. Bose, *Modern Power Electronics and AC Drives, First Edition.* Prentice Hall, 2002.

[2]   Edson H. Watanabe, Mauricio Aredes, "Compensation of Non-Periodic Currents using the Instantaneous Power Theory," *IEEE Power Engineering Society Summer Meeting, 2002*, vol. 2, July 2000

[3]   IEEE Recommended Practices and Requirements for Harmonic Control in Electric Power System, *IEEE Std 519-1992*

[4]   N. Mohan, A. K. Jain, Philip Jose, R. Ayyanar, "Teaching Utility Applications of Power Electronics in First Course on Power Systems," *IEEE Transactions on Power Systems*, vol. 19, no. 1, February 2004.

[5]   F. Wang, S. Rosado, T. Thacker, D. Boroyevich, "Power Electronics Building Blocks for Utility Power System Applications," *IEEE 4th International Power Electronics and Motion Control Conference*, vol. 1, August 2004.

[6]   Arindam Ghosh, Gerald Ledwich, *Power Quality Enhancement Using Custom Power Devices*. Kluwer Academic Publisher, 2002.

[7]   F. Z. Peng, George W. Ott, Jr., Donald J. Adams, "Harmonic and Reactive Power Compensation Based on the Generalized Instantaneous Reactive Power Theory for Three-Phase, Four-Wire Systems," *IEEE Transactions of Power Electronics*, vol. 13, no. 6, November 1998.

[8]   H. Akagi, Y. Kanazawa and A. Nabae, "Instantaneous Reactive Power Compensators Comprising Switching Devices Without Energy Storage Components," *IEEE Transactions on Industry Applications*, vol. 20, May 1984.

[9]   H. Akagi, "Active Filters and Energy Storage Systems Operated under Non-Periodic Conditions," *IEEE Power Engineering Society Summer Meeting, 2002*, vol. 2, July 2000.

[10]   F. Z. Peng, Jih-Sheng Lai, "Generalized Instantaneous Reactive Power Theory for Three-Phase Power System," *IEEE Transactions on Instrumentation and Measurement*, vol. 45, no. 1, February 1996.

[11]   Gerald M. Brown, Bernard J. Ebacher, Walter G. Koellner, "Increased Productivity with AC Drives for Mining Excavators and Haul Trucks," *IEEE Industry Applications Conference*, vol. 1, October 2000.

[12]   F. Z. Peng, Jih-Sheng Lai, "Dynamic Performance and Control of a Static Var Generator Using Cascade Multilevel Inverters," *IEEE Transactions on Industry Applications*, vol. 33, no. 3, May/June 1997.

[13]   Werner Leonhard, *Control of Electrical Drives, Third Edition.* Springer 2001.

[14]   Powerex IGBT and Diode data sheet. (www.pwrx.com)

[15]   Zhihong Ye, Timothy CY Wang, Gautam Sinha, Richard Zhang, "Efficiency Comparison for Microturbine Power Conditioning Systems," *IEEE Power Electronics Specialist Conference*, vol. 4, June 2003.

[16]   Jose R. Espinoza, Geza Joos, Luis Moran, "Decoupled Control of the Active and Reactive Power in Three-Phase PWM Rectifiers based on Non-Linear Control Strategies," *IEEE Power Electronics Specialist Conference*, vol. 1, July 1999.

[17] Frede Blaabjerg, John K. Pedersen, "An Integrated High Power Factor Three-Phase AC-DC-AC Converter for AC-machines Implemented in One Microcontroller," *IEEE Power Electronics Specialist Conference*, June 1993.

[18] Hidehiko Sugimoto, Siego Morimoto, Masao Yano, "A High Performance Control Method of a Voltage-Type PWM Converter," *IEEE Power Electronics Specialist Conference*, vol. 1, April 1988.

[19] Marc Bodson, John Chiasson, Robert Novotnak, "High Performance Induction Motor Control Via Input-Output Linearization," *IEEE Control System Magazine*, vol. 14, issue 4, August 1994.

[20] Leon M. Tolbert, F. Z. Peng, Thomas G. Habetler, "Multilevel Converters for Large Electric Drives," *IEEE Transactions on Industry Applications*, vol. 35, no. 1, January 1999.

[21] S. Khomfoi, V. Kinnares, P. Viriya, "Investigation into Core Losses due to Harmonic Voltages in PWM fed Induction Motors," *IEEE International Conference on Power Electronics and Drive Systems,* July 1999.

[22] Paul C. Krause, *Analysis of Electric Machinery.* McGraw Hill Book Company, 1986

[23] N. Mohan, T. M. Undeland, and W. P. Robbins, *Power Electronics: Converters, Applications, and Design, Third Edition.* John Wiley and Sons, 2003.

[24] Rangarajan M. Tallam, Rajendra Naik, Michael L. Gasperi, Thomas A. Nondahl, Hai Hui Lu, Qiang Yin, "Practical Issues in the Design of Active Rectifiers for AC Drives with Reduced DC-Link Capacitance," *IEEE Industry Applications Conference*, vol. 3, October 2003.

[25]   P. Brogan, R. Yacamini, "Harmonic Control Using an Active Drive," *IEEE Proceedings on Electric Power Applications*, vol. 150, issue 1, January 2003.

Vita

Pankaj Prabhakar Pandit is a citizen of India and was born in 1978. He received his bachelor's degree in the year 1999 from Government Engineering College Aurangabad, India. He graduated with M.S. in Electrical Engineering from the University of Tennessee in 2005. His area of interest is active front-end converters for motor drives.